Evaluating Hybrid Smiles by Inverse Transforms

Claus H. Jaroschek
Exeter College
University of Oxford

A thesis submitted in partial fulfillment of the MSc in
Mathematical Finance

20th July 2013

Vide hominem caecum dirigentes ad orbem,
te melius claudet oculos vestros,
incurvasti caputem tuum, expectare ricochetem,
... hinc aliquo modo esse, dixit scurra ad latronem,
illic est adeo confusionem, possum nihil levari,
percuties ipsum homo ibi, qui formidat uxor mea,
venire, et occupare meam quoque terram ...
... Ego sum agens chaos ... Non ego sum canebant artificis,
... quidam non possit emi, subiectae, cogitabant aut agebant,
... quidam iustus volo ad vigilate mundi exuret ...

Acknowledgments

I would like to express my sincere thanks to my supervisor Prof. Dr. Cornelis Oosterlee and his former PhD student Dr. Lech Grzelak for their patient advice, critical comments on my work in progress and the diligent corrections of the manuscript. I am very well aware that they might have had some difficult times to understand my thoughts, particularly as my progress on the subject was alternating between productive and less productive phases - usally directly related to the workload on my client projects. Even higher I value their continued support, and eventually the hope remains, that we have mutually profited from the collaboration.
I am also very grateful to the management of d-fine GmbH for introducing me to the Oxford MSc programme and the financial support of my participation.

Contents

List of Abbreviations

The following abbreviations are conventionally used throughout the text. Abbreviations are introduced for individual words recurring frequently and lengthy model names:

EQ	*equity*
IR	*interest rate*
DD	*displaced-diffusion*
SV	*stochastic volatility*

Model abbreviations:

H	*Heston* (model)
CH	*Cheyette* (model)
HW	*Hull-White* (model)
LMM	*Libor Market Model*

HHW	*Heston Hull-White* (model)
HCH	*Heston Cheyette* (model)
HCV	*Heston displaced-diffusion stochastic volatility Cheyette* (model)
HLMM	*Heston displaced-diffusion stochastic volatility Libor Market Model*

Abbreviations of affine hybrid model approximations:

H1HW	*Heston Hull-White* (model) *in the affine limit 1*
H1CH	*Heston Cheyette* (model) *in the affine limit 1*
H1CV	*Heston displaced-diffusion stochastic volatility Cheyette* (model) *in the affine limit 1*
H2CV	*Heston displaced-diffusion stochastic volatility Cheyette* (model) *in the affine limit 2*
H1LMM	*Heston displaced-diffusion stochastic volatility LMM in the affine limit 1*

Abbreviations are occasionally combined, i.e HDDCH corresponds to *Heston displaced-diffusion Cheyette* (model) - this is the HCV (model) without SV process.

Chapter 1

Introduction

Whenever inverse transform techniques are applicable to the evaluation of derivative products, the classical pricing methods based on solving Partial Differential Equations (PDE) or Monte-Carlo (MC) schemes are outclassed in computational performance (at least for non-Bermudan products). Consequently inverse transforms qualify as the methods of choice for model calibration purposes where striving for an optimum calibration set requires roaming potentially vast parameter spaces.
Accessibility of the characteristic function (CHF) is the prerequisite to employ inverse transform methods. A general formalism to obtain the CHF corresponding to a particular valuation model is known, whenever the underlying system of stochastic differential equations (SDEs) is representable in affine form.
The purpose of the thesis at hand is to derive an affine hybrid model which is capable to reproduce smile effects both in equity (EQ) and interest rate (IR) components. Such a model has the potential to evaluate derivative products sensitive to *hybrid smiles*. In this thesis the focus rests on a specific class of hybrid valuation models where the Heston stochastic volatility approach on the EQ side is combined with the Cheyette (CH) model on the IR side. Then, the complexity of the hybrid model is controlled by the concrete choice of the Cheyette model volatility specification. For constant IR volatility the plain Hull-White (HW) model is retained as limiting case of the Cheyette approach, and in combination with the Heston EQ process the Heston Hull-White (HHW) hybrid system ensues. The Cheyette model is amendable with the provision to include displaced-diffusion (DD) stochastic volatility (SV) specifications. By DD model extensions normal and log-normal characteristics in the IR component become entangled. Including an IR-SV process introduces smile effects on the IR side. In combination with the Heston EQ process the resulting hybrid model is named Heston DDSV Cheyette (HCV) model.
Depending on the number of correlated stochastic processes involved, hybrid models can be ordered according to dimensionality and complexity. At the lower end of complexity, the HHW combines the Heston process with a 1D short rate process. The HHW is capable to reproduce smile and skew effects solely in EQ. At the high end of complexity, the Heston DDSV Libor Market Model (HLMM) is constructed by coupling a Heston process in EQ with a multi-dimensional market model, further supplemented by DDSV extensions on the IR side. In the HLMM smile and skew features are representable both in EQ and IR components, however the high number of correlated processes makes

the model less tractible in practice. Affine versions of the HLMM require approximations making the model Markovian. This implies simplifications to the drift components of IR stochastic processes, usually associated with decisive reduction of the model dimensionality (for instance by *freezing* the initial Libor rates). In this context the HCV model resembles a trade-off between complexity and sophistication. The HCV incorporates hybrid smile features, and the approximations required to obtain an affine model version are less severe. Dimensionality of the model is determined by the specific choice of the stochastic volatility specification. In the simplest form the HCV is a 5D model, and hence, model complexity is between the extremes of HHW and HLMM.

Hybrid models like the HCV are in general non-affine, in particular when EQ-IR correlations are present. Central issue of the thesis at hand is to define and discuss approximations placing the HCV within the class of Affine Jump-Diffusion (AJD) processes with the constraint to retain the full set of correlations. The resulting affine model version is an approximation, but accessible to evaluation by inverse transform methods. Checking the validity and the limits of the approximations involved is also within the scope of the presented discussion. In this spirit the thesis is structured in the following fashion:

Chapter 2 sketches in brevity the theoretical basics of affine stochastic processes and selected inverse transform methods. Whenever SDEs adhere to the AJD process class, a general formalism exists to derive the CHF. Knowledge of the CHF is essential to apply inverse transforms. There is a broad variety of valuation techniques based on inverse transforms. However, the discussion refrains to two selected methods which are popular in practice as illustrative paradigms, since the main focus of the thesis rests on the study of affine approximations of the HCV model: The Carr-Madan Fast Fourier Transform (FFT) and the COS expansion techniques. Whenever affine models within the thesis are evaluated by inverse transforms, either of these two methods is applied.

Chapter 3 contains the essential points of the discussion: (i) At first, the affine approximations derived in previous studies for HHW and HLMM are introduced.

(ii) Then, the characteristics of the HCV hybrid model are detailed. The key to prescribe HCV model features is the volatility specification. The HCV features DD characteristics, and is in complexity between HHW and HLMM. Accordingly, the HCV can be viewed as linking element between HHW and HLMM: The HHW is the representative of low-dimensional hybrid models with IR component based on Gaussian short rates. The HLMM qualifies as the paradigm of high-dimensional hybrid models descending from log-normal market models.

(iii) Two affine limits are devised to place the HCV within the AJD process class. In the first affine limit the intial interest rates are *frozen* in the DDSV volatility specification - this affine limit is named H1CV model. The second affine limit is more subtle and retains DD features by *freezing* solely the initial volatility in the affine proxy of the IR component within the DDSV constraints - this approximation is named H2CV. The HCV and the corresponding affine approximations are central issues of the thesis at hand, in particular by virtue of the following points:

- The HCV model features true hybrid smile and skew, meaning that smile and skew traits are resembled in the EQ as well as in the IR component of the hybrid model. The Heston

model shapes the EQ-SV component, and DDSV extensions introduce smile and skew in the IR component.

- H1CV reproduces hybrid smiles excellently. H2CV is capable to represent both hybrid smile and skew.
- The HHW results from the HCV model presuming a constant volatility specification. DD extensions mix Gaussian model characteristics with log-normal contributions typical for the HLMM. Hence, simply by the problem-orientated choice of model parameters, the HCV is capable to assume characteristics either more closely related to the HHW, or to the HLMM, respectively.

(iv) Finally, the affine H1CV and H2CV models are validated with respect to model fidelity - this means in effect, how well the full HCV hybrid model features are retained in the approximations. Model validation is based on derivatives pricing results comparing the full model to the affine versions in the spot measure $\mathbb{Q}^B$ as well as in the terminal measure $\mathbb{Q}^T$.

In chapter 4 the qualities of the HCV model are compared with HHW and HLMM. Here, full models and corresponding affine approximations are actually employed in calibration settings and subsequent hybrid product pricing.

The discussion is concluded in chapter 5 where the basic findings are summarized, and weak points and critical issues are exposed as the inevitable loose ends to be tied up in future studies.

Chapter 2

Affine System and Inverse Transforms

The subsequent sections provide a brief introduction of theoretical prerequisites: The basic concept of an affine SDE system and the general formalism to obtain the corresponding CHF are exposed in section 2.1. Central issue of the thesis at hand is to derive the CHF of particular EQ-IR hybrid models, which are described by a system of correlated SDEs. By means of suitable approximations, the hybrid models under discussion are then placed within the AJD process class. As soon as the CHF is known, the valuation of derivative products by inverse transforms becomes feasible.
In order to illustrate the pricing by inverse transform techniques, the Carr-Madan Fourier Transform is introduced in section 2.3, and the basics of the COS expansion method are subsequently explained in section 2.4. The two methods are selected out of the broader spectrum of inverse transform pricing approaches, mostly because the methods are popular in practice and suitably well understood. The exposition of inverse transform techniques is necessarily brief without the claim for completeness - the details are found in the cited references. The focus of the thesis is on the derivation and discussion of the HCV model and affine approximations (cf. chapter 3); employing Carr-Madan or COS methods to evaluate affine models by inverse transforms is a deliberate as well as convenient choice.

2.1 Characteristic functions of affine processes

The hybrid models under discussion are represented by a system of correlated stochastic processes. Whenever the model system is within the class of affine jump-diffusion (AJD) processes, there exists a general formalism to derive the corresponding CHF [21]. The CHF derivation basically adheres to the following line of argumentation:
Consider an n-dimensional Markovian stochastic process with vector of state variables $\mathbf{X}_t$ on a fixed filtered probability space $(\Omega, \mathcal{F}, \mathbb{Q})$. In differential form

$$d\mathbf{X}_t = \mu(\mathbf{X}_t)dt + \sigma(\mathbf{X}_t)d\mathbf{W}_{\mathbf{x}}(t) \tag{2.1}$$

the model (without jumps) represents the mapping out of some pre-defined subspace $\mathbb{S} \in \mathbb{R} \to \mathbb{R}^n$ by a system of stochastic differential equations (SDE) with drift $\mu(\mathbf{X}_t) : \mathbb{S} \to \mathbb{R}^n$, instantaneous covariance $\Sigma_{\mathbf{X}} = \sigma(\mathbf{X}_t)\sigma^\dagger(\mathbf{X}_t) : \mathbb{S} \to \mathbb{R}^{n\times n}$, and $\mathcal{F}_t$-measurable independent Brownian drivers

$\mathbf{W}_{\mathbf{x}}(t) : \mathbb{S} \times \Omega \to \mathbb{R}^n$, respectively. The model is within the class of AJD processes when drift, instantaneous covariance and associated interest rate component $r(\mathbf{X}_t)$ are representable in the affine form:

$$\begin{aligned} \mu(\mathbf{X}_t) &= a_0 + a_1 \mathbf{X}_t \quad \forall\, (a_0, a_1) \in \mathbb{R}^n \times \mathbb{R}^{n\times n}, && (2.2)\\ \sigma(\mathbf{X}_t)\sigma^\dagger(\mathbf{X}_t) &= (c_0)_{ij} + (c_1)^\dagger_{ij} \mathbf{X}_t \quad \forall\, (c_0, c_1) \in \mathbb{R}^{n\times n} \times \mathbb{R}^{n\times n\times n}, && (2.3)\\ r(\mathbf{X}_t) &= r_0 + r_1^\dagger \mathbf{X}_t \quad \forall\, (r_0, r_1) \in \mathbb{R} \times \mathbb{R}^n. && (2.4) \end{aligned}$$

For an affine model the corresponding discounted CHF under the risk-neutral measure $\mathbb{Q}$ ensues to (cf. [21])

$$\hat{\phi}(\mathbf{u}, \mathbf{X}_t, t, T) = \mathbb{E}^{\mathbb{Q}}[e^{-\int_t^T r_s ds + i\mathbf{u}^\dagger \mathbf{X}_T} | \mathcal{F}_t] = e^{A(\mathbf{u},\tau) + \mathbf{B}^\dagger(\mathbf{u},\tau)\mathbf{X}_t} \tag{2.5}$$

discounted by the time-lag to maturity $\tau = T - t$. The CHF is by definition the Fourier transform of the probability density. For a random process represented by the state variables $\mathbf{X}_t = [x, ...]^\dagger$ and $\mathbf{X}_T = [y, ...]^\dagger$, and with the deliberate choice $\mathbf{u} = [u, 0, ..., 0]^\dagger$, the connection between discounted CHF and density gives us

$$\hat{\phi}(\mathbf{u}, \mathbf{X}_t, t, T) = \int_{-\infty}^{\infty} e^{iuy} \int_t^T e^{\zeta} f_{Y,\zeta}(y, \zeta | x) d\zeta\, dy = \int_{-\infty}^{\infty} \phi_Y(y|x) dy \tag{2.6}$$

with $\zeta = -\int_t^T r_s ds$, and $\phi(\cdot|x)$ the discounted risk-neutral probability density for given x, respectively. Here and throughout the thesis Fourier transforms are denoted by 'hatted' ($\hat{}$) variables.
As shown in [21] the coefficients obey complex-valued ordinary differential equations (ODE) of the following form

$$\begin{aligned} \frac{d}{d\tau} A(\mathbf{u}, \tau) &= -r_0 + \mathbf{B}^\dagger a_0 + \frac{1}{2}\mathbf{B}^\dagger c_0 \mathbf{B}, && (2.7)\\ \frac{d}{d\tau} \mathbf{B}(\mathbf{u}, \tau) &= -r_1 + a_1^\dagger \mathbf{B} + \frac{1}{2}\mathbf{B}^\dagger c_1 \mathbf{B}, && (2.8) \end{aligned}$$

where $\mathbf{B}(\mathbf{u}, \tau)$ is the vector of state variables in Fourier space with a spectrum of wave numbers $\mathbf{u} \in \mathbb{C}^n$, and $A(\mathbf{u}, \tau)$ is the time-lag component, respectively.
With the choice $\mathbf{u} = [u, 0, ..., 0]^\dagger$ (with $u \in \mathbb{R}$) at time $t = T$ the apparent boundary condition is obtained

$$\hat{\phi}(\mathbf{u}, \mathbf{X}_T, t = T, T) = \mathbb{E}^{\mathbb{Q}}[e^{i\mathbf{u}^\dagger \mathbf{X}_T} | \mathcal{F}_T] = e^{iux_T}. \tag{2.9}$$

This boundary condition fixes the set of initial conditions $A(u, 0)$ and $\mathbf{B}(u, 0)$ at $\tau = 0$ of the corresponding first order ODE system, thereby determining the CHF coefficients in equations (2.7), (2.8) above.
The discussion of interest rate processes is often simplified by the choice of an appropriate probability measure. Transformations of probability measure from the risk-neutral spot measure $\mathbb{Q}^B$ to the time T-forward measure $\mathbb{Q}^T \equiv \mathbb{T}$ rely on the dynamics of the zero-coupon bond. Prices of zero-coupon bonds $P(t, T)$ maturing at T are obtained at time t from the affine exponential representation of the CHF shown above by simply setting $\mathbf{u} = \mathbf{0}$:

$$P(t, T) = \hat{\phi}(\mathbf{u} = \mathbf{0}, \mathbf{X}_t, t, T) = e^{A(\mathbf{0},\tau) + \mathbf{B}^\dagger(\mathbf{0},\tau)\mathbf{X}_t} \tag{2.10}$$

This way the zero-bond prices for the various hybrid models discussed in the main thesis chapters are retained.

2.2 Pricing equation and inverse transforms

For a contingency claim on the underlying with value S_t (at time t), the pricing equation is straightforwardly formulated as the risk-neutral expectation

$$V(t,S_t;K) = \mathbb{E}^{\mathbb{Q}}\left[e^{-\int_t^T r_s ds} V(T,S_T;K)|\mathcal{F}_t\right], \tag{2.11}$$

$$\tilde{V}(t,x;k) = \int_{-\infty}^{\infty} \bar{V}(y;k)\phi_Y(y|x)dy, \tag{2.12}$$

of the derivative payoff $V(T,S_T;K)$ at maturity T. An equivalent alternative is the formulation as integral over probability density with the logarithms $k \equiv \ln K$ of the strike, $y \equiv \ln S_T$ of the asset value at expiry T, and $x \equiv \ln S_t$ of the spot asset value, respectively. For a simple call option the payoff then assumes $V(T,S_T) = (S_T - K)^+$, or in alternative formulation $\bar{V}(y;k) = (e^y - e^k)^+$.
Whereas the probability density is rarely known in practice, the CHF as the corresponding Fourier transform is often available. So the intriguing point is to formulate the pricing equation in a form where the CHF is used instead of the integral over probability density, and then to obtain the derivative price by applying the corresponding inverse transform.
This is done in the Carr-Madan method by a Fourier-Laplace transformation of the pricing equation (as shown in section 2.3 below), and by a cosine series expansion in the COS method (as outlined in section 2.4), respectively.
There are many other approaches to engage pricing problems by inverse transforms, promoted for instance in the work of Lewis [9b], Lee [9c], Lipton [22], Attari [23], and Bates [24], respectively. Within the present context the discussion is limited to the Carr-Madan and COS methods. All concrete numerical evaluations of affine models by inverse transforms within the thesis are done using either Carr-Madan or COS techniques.
The selective choice of these two methods is easily motivated: Carr-Madan is one of the first and most popular publications [9a] employing the basic Fourier-Laplace transform for derivative pricing. COS is one of the recent works within the field [5, 6], and exhibits extremely high evaluation performance. Both methods work in log-strike-space and, as a consequence thereof, are capable to price an entire vector of strikes simultaneously [11b]. This is beneficial for the discussion of smile effects, and when used in real-world calibration problems, well suited for the use in an optimization routine. Both methods are efficient, well-behaved in practical problems, and generally accepted in the financial community.

2.3 Fourier-Laplace transform: Carr-Madan pricing

The basic idea of the Carr-Madan method [9a] is to use the Fourier transform

$$\hat{C}(u) = \int_{-\infty}^{\infty} e^{iuk}\tilde{C}(t,x;k)dk \tag{2.13}$$

of the pricing equation of a European call option

$$\tilde{C}(t,x;k) = e^{\alpha k}\int_{-\infty}^{\infty}(e^y - e^k)^+\phi_Y(y|x)dy \tag{2.14}$$

$$\equiv e^{\alpha k}\tilde{V}(t,x;k). \tag{2.15}$$

This is actually the pricing equation exposed in equation (2.12) above, supplemented by an exponential damping factor with parameter α. The damping factor ensures integral convergence.
The original derivations of the Carr-Madan method assume deterministic interest rates. As EQ-IR hybrid models are central to the discussion at hand, we present here an extension towards stochastic interest rate scenarios.
With the Fourier transform of the call option price $\hat{C}(u)$, the actual call price is obtained in the Carr-Madan approach as result of the inverse transformation:

$$\tilde{V}(t,x;k) = \frac{e^{-\alpha k}}{\pi}\mathcal{R}\left[\int_0^{\infty} e^{-iuk}\hat{C}(u)du\right], \tag{2.16}$$

where $\mathcal{R}[\cdot]$ corresponds to the real part of any complex-valued argument. For the Carr-Madan results shown in this thesis, the inverse transform integral is numerically evaluated by the Fast Fourier Transform (FFT) after discretization with the Simpson rule. Numerical accuracy is determined by the number of discretization points N (should be a power of two for FFT performance), the extension of the integration domain (the upper cut-off of the semi-infinite integral), and a judicious choice for the damping parameter α. The typical number of discretization points in the Carr-Madan calculations performed in this thesis range from $N = 2^{12}$ to 2^{16}. The choice of the upper boundary u_{max} is problem-orientated (typical values are $u_{max} > 1000$) and determined in combination with the parameter α; the general constraint is that for given N the Carr-Madan result remains stable up to a pre-set accuracy even when the upper boundary is increased and the corresponding α is slightly varied.
In [9a] the Fourier transform of the call option price $\hat{C}(u)$ is derived explicity as function of the discounted CHF:

$$\hat{C}(u) = \int_{-\infty}^{\infty} dk\, e^{iuk}\int_k^{\infty} dy\, e^{\alpha k}(e^y - e^k)\phi_Y(y|x) \tag{2.17}$$

$$= \int_{-\infty}^{\infty}\phi_Y(y|x)\left(\frac{e^{(\alpha+1+iu)y}}{\alpha+iu} - \frac{e^{\alpha+1+iu}}{\alpha+1+iu}\right)dy \tag{2.18}$$

$$= \frac{\hat{\phi}(u-i(1+\alpha),S_t,t,T)}{\alpha^2+\alpha-u^2+iu(2\alpha+1)}. \tag{2.19}$$

To overcome difficulties in performing the contour path integration in the complex plane, Carr & Madan introduced a parallel shift along the real axis to avoid the discontinuity at the origin (please

refer to the original publication [9a] for details). In order to avoid numerical instability for high option values, in [9a] a modification to the pricing formula is derived in the form

$$\hat{c}(u) = (\hat{\gamma}(u - i\alpha) - \hat{\gamma}(u + i\alpha))/2, \tag{2.20}$$

$$\text{with} \quad \hat{\gamma}(u) = \frac{1}{1+iu} - \frac{1}{iu} - \frac{\hat{\phi}(u - i, S_t, t, T)}{u^2 - iu}, \tag{2.21}$$

in combination with the pricing equation

$$\tilde{V}(t, x; k) = \frac{1}{2\pi \sinh(\alpha k)} \int_{-\infty}^{\infty} \exp(-iuk)\hat{c}(u)du. \tag{2.22}$$

For the derivative payoffs calculated in this thesis, both pricing formulas give equivalent results. The derivations are shown for the particular case of a call option. The corresponding formulations for the put option payoff are obtained by the substitution $\alpha \to -\alpha$. These vanilla payoff types are sufficient for the present discussion, since calibration scenarios are limited to vanilla options on the EQ side, and caplets/floorlets/swaptions on the IR side. Derivative pricing by affine hybrid models is here deliberately restricted to combinations of vanilla instruments with these payoff types.
In the case of a call option the damping parameter α is necessarily positive with an upper limit α_{max} depending on the particular CHF employed. For the practical problems in the present discussion the typical value range of $0.1 \leq \alpha \leq 1.3$ is observed for call payoffs. There is no simple theory for the optimal choice of α. Therefore a 'pseudo-optimal' α_o is determined for each individual hybrid model evaluation problem by the general presumption, that the Carr-Madan result is expected to remain stable for slight variations around this α_o value.

2.4 Fourier series expansion: COS method

The COS method is based on the idea to expand the probability density in the pricing equation into its Fourier-cosine series. The COS method is a viable alternative to the Carr-Madan approach. For the affine hybrid models within this thesis, both COS and Carr-Madan methods are applied to pricing problems; mostly to cross-check results by using two alternative approaches and implementations, but in some instances also to study, whether one method shows superior performance in a particular pricing scenario.
The foundations of the COS method are elaborated in [5, 6], along with the key derivations regarding the application of the COS method to calculate the contingent claim prices with the COS technique for European, American and Bermudan type exercise conditions. Selected results originally derived in [5] are reproduced in the following.
The Fourier-cosine series is capable to represent a function $\phi_1(x)$ supported on a finite interval $\Omega \in [a, b]$ with $a, b \in \mathbb{R}/\{-\infty, +\infty\}$:

$$\phi_1(x) = \lim_{N\to\infty} {\sum_{k=0}^{N-1}}' A_k \cos\left(\frac{x-a}{b-a}k\pi\right) \tag{2.23}$$

$$\text{with} \quad A_k = \tfrac{2}{b-a}\mathcal{R}\left[\hat{\phi}_1\left(\frac{k\pi}{b-a}\right)e^{-i\frac{a}{b-a}k\pi}\right] \tag{2.24}$$

$$\text{and} \quad \hat{\phi}_1(x) = \tfrac{1}{2\pi}\int_a^b e^{ixu}\phi(u)du. \tag{2.25}$$

The modified symbol $\sum'$ indicates, that the initial term in the sum is weighed by $\frac{1}{2}$. The inverse Fourier integral can be well approximated by $\phi_1(x)$ on the truncated domain $\Omega \in [a,b]$ as

$$\hat{\phi}(x) = \tfrac{1}{2\pi}\int_{\mathbb{R}} e^{ixu}\phi(u)du \quad \simeq \quad \hat{\phi}_1(x) = \tfrac{1}{2\pi}\int_{\Omega} e^{ixu}\phi(u)du. \tag{2.26}$$

Such approximative presumptions generally work well with probability densities $\phi(x)$ as underlying functions, as these functions are well-behaved *entire* functions (for clean definitions regarding this terminology pls. cf. [38]) decaying sufficiently rapidly with x moving towards infinity.
As additional approximations of the COS method, the cosine series coefficients are calculated from the CHF based on the untruncated Fourier integral

$$F_k \quad = \quad \tfrac{2}{b-a}\mathcal{R}\left[\hat{\phi}\left(\frac{k\pi}{b-a}\right)e^{-i\frac{k\pi}{b-a}a}\right] \simeq A_k, \tag{2.27}$$

and the cosine series are cut-off at a finite (usually small) $N = N_{max}$. For typical pricing problems within this thesis $N_{max} = 2^8$ is used.
These are specifics of the COS method required as prerequisite to evaluate derivative payoffs within the affine hybrid models studied in the next chapters.
In general, the time-t value $V(t,S_t)$ of a contingent claim with strike K on the underlying asset S_t with European exercise condition at expiry T is obtained as conditional expectation in the risk-neutral measure

$$\begin{aligned} V(t,S_t) \quad &= \quad \mathbb{E}^{\mathbb{Q}}\left[e^{-\int_t^T r_s ds}V(T,S_T)|\mathcal{F}_t\right] = \int_{\Omega} V(T,y)e^{\zeta}\phi_{Y,\zeta}(y,\zeta|x)dy, \\ \text{with} \qquad & \zeta = -\int_t^T r_s ds, \\ \text{and} \qquad & x \equiv \ln(S_0/K), \quad y \equiv \ln(S_T/K), \end{aligned} \tag{2.28}$$

where S_T corresponds to the asset price at maturity. This is actually a slightly adapted version of the pricing equation introduced in equation (2.12) above. The particular choices $\mathbf{u} = [u,0,...,0]^{\dagger}$ and $\mathbf{X}_T = [y,...]^{\dagger}$ lead to

$$\begin{aligned} \hat{\phi}(u,\mathbf{X}_t,t,T) \quad &= \quad \mathbb{E}^{\mathbb{Q}}[e^{\zeta+i\mathbf{u}^{\dagger}\mathbf{X}_T}] \\ &= \quad \int_t^T d\zeta \int_{\Omega} e^{\zeta+iuy}\phi_{Y,\zeta}(y,\zeta|x)dy \equiv \int_{\Omega} e^{iuy}\psi_Y(y|x)dy, \end{aligned} \tag{2.29}$$

for the discounted CHF. According to [5] the conditional expectation is represented via cosine expansions as follows,

$$\psi_Y(y|x) \quad = \quad \sum_{k=0}^{N-1}{}' A_k(x)\cos\left(\frac{y-a}{b-a}k\pi\right), \tag{2.30}$$

$$\text{with} \quad A_k(x) \quad = \quad \tfrac{2}{b-a}\int_a^b \psi_Y(y|x)\cos\left(\frac{y-a}{b-a}k\pi\right)dy = \tfrac{2}{b-a}\mathcal{R}\left[\hat{\psi}\left(\frac{k\pi}{b-a}\right)e^{-i\frac{a}{b-a}k\pi}\right],$$

and the derivative value is given by

$$\begin{aligned} V(x,t) &= \tfrac{b-a}{2}\sum_{k=0}^{N-1}{}'A_k(x)V_k, \qquad (2.31)\\ \text{with} \quad V_k &= \tfrac{2}{b-a}\int_a^b V(T,y)\cos\left(\frac{y-a}{b-a}k\pi\right)dy. \end{aligned}$$

For the specific case of a European call payoff the COS pricing equation finally results in the following explicit form [5]:

$$\begin{aligned} V_k^{call} &= \tfrac{2}{b-a}\int_0^b (e^y-1)K\cos\left(\frac{y-a}{b-a}k\pi\right)dy = \tfrac{2}{b-a}K(\chi_k(0,b)-\psi_k(0,b)), \qquad (2.32)\\ &\text{with}\\ \chi_k(c,d) &= \frac{1}{1+(\frac{k\pi}{b-a})^2}\left[\cos\left(\tfrac{d-a}{b-a}k\pi\right)e^d - \cos\left(\tfrac{c-a}{b-a}k\pi\right)e^c\right]\\ &+ \tfrac{k\pi}{b-a}\sin\left(\tfrac{d-a}{b-a}k\pi\right)e^d - \tfrac{k\pi}{b-a}\sin\left(\tfrac{c-a}{b-a}k\pi\right) \qquad (2.33)\\ &\text{and}\\ k\neq 0: \quad \psi_k(c,d) &= \tfrac{b-a}{k\pi}\left[\sin\left(\tfrac{d-a}{b-a}k\pi\right) - \sin\left(\tfrac{c-a}{b-a}k\pi\right)\right], \qquad (2.34)\\ k=0: \quad \psi_k(c,d) &= d-c. \end{aligned}$$

An analogous derivation leads to the explicit expressions for put options (cf. [5] for details).

Chapter 3

Full-Scale Hybrid Models

3.1 The Problem: Hybrid Evaluation by Inverse Transforms

The discussion at hand focuses on hybrid models comprised by EQ and IR asset class components. Such kind of hybrid models exist in various degrees of sophistication. Financial models strive to reproduce characteristic features observable in real world markets. A feature is observable in case it is relevant to the pricing of financial instruments. When equating sophistication with the number of individual features the model incorporates quantitatively in high fidelity, more sophisticated models are comprised by a higher number of underlying stochastic processes. Higher dimensionality corresponds to higher complexity, especially when the model components are likewisely correlated. Within the present context hybrid models containing EQ-IR correlation are denoted as full-scale models.

For the hybrid models under discussion, the highest level of complexity is defined by models where implied smile and skew of market quotes are represented individually in the equity (EQ) as well as the interest rate (IR) parts, and both model components are correlated. On the EQ side, the focus rests on the Heston stochastic volatility (SV) model where the corresponding characteristic function (CHF) is well known. On the IR side, various models are linked: A straightforward approach is to use 1D short-rate models, though Hull-White based short rate models show deficits to incorporate *smiles and skews* in the IR component. On the highest complexity level the IR side is represented by Libor market models (LMM). The concepts of local and displaced-diffusion stochastic volatility (DDSV) as extension of the standard LMM [32, 33] are capable to capture an IR skew and smile observed in the market. LMMs are by design of the drift term high-dimensional, non-Markovian and non-affine, rendering the application of inverse transform methods impossible without restrictive approximation assumptions.

Application of Fourier methods relies on the CHF to be representable at least in semi-closed form. With increasing sophistication of the hybrid model at hand, the approximations necessary to obtain the CHF become progressively more involved.

The following three sections contain the foundations and central derivations of the thesis. In section 3.2 the Heston Hull-White (HHW) model as the most simple hybrid model under consideration is

introduced. The HHW model interlinks implied volatility smile features in the Heston EQ component ('equity smiles') with a 1D short rate process on the IR side. The essentials of the Heston, HW and HHW models are exposed together with the derivation of the corresponding CHFs. Details of the CHF calculation are explicitly shown in the referenced appendices. The approximations of non-affine terms in the HHW are described following the work in [1, 2, 3]. The CHF derivations of the basic processes contain the techniques and pertinent details applied in the subsequent CHF calculation of the more complex hybrid models.

Section 3.3 describes an implementation of the Heston DDSV LMM (HLMM) model and the corresponding affine approximation as originally derived in [4]. The HLMM is capable to represent smile and skew in the IR component. In combination with the Heston model, the smile effects in EQ and IR are linked, and hence, the HLMM can reproduce *hybrid smiles*. The HLMM is the most complex model under consideration and severe approximations are required to obtain an affine version of the HLMM.

In section 3.4 the concept of the Heston DDSV Cheyette (HCV) model is introduced. The HCV model is an attempt to bridge between the practical feasibility of SV short rate approaches and the complexity of DDSV LMMs. We intend to substantiate the idea of coupling the Heston SV model for EQ and a low-dimensional Markovian IR process (with displaced-diffusion SV extensions) in the HCV model. The HCV model can represent IR skew and smile effects in hybrid derivatives. Hence, the HCV can represent hybrid smiles, while being less complex than the HLMM. By virtue of approximations the HCV is placed within the AJD process class. Affine HCV approximations are evaluable by inverse transform methods.

3.2 Heston Hull-White Model (HHW)

The Heston Hull-White (HHW) model combines the Heston model in equity (EQ)

$$dS_t = r_t S_t dt + \sqrt{v_t} S_t dW_x(t), \tag{3.1}$$

$$dv_t = \kappa(\bar{v} - v_t)dt + \gamma\sqrt{v_t} dW_v(t), \tag{3.2}$$

with a classical Hull-White (HW) mean reversion process on the interest rate (IR) side

$$dr_t = \lambda(\theta(t) - r_t)dt + \eta dW_r(t). \tag{3.3}$$

In this section the basic facts about the HHW hybrid model are summarized; this also encompasses both constituent processes, the Heston model for the EQ, and the HW model to represent the IR component, respectively. Heston and HW models are both well-studied and discussed in a variety of original publications. Therefore, the summary here is very selective with one pervasive motivation: To show how the CHFs corresponding to these models are derived, and whenever applicable, to explain, which approximations are devised to make the models affine. All CHF derivations are included; however, the complete derivations are deferred to appendices to keep the recapitulation of previous work and basic findings concise within this section. In the following only particular

aspects of the derivations in the appendices are highlighted, as these results are important for the later discussion. We start with the summary of basic facts and model acronyms conventionally used throughout the thesis:

(i) Heston EQ-SV model:

The Heston model [8] assumes a SV process for EQ prices S_t ($x_t = \log S_t$) and mean-reverting dynamics for the stochastic variance process v_t. The corresponding Brownian drivers are related by the EQ-SV correlation coefficient $\rho_{xv}dt = dW_x dW_v$. All Heston process variables are described in detail in Appendix A.1. The CHF of the Heston process is also derived in Appendix A.1 following the method of [21]. The Heston process in log-space is already affine, and therefore the CHF is obtainable without any approximations. When calculating the CHF according to [21], each equation of the underlying SDE system transfers to one Fourier coefficient (as solution of one first order ordinary differential equation as elaborated in section 2.1 above). According to the derivations in Appendix A.1 the EQ-SV process (represented by v_t) relates to the Fourier coefficient $D(u,\tau)$ in the Heston CHF as

$$\hat{\Phi}_H(u, \mathbf{X}_t, t, T) = e^{A(u,\tau)+B(u,\tau)x_t+D(u,\tau)v_t}. \tag{3.4}$$

$D(u,\tau)$ is obtained in closed form as solution to an analytically solvable Riccati differential equation (for the explicit form of $D(u,\tau)$ please see Appendix A.1, equation A.12). The Riccati equation has an analytic solution whenever the coefficients are at least piece-wise constant. The Fourier coefficient $D(u,\tau)$ persists in the CHF solution of all hybrid models in this thesis where an Heston EQ-SV model is involved. The mathematical form of $D(u,\tau)$ remains the same, irrespective of whether the models are derived in the spot measure $\mathbb{Q}^B$ or the terminal measure $\mathbb{Q}^T$ (this fact will be elaborated for the hybrid models in several sections below, and becames evident by comparison of the explicit derivations shown in Appendices B and C, where hybrid models are derived unter $\mathbb{Q}^B$ as well as $\mathbb{Q}^T$, respectively). Please note that the statement is entirely true only when the EQ-SV and IR process are not correlated (corresponding to $\rho_{vr} = 0$, which is presumed for all the discussions within this thesis). This quality of the SV process on the EQ side is distinct from the SV process on the IR side of hybrid models. As shown in section 3.5.1 (the HCV model under $\mathbb{Q}^B$) and section 3.5.2 (the HCV model under $\mathbb{Q}^T$) the mathematical representation of the IR-SV process is susceptive to changes of measure. The pure Heston model results as limiting case whenever the hybrid models under discussion are considered in a parameter limit where stochastic IRs become deterministic. All numerical implementations of hybrid models employed in the present context are validated in the Heston limit against the Heston parameter sets listed in Appendix D.1). The model test sets encompass cases where the Feller condition $\gamma^2 < 2\kappa\bar{v}$ is violated (i.e. the stochastic variance process can become zero *a.s.*), as is observed in realistic calibration scenarios.

(ii) HW IR model:

The HW process serves as paradigm for Gaussian short rate models and is well-studied in the

literature. Details of the HW process are introduced in Appendix A.2. The HW IR model is already affine, and hence, the corresponding CHF is derivable without approximations as shown in Appendices A.2.1 and A.2.2. For the HW model the prices of zero bonds and certain European contingent claims (i.e. IR caplets) exist in analytic form (cf. Appendix A.3.2). The analytic values of HW zero bond and caplet prices serve as cross-check for all numerical implementations of hybrid models in this thesis. Furthermore, the numerical HW model implementations are cross-checked with literature results for a selected model test set (cf. Appendix D.2). The HW model is the limiting case of the Cheyette model for constant volatility specification $\eta_t \to \eta$. The connection between the HW and Cheyette model is detailed in Appendix A.3.1.1. This connection is also used in consistency checks throughout the thesis.

(iii) 3F-HHW ('Three-Factor-HHW') model:
In the HHW SDE system with Brownian drivers for EQ (W_x), SV (W_v), and IR (W_r), three different likewise correlations are possible: EQ-SV ρ_{xv}, EQ-IR ρ_{xr}, and IR-SV ρ_{rv} correlation (here IR-SV denotes the relation between the IR process and the SV process of the EQ component), respectively. When the full set of all three correlation factors is non-zero, the system is called the 3F-HHW model. The 3F-HHW model is not within the class of Affine-Jump-Diffusion (AJD) processes. Therefore the CHF corresponding to the 3F-HHW model is unknown.

(iv) *Full-scale* hybrid model and the *full-scale* HHW model:
The crucial point for the hybrid models under discussion is the non-vanishing EQ-IR correlation ($\rho_{xr} \neq 0$). This correlation determines the coupling between the EQ and IR asset classes. All hybrid models in this thesis have the Heston ansatz with non-vanishing EQ-SV correlation ($\rho_{xv} \neq 0$) as the EQ component. In combination with non-vanishing EQ-IR correlation $\rho_{xr} \neq 0$ we call this a *full-scale* hybrid model, since the stochastic processes on the EQ side and the IR side of the hybrid model are coupled.
It should be noted that the *full-scale* hybrid model is not necessarily capable to represent *hybrid smiles*. *Hybrid smiles* imply that the model features smile/skew effects in the EQ as well as the IR component. Whereas the Heston model introduces smile/skew effects on the EQ side, the HW model cannot reproduce smile effects and shows only the skew inherent to Gaussian models on the IR side. In the later sections we introduce hybrid models with a SV process on the IR side in order to capture IR smiles and skew. In combination with the Heston EQ component, such models then feature *hybrid smiles*.
Throughout the thesis we deliberately neglect the correlation between the IR side and the SV process on the EQ side ($\rho_{rv} \equiv 0$), and hence, strictly speaking we consider a 2F-HHW model. Both 2F-HHW and 3F-HHW models are non-affine, and within the present context both are denoted as *full-scale* hybrid models. This denotation is adopted for all models derived in this thesis. Whenever the EQ-IR correlation is non-zero, we speak of a *full-scale* hybrid model. Presuming $\rho_{rv} \equiv 0$ in the HHW model is simply out of convenience; as shown in [1] the methods devised to make the 2F-HHW model affine are straightforwardly extended towards

the 3F-HHW model. The construction of approximations to place *full-scale* hybrid models within the AJD process class and derive the corresponding CHF is the central motivation of this thesis. In section 3.2.1 below, we introduce the affine approximations devised in [1] to make the 2F-HHW and 3F-HHW models affine. The 2F-/3F-HHW concepts are capable to capture implied volatility smile and skew effects in the EQ component, and to incorporate certain peculiarities of a realistic interest rate term structure for EQ derivative contracts with long time to maturity [10a].

(v) 1F-HHW ('One-Factor-HHW') model - the 'uncorrelated' HHW model:
When Heston EQ-SV and HW IR components are combined into a hybrid model, but remain uncorrelated ($\rho_{xr} \to 0$), the 1F-HHW model results. Negligible EQ-IR correlation is the decisive difference with respect to a full-scale hybrid model. The 1F-HHW still retains the affine characteristics of the constituent processes and the CHF is analytically derivable in closed form, as detailed in Appendix B.1:

$$\hat{\Phi}_{1F-HHW}(u, x_t, v_t, r_t, T, t) = e^{A_{1F}(u,\tau)+B(u,\tau)x_t+D(u,\tau)v_t+C(u,\tau)r_t} \tag{3.5}$$

Explicit solutions and interpretation of the Fourier coefficients $A_{1F}(u,\tau)$, $B(u,\tau)$, $C(u,\tau)$ and $D(u,\tau)$ are deferred towards Appendix B.1 (and relevent cross references therein). The CHF is reiterated here to emphasize the point that the CHF corresponding to the affine approximations of the 1F-/2F-/3F-HHW model differ solely in the functions $A_{1F}(u,\tau)/A_{2F}(u,\tau)/A_{3F}(u,\tau)$, respectively; the effect of non-vanishing EQ-IR correlation ρ_{xr} is included in this Fourier coefficient.
The 1F-HHW serves as paradigm for the derivation of the CHF of EQ-SV IR hybrid models. The CHF is the analytic reference case for all hybrid model implementations in the limit $\rho_{xr} \to 0$. For the 1F-HHW model analytic pricing formulas exist for European contingent claims in equity. Call option prices within the 1F-HHW framework are derived in Appendix B.1.2 and are applied to model validation throughout the discussion.

3.2.1 Affine Heston Hull-White (H1HW)

Affine model approximations are based on the idea to project non-affine model components on deterministic functions. In [1] the problem of the CHF for the *full-scale* Heston Hull White (= HHW with full set of correlations, in particular including the essential 'hybrid' connection between EQ und IR components by assuming non-vanishing ρ_{rx}) is addressed. The instantaneous covariance

matrix of the HHW model (associated with the SDE system shown in equations (3.1) to (3.3))

$$\begin{aligned}
\Sigma_{\mathbf{X}_t} &= \begin{pmatrix} v_t & \rho_{xv}\gamma v_t & \rho_{xr}\eta\sqrt{v_t} \\ \rho_{vx}\gamma v_t & \gamma^2 v_t & \rho_{vr}\gamma\eta\sqrt{v_t} \\ \rho_{rx}\eta\sqrt{v_t} & \rho_{rv}\gamma\eta\sqrt{v_t} & \eta^2 \end{pmatrix} \\
&= L_{\mathbf{X}_t} L_{\mathbf{X}_t}^{\dagger}, \\
\text{with} \quad L_{\mathbf{X}_t} &= \begin{pmatrix} \sqrt{v_t} & 0 & 0 \\ \rho_{vx}\gamma\sqrt{v_t} & L_{xv}\gamma\sqrt{v_t} & 0 \\ \rho_{rx}\eta & L_{rv}\eta & L_{rx}\eta \end{pmatrix}, \\
\text{and} \quad & L_{xv} = \sqrt{1-\rho_{xv}^2},\ L_{rv} = (\rho_{rv} - \rho_{rx}\rho_{xv})/L_{xv},\ L_{rx} = \sqrt{1-\rho_{rx}^2 - L_{rv}^2},
\end{aligned} \tag{3.6}$$

contains non-linear terms $\Sigma_{1,3} = \Sigma_{3,1}$ and $\Sigma_{2,3} = \Sigma_{3,2}$ in the state variable $\sqrt{v_t}$. $L_{\mathbf{X}_t}$ is the Cholesky decomposition of the covariance matrix to express the HHW process in differential form by uncorrelated Brownian drivers,

$$\begin{pmatrix} dx_t \\ dv_t \\ dr_t \end{pmatrix} = \mu(\mathbf{X}_t)dt + L_{\mathbf{X}_t} \begin{pmatrix} d\tilde{W}_x(t) \\ d\tilde{W}_v(t) \\ d\tilde{W}_r(t) \end{pmatrix}. \tag{3.7}$$

The HHW model is placed within the class of AJD models by approximating the non-affine terms $\sqrt{v_t}$ in the covariance matrix with its corresponding expectation value:

$$\sqrt{v_t} \simeq \mathbb{E}[\sqrt{v_t}]. \tag{3.8}$$

Though $\mathbb{E}[\sqrt{v_t}]$ is known analytically in closed form for CIR-type processes [30a], the expressions involve infinite sums of Γ functions and are therefore somewhat tedious to handle in computational approaches. In order to improve the computational tractability and efficiency, [1] introduces a projection of the expection onto a deterministic function

$$\mathbb{E}[\sqrt{v_t}] \simeq a + be^{-ct} \equiv \delta_v(t), \tag{3.9}$$

with constant model specific parameters a, b and c. For the original definition of these parameters pls. cf. [1] (in particular section 3.1 therein); details of the projection technique are given in section 3.5.1 below, where the applicability is extended towards the Heston Cheyette and Heston DDSV Cheyette models.

The full-scale HHW model with deterministic approximation of non-affine terms is referenced as H1HW (the acronym is from [1]) and is within the AJD model class since the covariance matrix takes the form:

$$\Sigma_{\mathbf{X}_t} = \begin{pmatrix} v_t & \rho_{xv}\gamma v_t & \rho_{xr}\eta\delta_v(t) \\ \rho_{vx}\gamma v_t & \gamma^2 v_t & \rho_{vr}\gamma\eta\delta_v(t) \\ \rho_{rx}\eta\delta_v(t) & \rho_{rv}\gamma\eta\delta_v(t) & \eta^2 \end{pmatrix}. \tag{3.10}$$

For simplicity we presume $\rho_{rv} = 0$ for the moment, but as shown in [1] the entire argumentation holds for non-vanishing ρ_{rv} equally well. Derivation and solution of the defining ODEs for CHF Fourier coefficients are completely analogous to the 1F-HHW case elaborated in Appendix B.1. The Fourier coefficients $B(u,\tau), D(u,\tau), C(u,\tau)$ are equivalent to the 1F-HHW case, the sole deviation is an additional term in

$$A_{H1HW}(u,\tau) = A_{1F-HHW}(u,\tau) + \rho_{rx}\eta \int_0^\tau \delta_v(T-\tau)B(u,\tau)C(u,\tau)\,d\tau, \tag{3.11}$$

with solution

$$\begin{aligned}
&\rho_{rx}\eta \int_0^T \delta_v(T-\tau)B(u,\tau)C(u,\tau)\,d\tau = iu(iu-1)\tfrac{\rho_{xr}\eta}{\lambda} \\
&\quad \left[-\tfrac{b}{c}e^{-cT}(1-e^{c\tau}) + a\tau - \tfrac{a}{\lambda}(1-e^{-\lambda\tau}) + \tfrac{b}{c-\lambda}(1-e^{-\tau(\lambda-c)})\right] \\
&= \rho_{rx}\eta I_4(u,\tau). \qquad (3.12)
\end{aligned}$$

Apparently the additional term is a pure function of u, and hence, the zero coupon bond value remains unaffected by ρ_{xr}. Consequently, the zero bond values for the single correlation 1F-HHW model and full-scale HHW model are equivalent (!).
Finally, with $A_{H1HW}(u,\tau)$ of equation (3.8) the CHF of the H1HW results in canonical fashion, i.e.

$$\hat{\Phi}_{H1HW}(u,x_t,v_t,r_t,t,T) = e^{A_{H1HW}(u,\tau)+B(u,\tau)x_t+D(u,\tau)v_t+C(u,\tau)r_t}, \qquad (3.13)$$

where the Fourier coefficients $B(u,\tau)$, $C(u,\tau)$ and $D(u,\tau)$ are described in detail in Appendix B.1. With affine hybrid model versions H1HW and the corresponding CHFs available, derivatives pricing with these models is accessible to inverse transform and direct integration techniques (at least for those kinds of derivatives which are in general evaluable by inverse transform methods). In general the results obtained in the spot and terminal measures are equivalent, albeit numerical errors are susceptive to the particular choice of measure. The relation between numerical error characteristics and choice of measure is detailed later in the discussion of the affine versions of the Heston DDSV Cheyette model.

3.3 Smiles in Equity and Interest Rate

3.3.1 Displaced-Diffusion Stochastic Volatility Libor Market Model

Hybrid models can be constructed with various different IR components. In the previous sections the IR component was defined by the HW model. The HW model is based on a 1D short-rate process with inherent limitations: For instance, the HW model is a Gaussian model showing inherently large skew features in IR implied volatilities. Furthermore, as 1D model the HW approach is incapable to represent IR derivatives depending on the evolution of more than a single forward rate, like i.e. CMS spread products which are based on the difference of forward rates with different tenor structure. In order to resolve such insufficiencies, market models were devised within the HJM framework. When the market model is based on Libor forward rates, the Libor Market Model (LMM) results as fundamentally different ansatz compared to the HW short-rate process previously discussed. The LMM is inherently high-dimensional, since for a given set of maturities $\mathcal{T} = \{T\}_k = \{T_0, T_1, T_2, ..., T_N\}$ each maturity is represented by one individual stochastic process for the corresponding Libor rate $L(t, T_{k-1}, T_k) = L_k(t)$ (with each Libor forward rate based on the tenor structure $\tau_k = T_k - T_{k-1}$). When presuming the Libor rates to be log-normally distributed, the implied volatilities associated with IR products modeled with the LMM are flat. In the original LMM model IR smile and skew features are absent.
In the following we discuss an extension of the LMM as IR component of hybrid models. The

extended LMM model is denoted as the Displaced-Diffusion (DD) Stochastic Volatility (SV) Libor Market Model (LMM). The DDSV LMM is capable to reproduce smile and skew features observed in the implied volatility surface derived from the interest rate market. IR skew features are introduced by the DD concept. IR smile is controlled by a correlated IR stochastic volatility (IR-SV) process, analogous to the EQ-SV process in the Heston model on the EQ side of the hybrid model.
In [31] the stochastic process driving each of the Libor forward rates,

$$dL_k(t) = \sigma_k(t)(\mu_k(t)dt + dW_k(t)), \tag{3.14}$$

was generalized towards a DD volatility specification of functional form

$$\sigma_k(t) \quad = \quad s_k(t)\Phi_k(t, L_k(t)). \tag{3.15}$$

This is the DD LMM where the overall stochastic volatility level in model characteristics is determined by the value of $s_k(t)$. The DD ansatz [32, 33] is based on the idea to mix normal and log-normal behaviour in the stochastic processes underlying the Libor rate evolution, thereby controlling the skew of implied IR volatilities with

$$\Phi_k(t, L_k(t)) \quad = \quad b_k(t)L_k(t) + (1 - b_k(t))L_k(0). \tag{3.16}$$

Therein $0 \leq b_k(t) \leq 1$ controls the mixture between log-normal and normal model contributions. IR skew and smile were successively introduced as amendments to the standard Libor Market Model (LMM). Then [32, 33] further augmented the DD LMM by a stochastic variance process z_t to establish the full DDSV LMM concept:

$$dL_k(t) \quad = \quad s_k(t)\Phi_k(L_k(t), t)\sqrt{z_t}(\sqrt{z_t}\mu_k(t)dt + dW_k(t)), \tag{3.17}$$

$$\text{with IR} - \text{SV process}$$

$$dz_t \quad = \quad \beta(\bar{z} - z_t)dt + \epsilon\sqrt{z_t}dW_z(t), \tag{3.18}$$

$$\text{and correlations}$$

$$dW_k dW_z \quad = \quad \rho_{kz}dt \quad \text{and} \quad dW_i dW_k = \rho_{ik}dt. \tag{3.19}$$

The IR-SV process is of Cox-Ingersoll-Ross (CIR) type like the EQ-SV equivalent in the Heston process, with mean-reversion rate β, mean-reversion level $\bar{z}$ (conventionally to be set to $\bar{z} = z_0 = 1$, since the overall IR-SV level is already adjustable via the choice of s_k), and volatility ϵ of the IR variance process, respectively.
In general, all aforementioned DDSV model parameters are time-dependent. However, the focus of the discussion at hand relies on affine model approximations accessible to evaluation by inverse transforms. Therefore the DDSV parameters s_k and b_k are presumed to remain constant as one of the approximations necessary to derive an affine version of the DDSV LMM.
Assuming simple compounding the tenor structure $\tau_k = T_k - T_{k-1}$ defines the connection between the Libor rates $L_k(t) = L(t, T_{k-1}, T_k)$, and the zero (coupon) bond $P(t, T_k) = P_{m(t)}(t)$ value, as

$$\frac{P(t, T_k)}{P(t, T_{k-1})} = \frac{1}{1 + \tau_k L_k(t)}, \tag{3.20}$$

with $m(t) = min(k : t \leq T_k)$. The choice of measure determines the drift term and numeraire corresponding to each Libor rate process. Conventional choices are the spot Libor (SM) measure $\mathbb{Q}^B$ (where the Libor process corresponding to the instantaneous forward rate at the respective moment is a martingale, and the numeraire is the rolling over bank account described by $dB_t = L_{m(t)}(t)B_t dt$ and $B_0 = 1$), or, alternatively, the $T^N \equiv \mathbb{Q}^T$ forward or terminal (TM) measure (where the terminal Libor rate at maturity T_{N+1} is a martingale, and all other Libor processes are transformed into this particular measure $\mathbb{Q}^T$). Then, drift and numeraire assume the following explicit form:

Measure	Drift	Numeraire
T^N-Fwd (TM) $\mathbb{Q}^T$	$\mu_k(t) = -\sum_{i=k+1}^{N} \frac{\tau_i s_i \Phi_i(t,L_i(t))}{1+\tau_i L_i(t)} \rho_{ik}$	$P(t,T_N) = \frac{P_{m(t)}(t)}{\prod_{i=m(t)+1}^{N} 1+\tau_i L(t,T_{i-1},T_i)}$
Spot Libor (SM) $\mathbb{Q}^B$	$\mu_k(t) = \sum_{i=m(t)}^{k} \frac{\tau_i s_i \Phi_i(t,L_i(t))}{1+\tau_i L_i(t)} \rho_{ik}$	$B(t) = P_{m(t)}(t) \prod_{i=1}^{m(t)} 1 + \tau_i L(t,T_{i-1},T_i)$

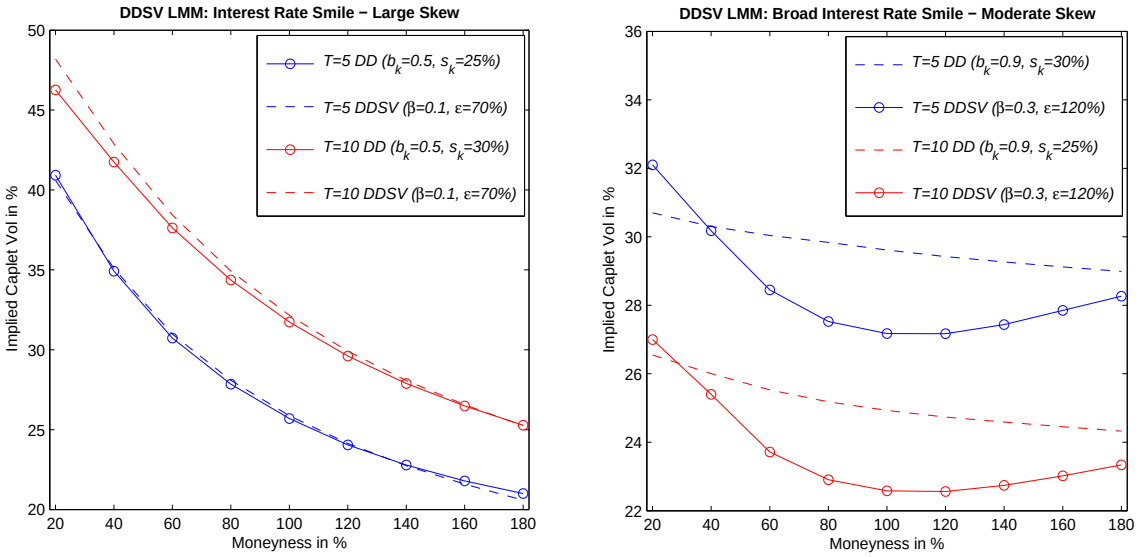

Figure 3.1: Comparison of Interest Rate (IR) smiles and IR skews observed in Monte-Carlo simulations of the DDSV LMM model. The overall implied volatility level is determined by the choice of s_k. Left: IR-SV scenario where normal and log-normal DD IR contributions have equal weight ($b_k = 0.5$). Data show in blue corresponds to maturity $T = 5$ and $s_k = 25\%$; data plotted in red is obtained at $T = 10$ and with $s_k = 30\%$. With Gaussian model contributions present, implied caplet volatilites show a significant skew. The solid lines correspond to the DD LMM case where the IR-SV process is absent. Overlayed in broken lines are the implied volatilities in the case IR-SV contributions are introduced ($\beta = 0.1$, $\epsilon = 70\,\%$). Right: The influence of short rate skew features diminuishes in the limit $b_k \to 1$ corresponding to the log-normal case, DD LMM model results shown as broken lines). Distinct IR-SV features are observed for IR-SV volatility assuming huge values of $\epsilon = 120\,\%$ (solid lines). For demonstration purposes the overall volatility level determined by s_k is permuted compared to the left part of the figure. $T = 5$ is the blue data with $s_k = 30\%$; data plotted in red is obtained for $T = 10$ with $s_k = 25\%$.

In Fig. 3.1 the impacts of DD and SV contributions on caplet implied volatilities are illustrated both as individual effects and in combination. Solid lines show implied volatility effects solely as result of DD contributions. The DD contributions plotted as solid lines are isolated in the limit $z_t \to \bar{z}$=1 (resulting from the choices $\beta \to 0$ or $\beta \gg 1$, and $\epsilon \to 0$), where modifications by the IR-SV process become negligible. This corresponds to the DD LMM model case. Here the base skew is disclosed by simulations without stochastic variance contributions. By tuning the DD parameter b_k, the relative weight of normal and log-normal components in the DDSV LMM is adjusted. The pure LMM case corresponds to b_k=1 with flat implied volatilities; the Gaussian model case is obtained in the limit $b_k \to 0$. In general the increase of Gaussian normal contributions is associated with pronounced skew features. Results are shown for $T = 5$ (blue) and $T = 10$ (red) years to maturity, initially presuming a flat forward curve at $L_k(0) = 5\%$ p.a. level for all initial Libor rates. The overall volatility level is determined by the choice of s_k in the DDSV LMM model. Implied caplet volatilities are obtained for $s_k = 25\%$ and $s_k = 30\%$ in both plots of Fig. 3.1 (in the left part $s_k = 25\%$ corresponds to maturity $T = 5$, in the right part results at maturity $T = 10$ are demonstratively shown for $s_k = 25\%$). In the left part of Fig. 3.1 a comparatively large base skew is generated by the skew parameter $b_k = 0.5$ (as b_k controls the mixture of log-normal and normal components of the LMM). Whether the IR smile is significant is controlled by mean-reversion rate β and volatiliy ϵ of the IR stochastic variance process; in the left panel $\beta = 0.1$ and $\epsilon = 70\%$ give rise to base skew with smile features. When calibrating to market data, ϵ values are usually below 50% - this already indicates the fact that IR smile contributions in realistic data of hybrid products are generally of course much smaller than EQ smile effects. In order to emphasize IR smile effects, the smile features are prominent for demonstration purposes in the right part of Fig. 3.1 by choosing small mean-reversion $\beta = 0.3$ and large volatility $\epsilon = 120\%$ in the IR-SV process. Here the base skew becomes much less prominent by the choice $b_k = 0.9$; then Libor rates are assumed to evolve 'quasi'-lognormal.

3.3.2 Heston DDSV Libor Market Model (HLMM)

By combining the DDSV LMM concept as IR component with the standard Heston process as EQ component, the Heston DDSV LMM (referenced by the acronym HLMM) hybrid model is constructed. The HLMM is a hybrid model by our conventional denotations used throughout the thesis: The entire discussion of HLMM results is based on the full-scale HLMM hybrid model with non-vanishing EQ-IR correlations (this means in effect, that the correlations between Heston EQ component and Libor rates are in general non-zero $\rho_{xk} \neq 0 \,\forall\, k$). Furthermore the HLMM features *hybrid smiles*: The Heston EQ component can represent EQ smile and skew effects, the DDSV LMM is capable to generate IR smile and skew observed in the IR markets, and EQ and IR smiles are likewisely correlated in the full-scale model.

In the numerical implementation as basis of the present discussion, the spot rate r_t in the Heston component is obtained as instantaneous Libor rate $r_t = L_{m(t)}(t)$ without any further interpolation.

The H1LMM as the affine approximation of the HLMM

In general, LMM models are due to the drift term strongly path-dependent, and consequently the DDSV LMM model is non-Markovian and non-affine. In [4] several approximations are imposed in order to render the HLMM SDE system in affine form. Particularly the Libor rates $L_k(t)$ are *frozen* to the initial value $L_k(0)$. This removes the path-dependency in the drift term arising from the sum over the Libor rates. The non-affine terms from the IR-SV process (see equation (3.15)) are approximated by assuming $z_t \simeq E[z_t] = \delta_z(t)$ in analogy to the approximations discussed in [1] (cf. section 3.2.1 above for H1CH/H1HW model approximations originally devised in [1]). In [4] all non-affine terms are rigorously linearized by adopting and extending the ideas published in [1]; for instance, EQ-SV and IR-SV processes are assumed to evolve independently and can be projected onto the corresponding expectations like $\sqrt{v_t}\sqrt{z_t} \simeq E[\sqrt{v_t}\sqrt{z_t}] \simeq E[\sqrt{v_t}]E[\sqrt{z_t}]$. Thereby the affine version of the HLMM SDE system in the terminal measure $\mathbb{Q}^T$ (referenced by the acronym H1LMM in the following) is placed within the AJD process class.
Details of the H1LMM derivation are found in the original publication [4]. In the following sections the full-scale HLMM model is implemented employing Monte-Carlo schemes, and the Carr-Madan and COS methods are prepared to price within the affine version H1LMM. These implementations are benchmarked for selected simulation parameters and derivative products. Particular traits of the Monte-Carlo implementation are exposed briefly below.

Benchmarking HLMM/H1LMM implementations

In order to validate the Heston DDSV LMM model implementations, the results obtained by Monte-Carlo (MC) simulation and inverse transform techniques (COS and Carr-Madan method) are compared with the reference results in [4], section 5.1 (with a particular focus on table 5.1 therein). The simulation setup and the choice of parameters are as described in [4], section 5.1:
The Heston model is set up with $\kappa = 1.2$, $\bar{v} = v_0 = 0.1$, $\gamma = 0.5$, and $\rho_{xv} = -0.3$, respectively. The Heston model model is coupled with $\rho_{xk} = 0.5$ to a DDSV LMM with $s_k = 0.25$, $b_k = 0.5$, $\beta = 1$, $\bar{z} = 1$, and $\epsilon = 0.1$, respectively. The IR-SV process is neither correlated to the EQ nor the IR model components ($\rho_{xk} = 0$ and $\rho_{kz} = 0$ for all Libor rates L_k, $\rho_{xz} = 0$); the correlation matrix of the Libor rates is $\rho_{ik} = 0.98$ for $i \neq k$, and unity otherwise.
The results obtained by inverse transform evaluation of an equity call option with the affine deterministic approximation of the Heston Libor Market Model (H1LMM) show excellent agreement (cf. Fig. 3.2, left part), Monte-Carlo results obtained for the full-scale HLMM model are in reasonable agreement (cf. Fig. 3.2, right part) with the reference results published in [4].
Another benchmark of the MC implementation of the HLMM follows from pricing a hybrid product as suggested in [4] (section 5.3 therein), where the hybrid named *Minimum of Several Assets* is priced. Hybrid products are considered in some detail in chapter 4 below, and the description of the specifics of the *Minimum of Several Assets* payoff construction is found in section 4.2. For the parameter set employed in [4], this hybrid derivative contains EQ and IR asset class components and is evaluated as function of the relative EQ contribution k in Fig. E.6. The calculated hybrid

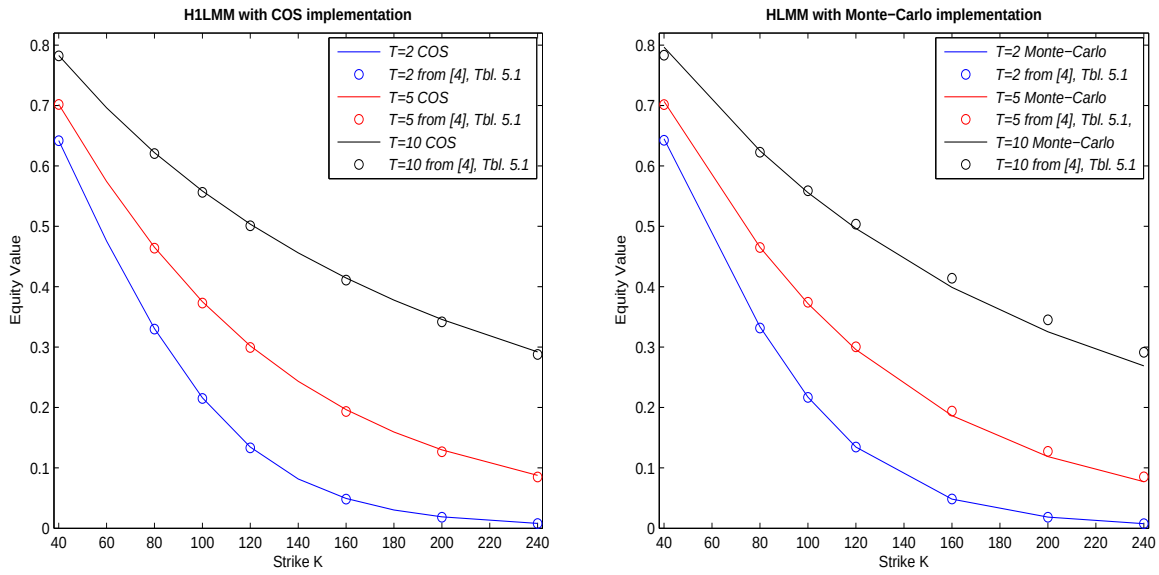

Figure 3.2: Comparison of equity call option values obtained within the Heston DDSV LMM (HLMM) and the corresponding affine model version H1LMM. Model parameters follow the description in [4] (section 5.1 and Appendix E therein). Left: Comparison of COS method results for the affine H1LMM model with [4], Table 5.1 therein. Right: Comparison of Monte-Carlo implementation results of the full-scale HLMM model with [4], Table 5.1 therein. MC resullts are obtained with $2 \cdot 10^6$ simulations and $k_s = 20$. The typical MC standard error level is 45 bp.

prices are in very good agreement with the results presented in [4], giving credit to the validity of the HLMM implementation.

Certain supplementary consistency checks were applied prior to the aforementioned pricing results:

- For $b_k = 0$, $s_k = 1$ the displaced-diffusion contribution cancels out. When the stochastic variance process is fixed at $z_t = z_0 = \text{const}$; this corresponds to the limit $\beta \to \infty$ and $\eta \to 0$. Then, the IR-SV process becomes quasi-deterministic and the LMM model remains.

- The Andersen QE scheme has been validated separately for the Heston case with the parameter sets of the original publication [7], and via cross-check with the analytical solution for the test parameter sets listed in Appendix D.1.

Monte-Carlo implementation of the full-scale HLMM model

The HLMM is implemented in one version where the DDSV LMM component is based on the spot Libor (SM) measure $\mathbb{Q}^B$, and an alternative version where the DDSV LMM component is evaluated in the terminal measure (TM) $\mathbb{Q}^T$. Crucial point in LMM implementations is the efficient evaluation of the drift term. Under $\mathbb{Q}^T$ the drift term is calculated by an iterative predictor-corrector (IPC) scheme (cf. [17] for details), which is adapted to account for the DDSV amendments to the model. The IPC scheme allows to use tenor-based time stepping (in [17] this is called *long stepping*) . Quite contrarily, the $\mathbb{Q}^B$ implementation employs a straightforward Euler scheme for the drift calculation, and the discretization errors introduced compared to the IPC scheme are compensated by introducing

substeps within each maturity tenor interval $T_i \leq t_k < T_{i+1}$ with $1 \leq k \leq k_s$ and $k_s = 20$ a typical number for the simulations presented in the discussion at hand.
For each Monte-Carlo path the following routine is completed for each time step $t \to t + \Delta t$ along the entire time frame $0 \leq t \leq T_N$ of the discretization:

1. Advance the IR-SV process variable $z_t \to z_{t+1}$ by an adaption of Andersen's QE scheme [7].

2. Proceed an individual time step in the DDSV LMM implementation, either in the spot measure $\mathbb{Q}^B$ or the terminal measure $\mathbb{Q}^T$.

3. Advance the Heston stochastic volatility process, based on Andersen's Quadratic Exponential (QE) scheme with martingale correction. Depending on the realization of the DDSV LMM component, either the EQ spot or forward stock prices are employed. The Libor spot rate is obtained from DDSV LMM results by setting $r_t = L_{m(t)}(t)$ without further interpolations.

3.4 Bridging between Short Rate and Market Model: The Cheyette Approach

3.4.1 Markovian Dynamics by Separable Volatility Specification

Hybrid models with a Hull-White IR component are well understood and, due to the low-dimensionality of the underlying system of SDEs, are widely used in practical applications. However HW short rate based models fail to capture market features like IR smiles. Striving to represent as much market observables as possible, market models are designed to model the entire forward curve by an HJM based volatility specification when computationally feasible, and are combined with concepts like displaced diffusion and an additional stochastic volatility process in order to account for IR smile and skew. DDSV LMMs are inherently non-Markovian and high-dimensional, and hence, by design not well suited for the application in calibration problems or dynamic hedging algorithms.
A viable approach to bridge between the simplicity of HW and sophistication of market models is to control the volatility structure of the Heath-Jarrow-Morton (HJM) framework by 'a priori' assumptions on the functional constraints by the Cheyette model [17c]. The result is a Markovian system with adaptable degree of dimensionality which allows for displaced-diffusion and stochastic volatility extensions. In the following, the Cheyette model is introduced within the context of the DDSV concept. Then, the DDSV Cheyette system as IR component is combined with a Heston EQ component to constitute a new hybrid model framework. Finally, affine approximations are studied which place the Heston DDSV Cheyette model within the AJD process class and open the path to efficient evaluation by inverse transform techniques. Benchmarking the quality of the affine versions (referenced by the acronyms H1CV and H2CV) with the full Heston DDSV Cheyette model, gives an indication of the validity of affine approximations and prepares to understand the comparison with the other short rate and LMM based hybrid models in the calibration and hybrid product valuation scenarios of the next chapter.

Cheyette Model Characteristics and Affine Model Features

The HJM framework [17b] is based on the idea to model the risk-neutral time evolution of the entire yield curve by the dynamics of the forward rate $f_t(T)$:

$$df_t(T) \quad = \quad \delta(t,T)dt + \sigma^f(t,T)dW(t) \qquad \text{for} \quad T \geq t, \tag{3.21}$$

where $\delta(t,T)$ is the corresponding drift and $\sigma^f(t,T)$ the volatility of each forward rate, respectively. According to [17b] the risk-neutral forward rate dynamics are completely determined by the initial market yield curve $f_0^M(T)$ as exogenous model input in combination with a given volatility structure $\sigma^f(t,T)$. In this form the HJM framework has practical drawbacks: The yield curve consists of an infinite number of individual stochastic processes (in the LMM this is overcome by defining a discretization on the basis of Libor rates with given tenor structure), and the drift is highly path dependent and non-Markovian. Essential point of the Cheyette model [17c] is to separate the forward rate stochastic volatility structure of the HJM framework

$$\sigma_i^f(t,T) = \sum_{k=1}^{n} g_k(T) H_t^k, \qquad i = 1, ..., n \quad , \tag{3.22}$$

into a product of a deterministic function $g_k(T)$ depending on maturity T and a Markovian process H_t^k. The Cheyette separable volatility model removes path dependency, and hence, the model is within the applicability of the Feynman-Kac theorem. In the case of single factor volatility $n = 1$ the Cheyette model with state vector $\mathbf{X}_t = [x_{c,t}, y_t]^\dagger$ in differential form reads:

$$dx_{c,t} \quad = \quad (y_t - \lambda x_{c,t})dt + \eta_t dW_c(t), \tag{3.23}$$

$$dy_t \quad = \quad (\eta_t^2 - 2\lambda y_t)dt, \tag{3.24}$$

where

- $x_{c,t}$ represents the Markovian Cheyette process (this is basically the short rate) with Brownian driver $W_c(t)$;
- y_t is the second state variable, coupling the mean-reversion level and the volatility. In the special und restrictive case of deterministic volatility $\eta_t = \eta(t)$ the second dimension becomes deterministic, $y_t = y(t)$. The essential advantage of the Cheyette model compared to the classical short rate models is the option to incorporate a stochastic volatility specification $\eta_t = \eta(t, x_{c,t}, y_t, z_t)$, the integral part of the discussion at hand. The particular choice of the stochastic volatility process z_t for the interest rate (IR) component controls the model features encompassing an IR smile.
- λ is the reversion rate of $d\tilde{x}_{c,t} = -\lambda \tilde{x}_{c,t} dt + \eta dW_c(t)$ of the first state variable.

The dimensionality of the Markovian Cheyette system is basically controlled by the specific form of the single-factor volatility:

- 3D Markovian Cheyette systems are obtained in case of full stochastic volatility specification $\eta_t = \eta(t, x_{c,t}, y_t, z_t)$, where the volatility connects to the state variable $x_{c,t}$ of the basic interest rate process and is combined by a separate SV process z_t. The DDSV Cheyette concept discussed below is inherently 3D. In general, the situation that η_t depends on other state variables gives rise to non-affine characteristics. Then, suitable approximations bring the system within the AJD process class and make inverse transform techniques applicable.
- 2D Markovian Cheyette systems result in configurations where $\eta_t = \eta(t, x_{c,t})$ connects at least to the Brownian driver $W_c(t)$ of the basic IR process.
- 1D Markovian Cheyette systems are generated by presuming deterministic $\eta_t = \eta(t)$; narrowing the constraints towards η_t=const to be constant results in system features with straightforward correspondence to the HW short rate model.

3.4.2 Displaced-Diffusion Stochastic Volatility (DDSV) Concept in the Cheyette Model

In principle the Displaced Diffusion (DD) concept as originally introduced into the LMM framework [31] is directly transferable into the Cheyette setting by adapting the volatility specification:

$$\begin{aligned} \eta(t, x_{c,t}, z_t) &= s_k(t)(b_k(t)\pi_t + (1 - b_k(t))\pi_0)\sqrt{z_t} \equiv s_k(t)\Phi_k(t), \qquad (3.25) \\ \text{with} \quad \pi_t &= f(0,t) + x_{c,t} \end{aligned}$$

The volatility is constructed by defining a certain basis level $s_k(t)$ and a IR skew parameter $b_k(t)$. The Cheyette system assumes the basis level in the limit $b_k \to 0$ and $z_t \to \bar{z}$=1 where implied volatility flattens out. In the limiting case $b_k \to 1$ the DD conformalization assumes log-normal behaviour corresponding to flat implied volatility structure without skew modifications. With b_k decreasing towards 0 as lower boundary, by η_t the skew features in the implied volatility structure are pronounced. Though $s_k(t)$ and $b_k(t)$ are in general time-dependent, in the present discussion the DDSV Cheyette system is based on constant DD parameters. IR smiles are introduced by a separate stochastic variance (IR-SV) process analogous to the Heston SV component on the EQ side, i.e.

$$z_t = \beta(\bar{z} - z_t)dt + \epsilon\sqrt{z_t}dW_z(t), \qquad (3.26)$$

where $\beta(t) = \beta$=const and $\epsilon(t) = \epsilon$=const correspond to the IR-SV mean reversion and volatiliy of variance, respectively, assumed to be constant here.
Consistency with the DDSV LMM approach is enforced by denoting the following connection to the forward rate volatility structure (cf. [33] for details on the derivation):

$$\begin{aligned} \eta(t, x_{c,t}, z_t) &= -[\tfrac{\partial}{\partial T}B_c(t,T)]^{-1} s_k(t)(b_k\pi_t + (1 - b_k)\pi_0)\sqrt{z_t} \qquad (3.27) \\ &= e^{\lambda(T-t)}(b_k\pi_t + (1 - b_k)\pi_0)\sqrt{z_t}. \qquad (3.28) \end{aligned}$$

The quantity $B_c(t,T)$ is the drift component in the Cheyette zero bond formulation (cf. section A.3.2).

3.4.3 HHW as limiting case of the Heston Cheyette model (HCH)

The HHW model is equivalent to the Heston Cheyette model (HCH) when certain constraints are imposed on the Cheyette model as the IR component. As the HHW and the associated affine approximations are well-studied in previous publications [1, 2], we use the HHW as limiting case to cross-check the derivations and implementations of the introduced HCH and HCV models. In section 3.4.1 the Cheyette (CH) model was introduced as a Markovian IR model with variable degrees of freedom. The dimensionality and complexity of the Cheyette model is controlled by the underlying volatility specification $\eta_t = \eta(t, x_t^i)$, where $x_t^i \; i \in \{1, ..., n\}$ are the Markovian state variables of the n-dimensional system. The Cheyette concept is based on introducing constraints on the volatility specification of market models; Cheyette models are Markovian by design and rendered as specific group within the IR models created by the Heath-Jarrow-Morton (HJM) framework.
In the limiting case of a Cheyette system under the constraint of constant volatility $\eta_t \to \eta$=const, the state variable y_t decouples from $x_{c,t}$ and becomes deterministic (cf. section 3.4.1 for a description of the Cheyette state variables and Appendix A.3 for calculation details):

$$y(t) \quad = \quad \tfrac{\eta^2}{2\lambda}(1 - e^{-2\lambda\tau}) \tag{3.29}$$

For constant volatility η the connection between the CH and HW models is then contained in the relation between CH and HW mean reversion levels, i.e.

$$\theta(t) \quad = \quad f(0,t) + \tfrac{1}{\lambda}\tfrac{\partial}{\partial T} f(0,t) + \tfrac{1}{\lambda} y(t). \tag{3.30}$$

The CH/HW connection is equally valid for the corresponding CHFs - the connection between CH CHF and HW CHF Fourier coefficients is shown in Appendix A.3.1.1 and based on the relation

$$Y_B(u,\tau) \quad = \quad -\tfrac{1}{2(1-iu)} C_B^2(u,\tau), \tag{3.31}$$

where $Y_B(u,\tau)$ is the Fourier transform coefficient of the $y(t)$ process, and $C_B(u,\tau)$ the corresponding Fourier coefficent of the IR process r_t, respectively. The subscript B indicates that the relation is derived under the spot measure $\mathbb{Q}^B$. Following the same line of thoughts, the connection of CH/HW IR components is carried into the corresponding hybrid models. The HHW/HCH correspondence is based on the integral relations of Fourier coefficients

$$\begin{aligned} \int_0^\tau Y_B(u,\tau)\, d\tau \quad &= \quad -\tfrac{1}{2(1-iu)} \int_0^\tau C_B^2(u,\tau)\, d\tau \\ &= \quad -\tfrac{1}{2(1-iu)} I_3(u,\tau) = \int_0^\tau C_B(u,\tau) y(t) d\tau \end{aligned} \tag{3.32}$$

These integral relations are detailed in Appendix B.2 and actually represent substantial parts of the affine H1CH/H1HW model Fourier coefficients $A_{H1CH}(u,\tau)$ and $A_{H1HW}(u,\tau)$ as discussed in section 3.2.1.
These model characteristics are previewed here to emphasize the following line of argumentation: The connection between HW and CH IR components and corresponding affine hybrid H1HW and H1CH models in the limiting case η=const is well-defined. All numerical implementations presented are validated in the sense that when parameters are tuned to assume this limit, the theoretically expected

connection between these models is observed numerically when employing inverse transforms or direct evaluation methods.
For the HHW/HCH IR components analytic prices of contingent claims are available as derived in Appendix F. Such analytic prices are used to cross-check the numerical implementations as is further detailed in Appendix F.

Affine model derivation in the spot $\mathbb{Q}^B$ and the terminal measure $\mathbb{Q}^T$

The derivation of the affine version of the full-scale Heston Cheyette (HCH) hybrid model (throughout the present discussion referenced by the acronym H1CH) proceeds in analogy to the H1HW derivations outlined above. The details of the H1CH derivation in the spot measure $\mathbb{Q}^B$ are given in Appendix B.2.
There are two intriguing features of the affine H1HW and H1CH models: (i) When the EQ-SV process and IR process are uncorrelated ($\rho_{vr} = 0$, which is the case for all instantaneous covariance structures within this thesis), the explicit form of the stochastic variance process on the EQ side is independent of the choice of measure; however, the IR component transforms according to the specific measure applied. (ii) The discounting decouples from the EQ-SV component upon transformation from $\mathbb{Q}^B$ to the terminal measure $\mathbb{Q}^T$.
The H1HW model derivation in the terminal measure $\mathbb{Q}^T$ is detailed in Appendix C.1, and in the same line of argumentation the transformation to the terminal measure is transferred to the H1CH model in Appendix C.2.
The Fourier cofficient $C(u,\tau)$ corresponding to the IR component is equivalent for both hybrid models assuming the form

$$C_B(u,\tau) \quad = \quad \tfrac{1}{\lambda}\left((1+iu\lambda)e^{-\lambda\tau}-1\right) = -\tfrac{1}{\lambda}(1-e^{-\lambda\tau}) + iue^{-\lambda\tau}, \tag{3.33}$$

under the spot measure $\mathbb{Q}^B$, and

$$C_T(u,\tau) \quad = \quad -\tfrac{1}{\lambda}(1-e^{-\lambda\tau}), \tag{3.34}$$

under the terminal measure $\mathbb{Q}^T$, respectively.
It is important to note that the decoupling of the EQ-SV and IR processes under the measure $\mathbb{Q}^T$ means that both processes evolve and can be modeled separately. However, the EQ-SV and IR processes remain correlated, so the hybrid correlation in the full-scale models remains. The corresponding EQ-SV/IR coupling parameters ρ_{xr} and ρ_{xc} are included in the Fourier coefficients $A_{H1HW}(u,\tau)$ and $A_{H1CH}(u,\tau)$, respectively.
The decoupling is indicated by subdividing the covariance matrices of the hybrid models as indicated by the broken lines in the relevant Appendix C.1 for the H1HW and C.2 for the H1CH. The separation of the hybrid components has favorable consequences for the numerical implementations (in particular of Monte-Carlo and PDE schemes), since the EQ-SV part can be modelled as a 2D process in the forward measure, where discounting is accomplished straightforwardly by an analytically determined zero bond value. The advantages in computational performance are obvious in contrast to the full 3D SDE system present under the spot measure $\mathbb{Q}^B$.

As already pointed out, the crucial point is that the change of measure solely affects the Fourier coefficients associated to the IR process component. The EQ-SV component of the hybrid model remains unaffected. When discussing the Heston DDSV-Cheyette model below, the essential difference is the introduction of an IR-SV process; then the SV component on the IR side will also be responsive to changes of measure. This is the difference in SV contributions between the EQ and IR side.
The implications are multiple, as for Heston DDSV Cheyette models the EQ-SV and IR-SV components remain entangled upon transformation from $\mathbb{Q}^B$ to $\mathbb{Q}^T$, and hence, the dimensional reduction observed by the separation of hybrid components is not applicable, putting constraints on the numerical implementations!

3.5 Hybrid Smiles in Markovian Systems

3.5.1 The Heston DDSV Cheyette Model in the Spot Measure

Combining the Heston process as equity component with the DDSV Cheyette model on the interest rate side creates a correlated SDE system governing the Heston DDSV Cheyette model, thereafter referenced by the acronym HCV:

$$\begin{aligned}
dx_{s,t} &= (\pi_t - \tfrac{v_t}{2})dt + \sqrt{v_t}dW_x(t), \\
dv_t &= \kappa(\bar{v} - v_t)dt + \gamma\sqrt{v_t}dW_v(t), \\
dx_{c,t} &= (y_t - \lambda x_{c,t})dt + \eta_t dW_c(t), \\
dz_t &= \beta(\bar{z} - z_t)dt + \epsilon\sqrt{z_t}dW_z(t), \\
dy_t &= (\eta_t^2 - 2\lambda y_t)dt, \\
&\text{with} \\
\pi_t &= f(0,t) + x_{c,t}, \\
\eta_t &= \sqrt{z_t}s_k(t)(b_k(t)\pi_t + (1 - b_k(t))\pi_0) \equiv \sqrt{z_t}s_k(t)\Phi_k(t),
\end{aligned} \tag{3.35}$$

and correlations $\rho_{xv}dt = dW_x dW_v$, $\rho_{cx}dt = dW_c dW_x$, $\rho_{cz}dt = dW_c dW_z$, $\rho_{cv}dt = dW_c dW_v$, $\rho_{vz}dt = dW_v dW_z$. The SV processes of the EQ and IR components are 'a priori' presumed to be uncorrelated ($\rho_{zv} = 0$). Furthermore, to simplify the analysis the correlation between EQ-SV and IR processes are also assumed to be negligible $\rho_{cv} = 0$; this is for the sake of clarity, since an extension to include this correlation type is straightforward. For the discussion at hand an interest rate with a single-factor Cheyette volatility, $k \equiv 1$, and constant parameters for the volatility $s_k(t) \equiv s_k$ of the IR variance process and displaced-diffusion conformalization $b_k(t) \equiv b_k$ are considered. In the later discussion an extension towards the multi-factor volatility framework becomes feasible.

3.5.2 The Heston DDSV Cheyette Model in the Terminal Measure

The forward stock price,

$$F_t \quad = \quad \frac{S_t}{P(t,T)} \equiv \frac{S_t}{P_t} \tag{3.36}$$

is a martingale under the T-forward measure. For specific EQ-IR hybrid systems like the HHW/HCH systems the transformation from the risk-neutral measure ($\mathbb{Q}^0$) to the T-forward (terminal) measure ($\mathbb{Q}^T$) gives rise to advantages: In the SDE hybrid system the equations governing the IR process are decoupled from the equations determining the forward price process. Consequently, the Heston EQ-SV component can be modeled separately from the IR process. The transformation $\mathbb{Q}^0 \to \mathbb{Q}^T$ is elaborated in detail in Appendices C.1 and C.2 for the HHW and HCH models, respectively. The influence of EQ-IR correlations is still represented by the correlation parameters ρ_{xr}, ρ_{xc} contained within the EQ-SV model components under the forward measure. The dimensional reduction from 3D in the spot to 2D in the forward measure has favourable effects on the computational implementations.

However, the situation gets more involved, as soon as an IR-SV component is included in the hybrid model. The essential point of the Heston DDSV Cheyette (HCV) system is that the volatility of the IR component $\eta_t = \eta(t, z_t)$ is driven by a stochastic variance process; then, y_t becomes a stochastic variable, and consequently the IR-SV Cheyette component is a 3D Markovian system. The DDSV IR component is introduced into the HCV system by

$$\eta_t = \sqrt{z_t} s_k \Phi_k(t, x_{c,t}) = \sqrt{z_t} s_k (b_k \pi_t + (1 - b_k)\pi_0) \quad \text{with} \quad \pi_t = f(0,t) + x_{c,t} \equiv r_t. \tag{3.37}$$

Though the zero bond value in the DDSV Cheyette model is solely a function of $x_{c,t}$ and y_t, the influence of the IR-SV process is contained implicitly in y_t and shows in the zero bond dynamics as is detailed in the derivations below.

By transformation to the forward measure, IR-SV contributions are contained in the forward EQ price dynamics, and hence, the Heston EQ-SV system contains the IR-SV variable z_t as additional third dimension. However, the situation becomes more involved in the presence of DD contributions, since then the IR volatility specification

$$\eta_t = \eta(t, z_t, x_{c,t}) = \sqrt{z_t} s_k \Phi(t, x_{c,t}), \tag{3.38}$$

becomes a function of both z_t and $x_{c,t}$. This volatility specification is present in the zero bond dynamics dP_t/P_t and thereby carried into the forward dynamics dF_t/F_t.

The connection between the specific choice of measure and the dimensionality of the SDE system is for the HCV model summarized as follows:

- The full-scale HCV model is an inherently 5D system both in the spot measure $\mathbb{Q}^B$ as well as in the terminal measure $\mathbb{Q}^T$. The underlying SDE system as well as the CHF depend on all five Markovian state variables $S_t, v_t, x_{c,t}, y_t, z_t$, irrespective of the specific choice of measure.

- When DD contributions are not taken into account and only the pure IR-SV process is present, the volatility specification simplifies to

$$\eta_t = \eta(t, z_t) = \sqrt{z_t} s_k \Phi_k(t). \tag{3.39}$$

  This is achieved for instance by *freezing* the interest rates in the initial state in the volatility specification, as is elaborated below within the constraints of the affine deterministic limit H1CV of the HCV model. The H1CV model, which represents a 5D Markovian system under the spot measure $\mathbb{Q}^B$, then separates into EQ-SV $\times$ IR-SV $\equiv$ 3D $\times$ 3D SDE systems upon transformation to the forward measure $\mathbb{Q}^T$. The IR-SV process variable z_t is the linking element between hybrid components.

- As soon as DD contributions are fully taken into account with Φ_k from equation (3.24) this implies a functional dependence of the form $\Phi_k = \Phi_k(t, x_{c,t})$, and hence, the HCV model system remains 5D. In this case there is no obvious computational advantage gained upon switching towards $\mathbb{Q}^T$.

In the following the transformation of the HCV model from spot measure $\mathbb{Q}^B$ towards the terminal measure $\mathbb{Q}^T$ is discussed in detail.
We consider the general SDE system,

$$\mathrm{d}\mathbf{X}_t \;=\; \mu^0(\mathbf{X}_t)dt + L_{\mathbf{X}_t}\mathrm{d}\tilde{\mathbf{W}}^{\mathbf{0}}(t), \tag{3.40}$$

with state variable vector $[y_t, z_t, x_{c,t}, v_t, S_t]^\dagger$, drift term

$$\mu^0(\mathbf{X}_t) \;=\; \begin{pmatrix} z_t s_k^2 \Phi_k^2 - 2\lambda y_t \\ \beta(\bar{z} - z_t) \\ y_t - \lambda x_{c,t} \\ \hdashline \kappa(\bar{v} - v_t) \\ r_t \end{pmatrix}, \tag{3.41}$$

and instantaneous covariance matrix $\Sigma_{\mathbf{X}_t} = L_{\mathbf{X}_t} L_{\mathbf{X}_t}^\dagger$ in Cholesky decomposition

$$L_{\mathbf{X}_t} \;=\; \left(\begin{array}{ccc:cc} 0 & 0 & 0 & 0 & 0 \\ 0 & \epsilon\sqrt{z_t} & 0 & 0 & 0 \\ 0 & \rho_{cz} s_k \Phi_k \sqrt{z_t} & L_{cc} s_k \Phi_k \sqrt{z_t} & 0 & 0 \\ \hdashline 0 & \rho_{vz}\gamma\sqrt{v_t} & L_{vc}\gamma\sqrt{v_t} & L_{vv}\gamma\sqrt{v_t} & 0 \\ 0 & \rho_{xz}\sqrt{v_t} & L_{xc}\sqrt{v_t} & L_{xv}\sqrt{v_t} & L_{xx}\sqrt{v_t} \end{array}\right), \tag{3.42}$$

with components

$$\begin{aligned} L_{cc} &= \sqrt{1-\rho_{cz}^2},\; L_{vc} = \tfrac{1}{L_{cc}}\sqrt{\rho_{vc} - \rho_{vz}\rho_{cz}},\; L_{vv} = \sqrt{1 - \rho_{vz}^2 - L_{vc}^2}, \\ L_{xc} &= \tfrac{1}{L_{cc}}(\rho_{xc} - \rho_{xz}\rho_{cz}),\; L_{xv} = \tfrac{1}{L_{vv}}(\rho_{xv} - \rho_{xz}\rho_{vz} - L_{xc}L_{vc}),\; L_{xx} = \sqrt{1 - \rho_{xz}^2 - L_{xc}^2 - L_{xv}^2}, \end{aligned}$$

and the corresponding vector of uncorrelated Brownian drivers $\tilde{\mathbf{W}}^{\mathbf{0}}(t) = [\tilde{W}_y^0(t), \tilde{W}_z^0(t), \tilde{W}_c^0(t), \tilde{W}_v^0(t), \tilde{W}_x^0(t)]^\dagger$. The superscript $'0'$ indicates that at this point the drift and Brownian drivers are still considered in the spot measure $\mathbb{Q}^B$.
In detail, we deal with the stock dynamics

$$\begin{aligned} \frac{dS_t}{S_t} &= \pi_t dt + \sqrt{v_t} dW_x^0 \\ &= r_t dt + \rho_{xz}\sqrt{v_t} d\tilde{W}_z^0 + L_{xc}\sqrt{v_t} d\tilde{W}_c^0 + L_{xv}\sqrt{v_t} d\tilde{W}_v^0 + L_{xx}\sqrt{v_t} d\tilde{W}_x^0, \end{aligned} \tag{3.43}$$

and the zero coupon bond dynamics, as follows,

$$\begin{aligned}
\frac{dP_t}{P_t} &= \pi_t dt + \sqrt{z_t} s_k \Phi_k B_c dW_c^0 = \pi_t dt + B_c(\rho_{cz}\sqrt{z_t} s_k \Phi_k d\tilde{W}_z^0 + L_{cc}\sqrt{z_t} s_k \Phi_k d\tilde{W}_c^0) \\
&= \pi_t dt + \sqrt{z_t} s_k \Phi_k B_c(\rho_{cz} d\tilde{W}_z^0 + L_{cc} d\tilde{W}_c^0) \quad \text{with} \quad B_c(t,T) = -\tfrac{1}{\lambda}(1-e^{-\lambda\tau}), \\
\text{so that} \quad \left(\frac{dP_t}{P_t}\right)^2 &= z_t s_k^2 \Phi_k^2 B_c^2 dt \quad \text{and} \\
&- \left(\frac{dP_t}{P_t}\right)\left(\frac{dS_t}{S_t}\right) = -\sqrt{z_t}\sqrt{v_t} s_k \Phi_k B_c(\rho_{xz}\rho_{cz} + L_{cc}L_{xc}) dt. \qquad (3.44)
\end{aligned}$$

The zero bond dynamics contain the IR stochastic variance process explicitly, even though the stochastic variance appears only implicitly in the corresponding zero bond formula. Then, the forward dynamics are given in the following form:

$$\begin{aligned}
\frac{dF_t}{F_t} &= (z_t s_k^2 \Phi_k^2 B_c^2 - \rho_{xc} s_k \Phi_k B_c \sqrt{z_t}\sqrt{v_t}) dt + (\rho_{xz}\sqrt{v_t} - \rho_{cz} s_k \Phi_k \sqrt{z_t} B_c) d\tilde{W}_z^0 \\
&+ (L_{xc}\sqrt{v_t} - L_{cc}\sqrt{z_t} s_k \Phi_k B_c) d\tilde{W}_c^0 + L_{xv}\sqrt{v_t} d\tilde{W}_v^0 + L_{xx}\sqrt{v_t} d\tilde{W}_x^0. \qquad (3.45)
\end{aligned}$$

The Girsanov kernel obtained from the zero bond dynamics, to perform the transformation from the risk-neutral towards the T-forward measure $\mathbb{Q}^B \to \mathbb{Q}^T$, reads

$$\begin{pmatrix} d\tilde{W}_y^0 \\ d\tilde{W}_z^0 \\ d\tilde{W}_c^0 \\ \hline d\tilde{W}_v^0 \\ d\tilde{W}_x^0 \end{pmatrix} = \begin{pmatrix} 0 \\ \rho_{cz}\sqrt{z_t} s_k \Phi_k B_c \\ L_{cc}\sqrt{z_t} s_k \Phi_k B_c \\ \hline 0 \\ 0 \end{pmatrix} dt + \begin{pmatrix} d\tilde{W}_y^T \\ d\tilde{W}_z^T \\ d\tilde{W}_c^T \\ \hline d\tilde{W}_v^T \\ d\tilde{W}_x^T \end{pmatrix}. \qquad (3.46)$$

Since the forward price is a martingale under the T-forward measure $F_t = \mathbb{E}^T[F_T|\mathcal{F}_t]$, the forward dynamics need to be driftless, i.e.

$$\begin{aligned}
dF_t &= (\rho_{xz}\sqrt{v_t} - \rho_{cz} s_k \Phi_k \sqrt{z_t} B_c) d\tilde{W}_z^T + (L_{xc}\sqrt{v_t} - L_{cc} s_k \Phi_k \sqrt{z_t} B_c) d\tilde{W}_c^T \\
&+ L_{xv}\sqrt{v_t} d\tilde{W}_v^T + L_{xx}\sqrt{v_t} d\tilde{W}_x^T.
\end{aligned}$$

However, drift components arise in the log-transform, i.e.

$$\begin{aligned}
d\hat{x}_t = d\log F_t &= -\tfrac{1}{2}[(\rho_{xz}^2 + L_{xc}^2 + L_{xv}^2 + L_{xx}^2) v_t - 2\rho_{xz}\rho_{xc} s_k \Phi_k B_c \sqrt{z_t}\sqrt{v_t} + \rho_{cz}^2 s_k^2 \Phi_k^2 z_t B_c^2 \\
&- 2(\rho_{xc} - \rho_{xz}\rho_{cz}) s_k \Phi_k B_c \sqrt{z_t}\sqrt{v_t} + (1-\rho_{cz}^2) s_k^2 \Phi_k^2 B_c^2 z_t] dt + \\
&(\rho_{xz}\sqrt{v_t} - \rho_{cz} s_k \Phi_k z_t B_c) d\tilde{W}_z^T \\
&+ (L_{xc}\sqrt{v_t} - L_{cc} s_k \Phi_k \sqrt{z_t} B_c) d\tilde{W}_c^T + L_{xv}\sqrt{v_t} d\tilde{W}_v^T + L_{xx}\sqrt{v_t} d\tilde{W}_x^T \\
&= (-\tfrac{v_t}{2} + \rho_{xc} s_k \Phi_k \sqrt{z_t} B_c \sqrt{v_t} - \tfrac{1}{2} z_t s_k^2 \Phi_k^2 B_c^2) dt + (\rho_{xz}\sqrt{v_t} - \rho_{cz} s_k \Phi_k z_t B_c) d\tilde{W}_z^T \\
&(L_{xc}\sqrt{v_t} - L_{cc} s_k \Phi_k \sqrt{z_t} B_c) d\tilde{W}_c^T + L_{xv}\sqrt{v_t} d\tilde{W}_v^T + L_{xx}\sqrt{v_t} d\tilde{W}_x^T. \qquad (3.47)
\end{aligned}$$

3.5.3 Heston DDSV Cheyette Model: Monte-Carlo Implementations

The Monte-Carlo (MC) evaluations of contingent claims within the HCV model are implemented under the spot measure $\mathbb{Q}^B$ as well as under the T-forward measure $\mathbb{Q}^T$. For both measures unbiased schemes exist for the IR components detailed below. On the EQ side, there is the unbiased

Andersen QE scheme with martingale correction available for the Heston process; on the IR side, the QE scheme is adapted to be applicable to the IR-SV process.
In general, the results obtained under $\mathbb{Q}^B$ and $\mathbb{Q}^T$ are consistent. Whenever spurious deviations are observed, these are the consequence of different dimensionality in model formulations under the respective measures. The influence of a particular choice of measure on the quality and performance of numerical evaluations is part of the discussion below along with the model validation. The implementations are based on a forward MC scheme, so for every MC path the simulation proceeds forward in time by stepping along a predefined time grid from $t = 0$ towards maturity $t = T$.

Under the **spot measure** the HCV model resembles a full 5D system. At each step from t_k to t_{k+1} within the time discretization we perform the following steps:

- (i) Advance the IR-SV process via an adapted version of the Quadratic Exponential (QE) scheme [7] $z_{t_k} \to z_{t_{k+1}}$.
- (ii) Iterate the first IR component $y_{t_k} \to y_{t_{k+1}}$ by means of a straightforward Euler step.
- (iii) Perform another Euler step for $x_{c,t}$ employing the unbiased scheme in the spot measure $\mathbb{Q}^B$:

$$\begin{aligned} dx_{c,t_{k+1}} &= (y_{t_k} - \lambda x_{c,t_k})dt + \eta_{t_k} d\tilde{W}^0(t_k) \\ &= (y_{t_k} - \eta_{t_k}^2 B_c^2(t_k, t_{k+1}) - \lambda x_{c,t_k})dt + \eta_{t_k} d\tilde{W}^B(t_k) \end{aligned} \tag{3.48}$$

- (iv) Simulate the EQ-SV component $v_{t_k} \to v_{t_{k+1}}$ as first part of the Andersen QE scheme for the Heston process.
- (v) Simulate the log-transformed EQ state variable $\hat{x}_{t_k} = \log S_{t_k} \to \hat{x}_{t_{k+1}}$ as second part of the Andersen QE scheme.

With the EQ state variable at maturity $\hat{x}_T$ the derivative payoff

$$\Pi(t) = B(t)\mathbb{E}^B\left[\frac{1}{B(T)}\Pi(T)\right] = \mathbb{E}^B\left[\prod_{k=k(t)}^{k(T)-1} P(t_k, t_{k+1})\Pi(T)\right], \tag{3.49}$$

is calculated under $\mathbb{Q}^B$ and discounted to the present value, where the directly re-balanced money market account (discretely compounded on the pre-defined time grid)

$$B(t) = P(t,T)\prod_{k=k(t)}^{k(T)-1}\frac{1}{P(t_k, t_{k+1})}, \tag{3.50}$$

is chosen as numéraire.
In the **terminal measure** $\mathbb{Q}^T$ the HCV model is under certain conditions reduceable to a 3D system as argued in the preceding section. Whenever DD contributions are taken into account, the HCV model remains 5D and the IR component is based on the following unbiased scheme:

$$\begin{aligned} dx_{c,t_{k+1}} &= (y_{t_k} - \lambda x_{c,t_k})dt + \eta_{t_k} d\tilde{W}^0(t_k) \\ &= (y_{t_k} - \eta_{t_k}^2 B_c^2(t_k, T) - \lambda x_{c,t_k})dt + \eta_{t_k} d\tilde{W}^T(t_k). \end{aligned} \tag{3.51}$$

Under the $\mathbb{Q}^T$ measure the discounted derivative payoff assumes the form,

$$\Pi(t) \quad = \quad P(t,T)\mathbb{E}^T[\Pi(T)]. \tag{3.52}$$

3.6 Evaluation of the Heston DDSV Cheyette Model by Inverse Transform Techniques

The Heston DDSV Cheyette model (HCV) is in itself non-affine. With the state variable vector $X_t = [x_{s,t}, v_t, x_{c,t}, z_t, y_t]^\dagger$ the covariance matrix is given by

$$\Sigma_{\mathbf{X}_t} \quad = \quad \begin{pmatrix} v_t & \rho_{xv}\gamma v_t & \rho_{xc}s_k\Phi_k\sqrt{v_t}\sqrt{z_t} & 0 & 0 \\ \rho_{vx}\gamma v_t & \gamma^2 v_t & 0 & 0 & 0 \\ \rho_{cx}s_k\Phi_k\sqrt{v_t}\sqrt{z_t} & 0 & s_k^2\Phi_k^2 z_t & \rho_{zc}s_k\Phi_k\epsilon z_t & 0 \\ 0 & 0 & \rho_{zc}s_k\Phi_k\epsilon z_t & \epsilon^2 z_t & 0 \end{pmatrix}. \tag{3.53}$$

Acknowledging the fact that $s_k\Phi_k = s_k\Phi_k(x_{c,t})$ is a function of the state variable $x_{c,t}$, the following non-linear terms need to be considered when affine model constraints are to be prescribed:

$$\Sigma_{\mathbf{X}_t}(1,3) = \Sigma_{\mathbf{X}_t}(3,1) \quad = \quad \rho_{xc}s_k\Phi_k\sqrt{v_t}\sqrt{z_t}, \tag{3.54}$$

$$\Sigma_{\mathbf{X}_t}(3,4) = \Sigma_{\mathbf{X}_t}(4,3) \quad = \quad \rho_{xc}s_k\Phi_k\epsilon z_t, \tag{3.55}$$

$$\Sigma_{\mathbf{X}_t}(3,3) \quad = \quad s_k^2\Phi_k^2 z_t. \tag{3.56}$$

Basically, there are two possible strategies to place this model within the AJD process class:

- **Limit 1:** Remove the dependency of $s_k\Phi_k$ on the state variable $x_{c,t}$ and introduce affine approximations for the state variables v_t and z_t, for instance by employing the projection on proxies for the corresponding expectation values $\mathbb{E}\left[\sqrt{v_t}\right] \equiv \delta_v(t)$ and $\mathbb{E}\left[\sqrt{z_t}\right] \equiv \delta_z(t)$, as suggested in [1]. $s_k\Phi_k$=constant is straightforwardly achieved in the limit $b_k = 0$,

$$s_k\Phi_k = s_k\left(b_k(f(0,t)+x_{c,t}) + (1-b_k)(f(0,0)+x_{c,0})\right) \xrightarrow{b_k\to 0} s_k(f(0,0)+x_{c,0}) = s_k\Phi_k(0). \tag{3.57}$$

  The stochastic variables v_t and z_t describe classical CIR-type square root processes. The corresponding expectations $\mathbb{E}[\sqrt{v_t}]$ (as well as $\mathbb{E}[\sqrt{z_t}]$) exist in analytic form as derived in [30a]:

$$\mathbb{E}\left[\sqrt{v_t}\right] \quad = \quad \sqrt{2c_v(t)}e^{-\omega_v(t)/2}\sum_{k=0}^{\infty}\frac{1}{k!}\left(\frac{\omega_v(t)}{2}\right)^k\frac{\Gamma(\frac{1+d_v}{2}+k)}{\frac{d_v}{2}+k}, \tag{3.58}$$

$$\mathbb{E}\left[\sqrt{z_t}\right] \quad = \quad \sqrt{2c_z(t)}e^{-\omega_z(t)/2}\sum_{k=0}^{\infty}\frac{1}{k!}\left(\frac{\omega_z(t)}{2}\right)^k\frac{\Gamma(\frac{1+d_z}{2}+k)}{\frac{d_z}{2}+k}, \tag{3.59}$$

  with

$$c_v(t) \quad = \quad \tfrac{1}{4\kappa}\gamma^2(1-e^{-\kappa t}),\ d_v = \tfrac{4\kappa\bar{v}}{\gamma^2},\ \omega_v(t) = \tfrac{4\kappa v_0 e^{-\kappa t}}{\gamma^2(1-e^{-\kappa t})},$$

$$c_z(t) \quad = \quad \tfrac{1}{4\beta}\epsilon^2(1-e^{-\beta t}),\ d_z = \tfrac{4\beta\bar{z}}{\epsilon^2},\ \omega_z(t) = \tfrac{4\beta v_0 e^{-\beta t}}{\epsilon^2(1-e^{-\beta t})},$$

  and $\qquad \Gamma(x) = \int_0^\infty t^{x-1}e^{-t}dt \quad$ the $\Gamma-$function,

where simplifications to the hypergeometric series are employed, as originally introduced in [37]. Though an explicit form exists, the evaluation is time consuming in computational implementations. Therefore, it is advantageous to use a projection on time dependent functions of the following form

$$\mathbb{E}\left[\sqrt{v_t}\right] \simeq a_1 + b_1 e^{c_1 t} \equiv \delta_v(t), \tag{3.60}$$

$$\mathbb{E}\left[\sqrt{z_t}\right] \simeq a_2 + b_2 e^{c_2 t} \equiv \delta_z(t), \tag{3.61}$$

as proxies. As suggested in [1], the coefficients a_i, b_i, c_i $(i \in \{1, 2\})$ result as minimization of the norm

$$min_{\{a_1,b_1,c_1\}} ||\delta_v(t) - \Lambda_v(t)||_n, \tag{3.62}$$

$$min_{\{a_2,b_2,c_2\}} ||\delta_z(t) - \Lambda_z(t)||_n, \tag{3.63}$$

where $||...||_n$ is any n^{th} norm with respect to the respectively corresponding objective functions

$$\Lambda_v(t) = \sqrt{c_v(t)(\omega_v(t) - 1) + c_v(t)d_v + \frac{c_v(t)d_v}{2(d_v + \omega_v(t))}} \geq 0 \tag{3.64}$$

$$\Lambda_z(t) = \sqrt{c_z(t)(\omega_z(t) - 1) + c_z(t)d_z + \frac{c_z(t)d_z}{2(d_z + \omega_z(t))}} \geq 0. \tag{3.65}$$

Conducting the optimization is again tedious in practice with respect to computational performance. Therefore, following [1], approximative solutions are obtained by matching the $\Lambda_v(t)$, $\Lambda_z(t)$ in the limiting cases $t \to 0$, $t = 1$, and $t \to \infty$:

$$\begin{aligned}
\lim_{t\to\infty} \Lambda_v(t) &= \sqrt{\bar{v} - \frac{\gamma^2}{8\kappa}} = a_1 = \lim_{t\to\infty} \delta_v(t), \\
\lim_{t\to\infty} \Lambda_z(t) &= \sqrt{\bar{z} - \frac{\epsilon^2}{8\beta}} = a_2 = \lim_{t\to\infty} \delta_z(t),
\end{aligned} \tag{3.66}$$

$$\begin{aligned}
\lim_{t\to 0} \Lambda_v(t) &= \sqrt{v_0} = a_1 + b_1 = \lim_{t\to 0} \delta_v(t), \\
\lim_{t\to 0} \Lambda_z(t) &= \sqrt{z_0} = a_2 + b_2 = \lim_{t\to 0} \delta_z(t),
\end{aligned}$$

$$\begin{aligned}
\lim_{t=1} \Lambda_v(t) &= = a_1 + b_1 e^{-c_1} = \lim_{t=1} \delta_v(t), \\
\lim_{t=1} \Lambda_z(t) &= = a_2 + b_2 e^{-c_2} = \lim_{t=1} \delta_z(t),
\end{aligned}$$

Finally, the coefficients of the affine proxies $\delta_v(t)$ and $\delta_z(t)$ are obtained as follows:

$$a_1 = \sqrt{\bar{v} - \frac{\gamma^2}{8\kappa}}, \quad b_1 = \sqrt{v_0} - a_1, \quad c_1 = -\log[(\Lambda_v(1) - a_1)/b_1], \tag{3.67}$$

$$a_2 = \sqrt{\bar{z} - \frac{\epsilon^2}{8\beta}}, \quad b_2 = \sqrt{z_0} - a_2, \quad c_2 = -\log[(\Lambda_z(1) - a_2)/b_2]. \tag{3.68}$$

The approximations employed in the *affine limit 1* of the HCV model correspond to *freezing the initial interest rates* - a technique commonly used to reduce complexity in the drift calculation

of Libor Market Models. The original idea of the displaced-diffusion (DD) concept is to mix normal and log-normal behavior of interest rates; by the choice $b_k = 0$ the concept of mixing is abandoned and only normal model features are retained.
In any event the approach appears viable for discussion and the affine model resulting within this approximation limit 1 is elaborated below.

- **Limit 2:** In order to retain the original ideas of the DD concept, an alternative derivation appears relevant, where the non-affine components of the displaced-diffusion term are projected onto a time-dependent function $\alpha(t)$:

$$\begin{aligned} s_k \Phi_k^A(t) &= s_k \left(b_k (f(0,t) + \alpha(t)) + (1-b_k)(f(0,0) + x_{c,0}) \right), \qquad (3.69) \\ \text{and consequently} & \\ (s_k \Phi_k^A(t))^2 &= s_k^2 [b_k^2 \zeta^2(t) + 2 b_k (1-b_k) \pi_0 \zeta(t) + (1-b_k)^2 \pi_0^2], \qquad (3.70) \\ \text{with} & \\ \pi_t &= f(0,t) + x_{c,t}, \\ \zeta(t) &= f(0,t) + \alpha(t). \end{aligned}$$

Then, the affine approximation of the DDSV volatility specification results in

$$\begin{aligned} \eta_t^A &= \delta_z(t) s_k [b_k \zeta(t) + (1-b_k)\pi_0], \qquad (3.71) \\ (\eta_t^A)^2 &= z_t (s_k \Phi_k^A(t))^2. \end{aligned}$$

This strategy is referred to as *affine limit 2* in the following. The crucial point is to find a suitable time-dependent projection $\alpha(t)$ to serve as affine proxy of the stochastic variable $x_{c,t}$. A possible choice is to use the expected value of $x_{c,t}$ as time-dependent projection

$$\begin{aligned} \alpha(t) &= \mathbb{E}[x_{c,t}], \qquad (3.72) \\ \text{with} \quad \mathbb{E}[x_{c,t}] &= \tfrac{\eta_0^2}{2\lambda^2}(1 - e^{-\lambda t})^2. \end{aligned}$$

Applying the expectation in this form implicitly presumes $x_{c,t}$ to evolve with the undisturbed initial value of η_0 (as if DDSV effects would not be present). So the decisive difference between affine limits 1 and 2 are summarized as follows:
In the affine limit 2 the initial volatility η_0 of the affine proxy $\alpha(t)$ in the DDSV specification is presumed to be *frozen* to the initial value, whereas in the affine limit 1 the IR Markov variable $x_{c,t} = x_{c,0}$ is presumed to be *frozen*.
Apparently, the approximation assumptions are significantly more restrictive in the affine limit 1 than in the affine limit 2. Limit 1 completely removes any DD effects. Limit 2 is devised to retain an adequate representation of DD effects in the affine model version H2CV. In section 3.6.4 the comparison of the full HCV model with the H2CV model results proves that these particular choices of $\alpha(t)$ are viable proxies of $x_{c,t}$, and the affine limit 2 gives an accurate affine approximation of DDSV effects in the Heston DDSV Cheyette (HCV) model.

In the next section the essentials of the CHF of model limit 1 are detailed. In accordance with the previous abbreviations the model is named H1CV. The second limit option H2CV is considered subsequently.

3.6.1 Heston DDSV Cheyette Model in Affine Deterministic Limit (H1CV)

The derivation of the H1CV characteristic function (CHF) assuming the limit 1 approximations is detailed in Appendix B.3 resulting in:

$$\hat{\Phi}_{H1CV}(u, \mathbf{X}_t, t, T) = e^{A(u,\tau)+iux_{s,t}+D(u,\tau)v_t+C(u,\tau)x_{c,t}+Z(u,\tau)z_t+Y(u,\tau)y_t}. \tag{3.73}$$

The relevant Fourier coefficients are obtained as solutions of the defining ODEs from the affine system according to the techniques introduced in section 2.1 (Appendix B.3 and dependent appendices of relevance contain the details of the derivation).
Solutions for $B(u,\tau)$, $C(u,\tau)$ and $D(u,\tau)$ are equivalent to the affine Heston and HHW models. $Y(u,\tau)$ in (3.88) is obtained by variation of constants. According to the derivations in Appendix B.3 there is a connection between Fourier coefficients $Y(u,\tau)$ and $C(u,\tau)$:

$$Y(u,\tau) \quad = \quad -\tfrac{1}{2\lambda^2}(1-iu)(1-e^{-\lambda\tau})^2 = -\tfrac{1}{2(1-iu)}C^2(u,\tau). \tag{3.74}$$

$Z(u,\tau)$ in equation (3.83) is a Riccati-type differential equation for the SV of the IR component, where the coefficients are in this instance time-dependent. Employing the solutions for the other Fourier coefficients and presuming $\rho_{cz} = 0$, the defining ODE is of the form

$$\begin{aligned} \tfrac{d}{d\tau}Z(u,\tau) \quad &= \quad \tfrac{\epsilon^2}{2}Z^2(u,\tau) - \beta Z(u,\tau) + q_1(u,\tau), \\ \text{with} \quad q_1(u,\tau) \quad &= \quad \tfrac{iu}{2-2iu}C^2(u,\tau) = \tfrac{iu(iu-1)}{2\lambda^2}s_k^2\Phi_k^2(1-e^{-\lambda\tau})^2. \end{aligned} \tag{3.75}$$

One has to resort to standard numerical methods for ODE solution or to simplify towards $q_1(u,\tau) = q_1(u)$ (i.e. time independent parameters) where the solution is then just a variation of the well-known Heston-type Riccati equation as elaborated below.
Again by straightforward integration we find for $A(u,\tau)$

$$\begin{aligned} A(u,\tau) \quad &= \quad -\int_0^\tau f(0,t)\,d\tau + \kappa\bar{v}\int_0^\tau D(u,\tau)\,d\tau - \beta\bar{z}\int_0^\tau Z(u,\tau)\,d\tau \\ &+ \quad \tfrac{1}{2}\rho_{cx}s_k\Phi_k\int_0^\tau \delta_v(t)\delta_z(t)B(u,\tau)C(u,\tau)\,d\tau \\ &= \quad -\int_0^\tau f(0,t)\,d\tau + \kappa\bar{v}I_2(u,\tau) + \beta\bar{z}I_5(u,\tau) + \tfrac{1}{2}\rho_{cx}s_k\Phi_k I_7(u,\tau), \end{aligned} \tag{3.76}$$

where the integral $I_2(u,\tau)$ is from the derivation of the H1HW model in Appendix 3.2.1, $I_5(u,\tau)$ equals the integral resulting from the IR-SV process in the DDSV Cheyette model, and

$$\begin{aligned} I_7(u,\tau) \quad &= \quad -\tfrac{1}{\lambda}(1-iu)[a_1a_2(\tau + \tfrac{1}{\lambda}(e^{-\lambda\tau}-1)) + \tfrac{a_1b_2}{c_2}(e^{-c_2(T-\tau)} - e^{-c_2T}) + \tfrac{a_2b_1}{c_1}(e^{-c_1(T-\tau)-c_1T}) \\ &+ \quad \tfrac{b_1b_2}{c_1+c_2}(e^{-(c_1+c_2)(T-\tau)} - e^{-(c_1+c_2)T}) \\ &- \quad \tfrac{a_1b_2}{c_2-\lambda}e^{-c_2T}(e^{(c_2-\lambda)\tau}-1) - \tfrac{a_2b_1}{c_1-\lambda}e^{-c_1T}(e^{(c_1-\lambda)\tau}-1) \\ &- \quad \tfrac{b_1b_2}{c_1+c_2-\lambda}e^{-(c_1+c_2)T}(e^{(c_1+c_2-\lambda)\tau}-1))]. \end{aligned} \tag{3.77}$$

In order to render the CHF evaluation efficient, closed form analytic representations of all Fourier coefficients and corresponding integrals are of high value. Therefore, the coefficient $Z(u,\tau)$ is approximated yielding closed form expressions.
We presume $q_1(u,\tau)$ to be piecewise constant in time, i.e.

$$q_1(u,\tau) \simeq q_1(u,\tau_j) = \tfrac{iu(iu-1)}{2\lambda^2} s_k^2 \Phi_k^2 (1-e^{-\lambda\tau_j})^2, \tag{3.78}$$

on intervals $\tau_j \in [T_j, T_{j+1}[$ for a particular choice of refinement $0 \le j \le j_{max}$. Then, the Cheyette SV process is recursively given by

$$Z_j(u,\tau_{j+1}) = Z(u,\tau_j) + \tfrac{\xi_{j+1}^-}{\epsilon^2} \frac{1-e^{-d_{j+1}(\tau_{j+1}-\tau_j)}}{1-\frac{\xi_{j+1}^-}{\xi_{j+1}^+} e^{-d_{j+1}(\tau_{j+1}-\tau_j)}}, \tag{3.79}$$

with coefficients (3.80)

$$\begin{aligned} \hat{d}_{j+1} &= \sqrt{\beta^2 - 2\hat{\alpha}\epsilon^2}, \\ \hat{\xi}_j^{\pm} &= \beta \pm (d_{j+1}+d_j)/2 - \epsilon^2 Z_j, \\ \hat{\alpha} &= \tfrac{iu(iu-1)}{2\lambda^2} s_k^2 \Phi_k^2 (1-e^{-\lambda\tau_j})^2. \end{aligned}$$

The quality of the recursive approximation is shown in Fig. E.2 where the numerical evaluation of the ODE by a standard Runge-Kutta method is compared to the analytic approach of recursive $Z(u,\tau_i)$ computation on subsequent time intervals. For parameters typically obtained in calibration scenarios, the analytic approach shows high quality and superior performance in CPU time.
With the mean-reversion parameter λ sufficiently large (i.e. $\lambda > 1$ is actually a merely academic construction, since $10^{-2} \le \lambda \le 10^{-3}$ are typical calibration results), the time dependence in $q(u,\tau)$ is lost, as

$$q(u,\tau) \simeq \tfrac{iu(iu-1)}{2\lambda^2} s_k^2 \Phi_k^2 \check{q}(u), \tag{3.81}$$

appears as viable approach. Then,

$$\tfrac{d}{d\tau}\check{Z}(u,\tau) = \tfrac{\epsilon^2}{2}\check{Z}^2(u,\tau) - \beta\check{Z}(u,\tau) + \check{q}(u), \tag{3.82}$$

is of well-known Riccati-type, with elementary solution

$$\begin{aligned} \check{Z}(u,\tau) &= \check{\xi}^- \frac{1-e^{-\check{d}\tau}}{1-\check{g}e^{-\check{d}\tau}}, \\ \text{with} \quad \check{g} &= \frac{\check{\xi}^-}{\check{\xi}^+}, \\ \check{\xi}^{\pm} &= \tfrac{1}{\epsilon^2}\left(\beta \pm (\beta^2 - 2\check{\alpha}\epsilon^2)^{\frac{1}{2}}\right), \\ \check{\alpha} &= \tfrac{iu(iu-1)}{2\lambda^2} s_k^2 \Phi_k^2, \end{aligned} \tag{3.83}$$

and the corresponding integral results in the form

$$\int_0^\tau \check{Z}(u,\tau)\,d\tau = \check{\xi}^-\tau - \frac{2}{\epsilon^2}\ln\left[\frac{1-\check{g}e^{-\check{d}\tau}}{1-\check{g}}\right] \equiv \check{I}_2(u,\tau). \tag{3.84}$$

For the applications discussed in this thesis the recursive solution is the approach chosen.

3.6.2 Transformation of the H1CV to the T-forward measure

The stock price dynamics under the T-forward measure are derived in section 3.5.2 above. The CHF of the affine model approximation is given under the $\mathbb{Q}^T$ measure. For the state vector $\hat{\mathbf{X}}_t = [y_t, z_t, x_{c,t}, v_t, \hat{x}_t]^\dagger$ the affine decomposition of the SDE system in the T-forward measure assumes the form:

$$\begin{aligned}
\mu(\hat{\mathbf{X}}_t) &= a_0 + a_1 \mathbf{X}_t = \left(\begin{array}{c} s_k^2\Phi_k^2 z_t - 2\lambda y_t \\ \beta(\bar{z} - z_t) + \rho_{cz}\epsilon s_k \Phi_k B_c z_t \\ \hdashline y_t - \lambda x_{c,t} + s_k^2 \Phi_k^2 B_c z_t \\ \hdashline \kappa(\bar{v} - v_t) \\ \rho_{xc} s_k \Phi_k B_c \sqrt{v_t}\sqrt{z_t} - \frac{1}{2} s_k^2 \Phi_k^2 B_c^2 z_t - \frac{v_t}{2} \end{array}\right) \qquad (3.85) \\
&= \left(\begin{array}{c} 0 \\ \beta\bar{z} \\ 0 \\ \hdashline \kappa\bar{v} \\ \rho_{xc} s_k \Phi_k B_c \delta_v(t)\delta_z(t) \end{array}\right) + \left(\begin{array}{ccc:cc} -2\lambda & s_k^2\Phi_k^2 & 0 & 0 & 0 \\ 0 & -\beta & \rho_{cz}\epsilon s_k \Phi_k B_c & 0 & 0 \\ 1 & s_k^2\Phi_k^2 B_c & -\lambda & 0 & 0 \\ \hdashline 0 & 0 & 0 & -\kappa & 0 \\ 0 & -\frac{1}{2}s_k^2\Phi_k^2 B_c^2 & 0 & -\frac{1}{2} & 0 \end{array}\right) \left(\begin{array}{c} y_t \\ z_t \\ x_{c,t} \\ \hdashline v_t \\ \hat{x}_t \end{array}\right);
\end{aligned}$$

$$\begin{aligned}
\Sigma_{\hat{\mathbf{X}}_t} &= LL^\dagger = c_0 + c_1^\dagger \hat{\mathbf{X}}_t \qquad (3.86) \\
&= \left(\begin{array}{ccc:cc} 0 & 0 & 0 & 0 & 0 \\ 0 & 0 & 0 & \rho_{zv}\epsilon\gamma\delta_v\delta_z & \rho_{zx}\epsilon\delta_v\delta_z \\ 0 & 0 & 0 & \rho_{cv}\gamma s_k\Phi_k\delta_v\delta_z & \rho_{cx}s_k\Phi_k\delta_v\delta_z \\ \hdashline 0 & \rho_{vz}\gamma\epsilon\delta_v\delta_z & \rho_{vc}s_k\Phi_k\gamma\delta_v\delta_z & 0 & -\rho_{vc}\gamma s_k\Phi_k B_c\delta_v\delta_z \\ 0 & \rho_{xz}\epsilon\delta_v\delta_z & \rho_{xc}s_k\Phi_k\delta_v\delta_z & -\rho_{vc}\gamma s_k\Phi_k B_c\delta_v\delta_z & -2\rho_{xc}s_k\Phi_k B_c\delta_v\delta_z \end{array}\right) \\
&+ \left(\begin{array}{ccc:cc} 0 & 0 & 0 & 0 & 0 \\ 0 & \epsilon^2 & \rho_{zc}\epsilon s_k\Phi_k & 0 & -\rho_{cz}\epsilon s_k\Phi_k B_c \\ 0 & \rho_{cz}\epsilon s_k\Phi_k & s_k^2\Phi_k^2 & 0 & -s_k^2\Phi_k^2 B_c \\ \hdashline 0 & 0 & 0 & 0 & 0 \\ 0 & -\rho_{cz}\epsilon s_k\Phi_k B_c & -s_k^2\Phi_k^2 B_c & 0 & 0 \end{array}\right)^\dagger z_t + \left(\begin{array}{ccc:cc} 0 & 0 & 0 & 0 & 0 \\ 0 & 0 & 0 & 0 & 0 \\ 0 & 0 & 0 & 0 & 0 \\ \hdashline 0 & 0 & 0 & \gamma^2 & \rho_{xv}\gamma \\ 0 & 0 & 0 & \rho_{xv}\gamma & 1 \end{array}\right)^\dagger v_t; \\
r &= r_0 + \mathbf{r_1}^\dagger \hat{\mathbf{X}}_t = 0 + (0,1,0,0)^\dagger \hat{\mathbf{X}}_t. \qquad (3.87)
\end{aligned}$$

As indicated by the broken lines, under the T-forward measure the matrices separate into IR and EQ components without any cross terms. For the corresponding Fourier state vector $\mathbf{B} = [Y, Z, C, D, B]^\dagger$ the coefficients of the CHF follow from the defining ODEs:

$$\begin{aligned}
\tfrac{d}{d\tau}\mathbf{B}(u,\tau) &= -\mathbf{r_1} + a_1^\dagger \mathbf{B} + \tfrac{1}{2}\mathbf{B}^\dagger (c_1)_{\hat{\mathbf{X}}_t} \mathbf{B}, \quad \text{i.e.} \\
\tfrac{d}{d\tau}Y(u,\tau) &= -2\lambda Y + C, \\
\tfrac{d}{d\tau}Z(u,\tau) &= \tfrac{\epsilon^2}{2}Z^2 + (\rho_{cz}\epsilon s_k\Phi_k C(1-iu)\beta)Z(1-2iu)s_k^2\Phi_k^2 C^2, \\
\tfrac{d}{d\tau}C(u,\tau) &= -1 + \rho_{cz}\epsilon s_k\Phi_k B_c Z - \lambda C, \\
\tfrac{d}{d\tau}D(u,\tau) &= \tfrac{\gamma^2}{2}D^2 + (\rho_{xv}\gamma B - \kappa)D + \tfrac{B}{2}(B-1), \\
\tfrac{d}{d\tau}B(u,\tau) &= 0,
\end{aligned} \qquad (3.88)$$

$$
\begin{aligned}
\text{and} \quad \tfrac{d}{d\tau}A(u,\tau) &= -r_0 + \mathbf{B}^\dagger a_0 + \tfrac{1}{2}\mathbf{B}^\dagger c_0 \mathbf{B}, \\
\longrightarrow \tfrac{d}{d\tau}A_{EV}(u,\tau) &= -f(0,t) + \rho_{xc} s_k \Phi_k C \delta_v \delta_z (1 - B^2) \\
&+ D(\kappa\bar{v} - \rho_{vc}\gamma s_k \Phi_k C \delta_v \delta_z B), \\
\longrightarrow \tfrac{d}{d\tau}A_{IV}(u,\tau) &= Z(\beta\bar{z} + \rho_{vz}\epsilon\gamma\delta_v\delta_z D + \rho_{xz}\epsilon\delta_v\delta_z B) \\
&+ C(\rho_{vc} s_k \Phi_k \gamma \delta_v \delta_z D + \rho_{xc} s_k \Phi_k \delta_v \delta_z B).
\end{aligned} \tag{3.89}
$$

The defining ODE for $A(u,\tau)$ is already split into components contributing to EQ-SV components $A_{EV}(u,\tau)$, and IR-SV components $A_{IV}(u,\tau)$, respectively. Then, with initial conditions $B(u,0) = iu$, $Y(u,0) = 0$, $C(u,0) = 0$, $D(u,0) = 0$, $A(u,0) = 0$ and $\mathbf{u}^\dagger = [0,0,0,0,u]^\dagger$, the corresponding solutions are

$$
\begin{aligned}
Y(u,\tau) &= -\tfrac{1}{2}C^2(u,\tau), \\
C(u,\tau) &= -\tfrac{1}{\lambda}(1 - e^{-\lambda\tau}) = B_c(t,T) \quad (\text{when } \rho_{\text{cz}} = 0 \,\text{is presumed}), \\
B(u,\tau) &= iu, s \\
A_{H1CV}(u,\tau) &= \int_0^\tau [\tfrac{d}{d\tau}A(u,\tau)]d\tau.
\end{aligned}
$$

$Z(u,\tau)$ is the numerical solution described in equation (3.83). $D(u,\tau)$ is the standard Heston Riccati solution. Since the IR dynamics separate, the CHF of the H1CV in the T-forward measure reduces to

$$
\hat{\Phi}^T(\mathbf{u}, \hat{\mathbf{X}}_t, T, t) = \mathbb{E}^T\left[e^{i\mathbf{u}^\dagger \hat{\mathbf{X}}_t} | \mathcal{F}_t\right] = \mathbb{E}^T\left[e^{iu\hat{x}_t} | \mathcal{F}_t\right] = e^{A^T_{H1CV}(u,\tau) + B(u,\tau)\hat{x}_t + D(u,\tau)v_t}, \tag{3.90}
$$

with terminal condition $\hat{\Phi}^T(u, \hat{\mathbf{X}}_t, T, T) = e^{i\mathbf{u}^\dagger \hat{\mathbf{X}}_T} = e^{iu\hat{x}_T}$ and

$$
\begin{aligned}
\tfrac{d}{d\tau}A^T_{H1CV}(u,\tau) &= \tfrac{d}{d\tau}A_{EV} = -f(0,t) + \rho_{xc} s_k \Phi_k B_c \delta_v \delta_z (1 - B^2) \\
&+ D(\kappa\bar{v} - \rho_{vc}\gamma s_k \Phi_k B_c \delta_v \delta_z B).
\end{aligned} \tag{3.91}
$$

3.6.3 Impact of IR-SV and characteristics of the affine H1CV model

The Heston DDSV Cheyette (HCV) model is a full-scale hybrid model with two essential qualities:

- **(i) Stochastic volatility in interest rates generates hybrid smiles.** This actually means, that by virtue of the CIR type IR-SV process, the HCV model reproduces smile features in the IR component in analogy to the Heston process in EQ; in combination, EQ-SV and IR-SV constitute hybrid smiles - smile features originating out of both asset classes sensitive to the hybrid correlation ρ_{xc}. The stochastic volatility effects incorporated by the HCV model are consistent with market observations: The zero bond value in the Cheyette model depends solely on the state variables $x_{c,t}$ and y_t, the latter containing IR-SV contributions implicitly. Consequently a portfolio of zero bonds is insensitive to variations in IR-SV, whereas other IR

derivatives (like caplets, swaptions etc.) are sensitive to risk patterns introduced in the presence of IR-SV. Therefore IR-SV as additional risk factor cannot be hedged within a trading book simply consisting of zero bonds alone. This falls into place with the reality observed in IR markets. Hence, to point out this characteristic, the HCV model is called *true* IR-SV model.

- (ii) The HCV is a Markovian Gaussian model with volatility specification under the bond measure. The HLMM is a non-Markovian log-normal model based on Libor rate volatilities under the forward measure. **Short rate and market model features are mixed by DDSV extensions.** The Cheyette approach bridges between the short rate and market model: The number of state variables is controlled by the volatility specification and in the HCV exceeds the dimension of classical short rate models. Displaced-diffusion extensions introduce log-normal (i.e. market model) features into the classical Cheyette approach, allowing for implied volatility base skew conformalizations formerly only associated with market models.

In section 3.6.1 the H1CV model was derived as the approximation of the HCV model in the affine limit 1. In the following the H1CV model is discussed with focus on these aspects:

- **(i) Validation of affine model fidelity.** The first task is to clarify, whether the H1CV is an accurate representation of the HCV hybrid model. The approximation is accurate, when hybrid smile and skew features are correctly reproduced within a reasonable space of realistic scenario parameters. Hybrid smiles are understood as combination of smile characteristics originating on the EQ side by an EQ-SV process and on the IR side by a corresponding IR-SV equivalent. The EQ-IR hybrid correlation ρ_{xc} is the control parameter for cross-asset interaction and hybrid smiles.

  The quality of smile representations is judged by comparing the H1CV evaluated by inverse transforms and the corresponding full model in Monte-Carlo simulations. The comparison is done both in the spot measure $\mathbb{Q}^B$ and the terminal measure $\mathbb{Q}^T$, as function of moneyness, hybrid correlation ρ_{xc}, and maturity of hybrid derivative contracts, respectively. Aside from derivative prices, the Black implied volatilities corresponding to the individual model evaluations are used as basis. In general the model validation is based on the numerical experiments presented in the following.

- **(ii) Limits of affine approximations.** Approximations are not perfect and carry drawbacks in form of deviations from the original non-affine model. When scenario parameters are pushed towards unrealistic limits, the quality of affine approximations weakens, and spurious deviations in derivative prices between affine and full model evaluations arise.

  Deviations between affine and full model versions are in general not necessarily serious. Each model is based on a number of a priori assumptions and is designed to represent a variety of market features. Once calibrated, the model is supposed to have predictive power for futures states of market observables - ideally for a number of observables beyond the ensemble size of calibration instruments, and for a significant future period. We strive to discuss the limits of the affine approximations of the H1CV.

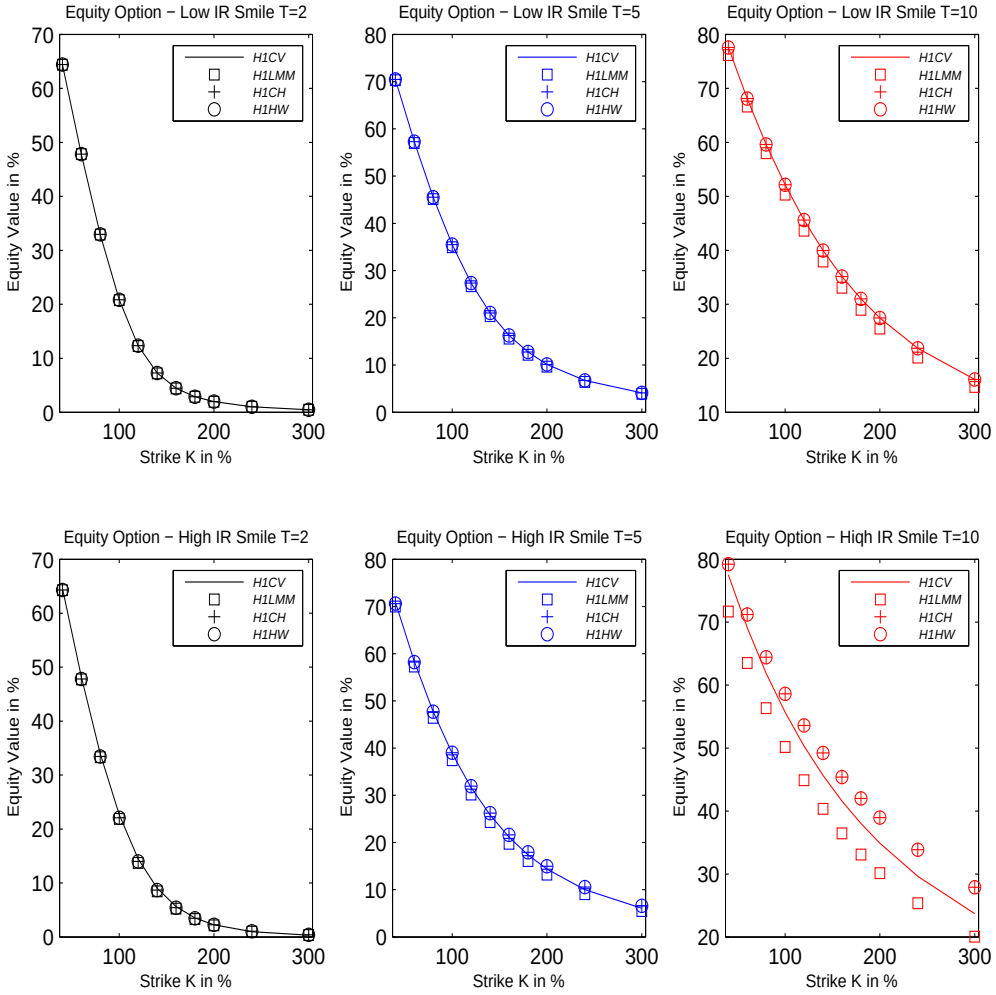

Figure 3.3: Comparison of EQ call option prices obtained with all affine hybrid models H1HW, H1CH, H1CV, and H1LMM at disposal. H1CV and H1LMM incorporate IR-SV contributions. All models are evaluated by the Carr-Madan FFT technique (damping factor $\alpha = 0.75$) for deliberately high EQ-IR correlation $\rho_{xc} = 0.9$ at times T=2, 5 and 10. Upper part: Model parameters reflect neglegible IR smile contributions with particular choices β=10^{-4} and ϵ=10^{-4} in order to confirm that the H1CV model based on the Heston SV Cheyette hybrid model smoothly reduces into the H1CH limit where deterministic IR volatilities are observed. Lower part: Emphasis on significant IR-SV contributions in hybrid prices by the extreme choices β=0.1 and ϵ=1.2 - mostly for illustrative purposes and to introduce the discussion about the quality and limits of affine approximations.

Affine H1CV model fidelity:

In order to judge the quality of affine H1CV model approximations, several consistency checks need to be performed to ensure the discussion is based on accurate and bias-free results. Affine models are evaluated by the Carr-Madan (CM) FFT and COS expansion techniques. Results obtained by both inverse transform methods are consistent, though for the discussion within the current section

the Carr-Madan results are shown. The choice to plot CM results is completely arbitrary, as the calculated values are indistinguishable (within numerical errors) between CM and COS methods. CM results rely on the judicious choice of the damping parameter α; an optimal choice of α can be found by careful analysis of the underlying CHF for each individual set of parameters, but is rather time consuming and not applicable in general model scenarios with broad parameter spectra. Therefore, α is tuned to values where results are stable and rather insensitive to variations of α; for the investigations at hand $\alpha = 0.75$ is typical, and is used as quasi-optimal choice. The COS method depends on the choice of a characteristic scale length L over which COS expansion methods are applied. L needs to be tuned heuristically presuming to obtain stable COS results insensitive to slight variations in L. For the evaluations presented here, L=10 to 17 is found to be suitable.
For CM evaluations a numerical grid consisting of 2^{16} points is used; the COS series expansion is cut-off typically at $N_{max} = 2^{10} - 2^{12}$. The equivalence of results for CHF evaluations in the spot measure $\mathbb{Q}^B$ and the terminal measure $\mathbb{Q}^T$, up to spurious numerical discrepancies, are the preconditons for the statement that the **results under discussion obtained by inverse transform techniques are consistent.**
The corresponding full models are evaluated via the Monte-Carlo (MC) schemes described in section 3.5.3. MC schemes in the spot $\mathbb{Q}^B$ and the terminal measure $\mathbb{Q}^T$ are inherently bias free in the IR component; Martingale corrections as suggested in [7] are employed to render EQ-SV and IR-SV process simulations also unbiased. Consequently, MC sampling and discretization errors remain as sources of simulation errors. Time discretizations are varied between 400 and 1600 time steps for each maturity interval $\Delta T = 1$. The reduction of the MC sampling error has been monitored over the range from $N = 10^5$ to $N = 10^8$ MC paths to ensure the MC standard error reduces according to the expected $\sim 1/\sqrt{N}$ behaviour.
Simulation results are presented for 800 timesteps per ΔT and 10^6 MC sampling paths. The interpretation of results relies only on the characteristics of the hybrid model under investigation. Results are supposed to be independent of the specific choice of the underlying simulation technique. In analogous argumentation as for the affine model evaluations before, the **results obtained by MC evaluation of the full non-affine original models are consistent.**
Another point to be clarified in the prologue of H1CV model validation is to sort out the scenario parameters and values of specific interest. Obviously, the choice of parameters is expected to point out the influence of IR-SV contributions. Therefore, hybrid model evaluations are studied for a fixed set of Heston parameters in order to have a pre-defined EQ component as reference. The selected Heston parameters are $\kappa = 0.8$, $\bar{v} = v_0 = 0.1$, $\gamma = 0.5$, $\rho_{xv} = -0.3$ and an at-the-money (ATM) security value of $S_0 = 100$. The Heston parameters are chosen deliberately to have a case where the Feller condition is violated - this is typical in realistic market environments. In order to get a first impression where IR-SV contributions become relevant in derivatives pricing, we vary parameters in Figs. E.1 and E.3. In both figures the affine hybrid model approximations are computed by the Carr-Madan FFT method where pricing is accomplished within split seconds. From Fig. E.1 it is evident that IR-SV contributions are most prominent at long maturities, high correlation ρ_{xc} between EQ and IR components, and in the regime where hybrid products are far out-of-the-money (OTM). Simulations are performed up to $T = 10$ with correlations up to $\rho_{xc} = 0.9$, and OTM EQ

option prices are calculated up to 300 % of the ATM baseline.

Fig. E.3 shows EQ prices and associated implied volatilities for all affine hybrid models at disposal. Evidently, the H1CV collapses to the H1HW/H1CH hybrid models in case of vanishing IR-SV contributions (as seen in the left half of the figure over the complete range of maturities). When IR-SV influences are significant for deliberately high IR-SV volatility $\epsilon = 1.2$ and high EQ-IR correlation $\rho_{xc} = 0.9$, the H1CV model shows characteristics distinguishable from the H1HW/H1CH model, and also from the H1LMM model, though the latter incorporates the same IR-SV process.

Out of these first findings the parameters for *low IR smile* and *high IR smile* scenarios are defined in Fig. 3.3. Based on the scenarios, the discussion of the H1CV model characteristics and model performance is presented in the subsequent figures.

In Fig. 3.4 the EQ call option prices obtained by the affine H1CV model are compared with the values from MC evaluation of the full non-affine HCV model. The comparison shows the quality of affine approximations, with particular emphasis on the representation of hybrid smiles at $\beta = 0.1$ and $\epsilon = 1.2$ when EQ-IR correlation is varied for $\rho_{xc} = \{0.2, 0.5, 0.9\}$ at long maturity $T = 10$. In order to assess the model fidelity the equivalent comparison is plotted for the H1CH and HCH as the respective affine and full model versions without IR-SV contributions (H1CH is equivalent to H1HW which is discussed in previous publications [1]). The figure shows two sets of scenario parameters, both are based on *high IR smile* contributions from the IR-SV process. Set 1 combines *high IR smile* parameters ($\beta = 0.3$ and $\epsilon = 1.2$) with HW model values ($\lambda = 0.1$, $s_k = 0.0125$) typically observed in realistic market settings; Set 2 uses even more extreme parameters as *high IR smile* scenario ($\beta = 0.1$ and $\epsilon = 1.2$) combined with very high HW model volatilities ($\lambda = 0.1$, $s_k = 0.025$) to show the limits of affine model approximations.

The affine H1CV performs extremely well for the scenario Set 1, exhibiting accuracy for any value of moneyness, EQ-IR correlation and maturity. The performance over the complete regime of maturities has been validated; accuracy is easily inferred from the results shown in Fig. 3.4 as any inherent divergencies would integrate with time and would yield discrepencies, whenever recognizable, at the highest maturity.

Consequently, the affine H1CV fidelity is satisfactory - an observation confirmed by the comparision in implied volatilities in Fig. 3.5. Implied volatilities are more sensitive to inherent model discrepancies, but even when affine approximations are employed under these constraints, the model fidelity proves to be essentially unchanged in this numerical experiment.

Up to this point the model discussion is based on the EQ prices of hybrid derivative products. However, the underlying IR-SV process and displaced-diffusion (DD) extensions affect IR derivatives such as caplets and swaptions. Caplet prices obtained from the IR component of the HCV model are shown for various DD choices with and without IR-SV contributions in Fig. 3.6. By construction the H1CV is an affine limit corresponding to $b_k = 0$, where the initial short rates are frozen in the DD volatility specification and the mixture with log-normal model features is neglected. This corresponds to the implied volatility surfaces shown in the left part of Fig. 3.6. Apparently, DD features become significant with increasing parameter b_k. Consequently, whenever log-normal features are present in the realistic IR markets (indicated by flattening out of the base skew of implied volatilities corresponding to IR products serving as benchmark instruments) the H1CV shows deviations from

the HCV model. This opens the subsequent discussion of the limits of affine H1CV approximations.

Limits of affine approximations in the H1CV:

As already noted the H1CV neglects DD contributions a priori, and hence, deviations from the full HCV model become apparent as soon as the DD base skew in the HCV model is introduced. By nature, the H1CV exhibits the orginal base skew inherent to all Gaussian short rate models. In case DD contributions would be correctly represented in the affine approximation H1CV, the implied volatilities would appear less skewed with increasing parameter b_k. In the same line of argument the HLMM, as log-normal model, shows flat implied volatilities. In the H1LMM however, since the same affine approximation is employed which is based on *freezing the inital state of IR rates* in the DDSV volatility, the H1LMM abandons the log-normal characteristics, and rather shows a base skew corresponding to normal models.
The caplet implied volatility surfaces in Fig. 3.6 are obtained from the IR component of the HCV, and expose the base skew characteristic to Gaussian models at $b_k = 0$; this base skew then flattens out when log-normal contributions are introduced towards higher b_k. The mixture of normal and log-normal model characteristics is of course the motivation for introducing the DD concept. This process is clearly resembled in the caplet implied volatility structures irrespective whether IR-SV contributions are superposed. As the H1CV is by construction incapable to reproduce DD log-normal features, it is instructive to study the impact on EQ derivative prices obtained by the hybrid model in the presence of DD base skew.
Fig. 3.7 shows implied volatilities of caplet and EQ call option prices as functions of the DDSV base skew. The comparison includes the affine H1CV and the corresponding full HCV model evaluations. Caplet implied volatilities are indicators of the IR component and call option implied volatilities benchmark the associated EQ component of the same hybrid model. Fig. 3.7 further includes the corresponding implied volatilities obtained by the H1CH model, where IR-SV contributions are neglected, but aside from that shares the same DD approximations as the H1CV; consequently, deviations from the affine DD approximations arise analogously when comparing H1CV with HCV and H1CH with HCH, respectively. In Fig. 3.7 deviations between full model and affine approximation are apparent in caplet volatilities for $b_k = 0.5$ and $b_k = 1.0$, where DD significantly reshapes the base skew. The deviations propagate via the EQ-IR correlations towards the EQ component of the hybrid model, where deviations in option values become significant throughout the entire OTM regime. Problems in model fidelity are observed equally in H1CV/HCV and H1CH/HCV, and hence, the deviations have DD approximations as origin and are supposedly insensitive to IR-SV contributions. A viable approach to include DD features in affine models is described in the next section where the affine H2CV model is detailed.
Another source of H1CV model weaknesses is observed when parameters become more extreme as in Set 2 (Fig. 3.4), where extreme IR-SV values are combined with challenging parameters in the HW / CH components. The resulting deviations between affine and full model are clearly observable in the corresponding implied volatilities shown in Fig. 3.5. It is wise to denote such limits in parameter space, even though put into context these appear not to impose restrictions with respect to

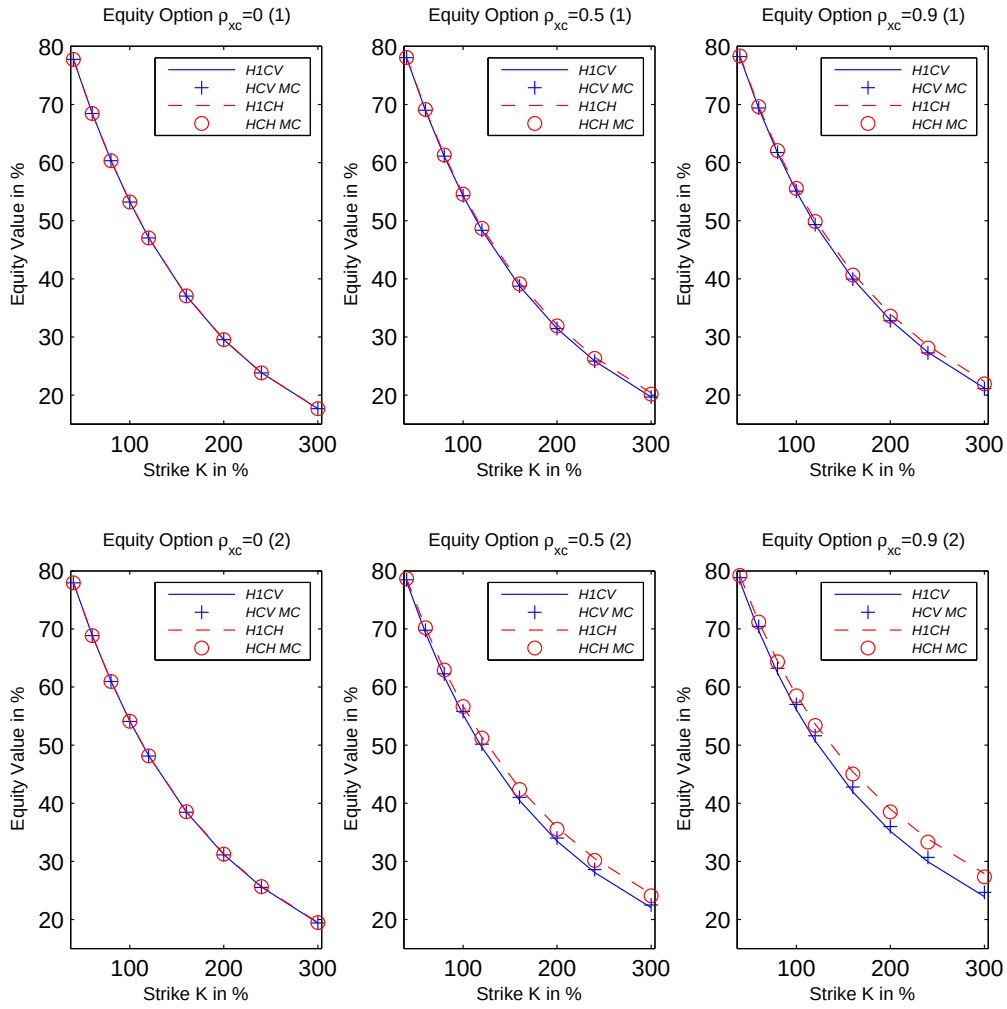

Figure 3.4: Crucial point to assess the quality and stability of affine approximations is the model behaviour with increasing EQ-IR correlation $\rho_{xc} = \{0, 0.5, 0.9\}$ as the decisive hybrid coupling parameter. Quality is contested by comparison with the full model evaluation; stability is stressed by the deliberate choice of extreme parameter sets. Equity option prices at T=10 are displayed for $\rho_{xc} = \{0, 0.5, 0.9\}$ and extreme choices of IR-SV model parameters: Set 1 is based on $\lambda = 0.1$, $s_k = 0.0125$ and $\beta = 0.3$, $\epsilon = 1.2$. Set 2 shows results for $\lambda = 0.1$, $s_k = 0.025$ and $\beta = 0.1$, $\epsilon = 1.2$. Affine models (H1CH/H1CV) are evaluated by the Carr-Madan method, full model equivalents (HCH/HCV) are obtained by Monte-Carlo (MC) simulations conducted in the spot measure $\mathbb{Q}^B$ with 10^6 paths and 800 time steps/ΔT (with ΔT=1). MC errors are below $8 \cdot 10^{-4}$ throughout all strikes shown, and hence, MC errors are below the size of marker symbols in all points.

model applicability in realistic scenarios. The deviations are not different from those observed in the H1HW/H1CH affine model approximations which are also plotted in Fig. 3.5 for comparison, and are studied and validated in earlier publications [1]. When HW volatilities assume values reasonable for realistic applications (actually corresponding to a general DDSV volatility level of $s_k \leq 0.02$), the affine approximations show the excellent model affinity as described above.

H1CV features in the context of H1HW/H1CH and H1LMM:

The H1CV model is connected to Gaussian short rate models, and shares a common choice for IR-SV contributions with the H1LMM. In addition the *freezing of initial Libors* introduces base skew features into the H1LMM, which are otherwise typical for short rate models. Hence, the H1CV is expected to expose characteristics inherent to both HW and DDSV LMM based hybrid model approaches. When DDSV extensions are included in the model, the overall volatility level is determined by the choice of s_k. HCV/H1CV and HLMM/H1LMM are related in linear order via $s_k^{H1CV}(t) = s_k^{H1LMM}(t) f_0(T)$ ($f_0(T)$ is the instantaneous forward rate as function of maturity T associated with the initial term structure at $t = 0$). For the discussion at hand $f_0 = 0.05$ is used, and therefore $s_k^{H1CV} = 0.0125$ and $s_k^{H1LMM} = 0.25$ correspond to quasi-equivalent basis levels in the volatility specification. The correspondence works well in practice as seen from Fig. E.3 where all affine model versions are compared. In case of negligible IR-SV contributions all models give comparable results, irrespective whether the affine model is Gaussian or log-normal based. At long maturities the different nature of the H1LMM shows small deviations in call option prices, though the differences become apparent only in implied volatilities at $T = 10$. When IR-SV contributions are significant (right side of Fig. E.3), the H1CV and H1LMM both exhibit hybrid smiles. The IR-SV process is equivalent in H1CV and H1LMM, but the DDSV volatility specification (or rather only the SV volatility specification, since DD effects are eliminated in the affine limit 1) is propagated in different fashion in H1CV and H1LMM as observable in Fig. E.3 (right side) in the valuation differences towards longer maturities. These differences are then patterns which are characteristic to whether the affine model has Cheyette or LMM based full model IR components, respectively. Pricing differences due to model specific characteristics are most interesting for hybrid products and are the central point of the discussion in chapter 4 below.

3.6.4 Heston DDSV Cheyette Model in Affine Limit 2 (H2CV)

In Fig. 3.8 the validity of the affine approximations in the limit 2 is studied by comparison with the full HCV model results for significant DD contributions at $b_k = 0.5$ and $b_k = 1.0$. At these b_k levels the H1CV model showed deficits in reproducing the DD features present in the HCV model. The implied caplet volatilities (top level plot series in Fig. 3.8) indicate that the H2CV model can basically follow the base skew prescribed by the DD model extensions, whereas the H1CV model (given as broken line for comparison) shows difficulties to reproduce DD base skew modifications. Consequently, the H2CV model succeeds in incorporating the mixture of normal and log-normal model contributions, and thereby retain DD effects in the limit of affine approximations. The affine limit 2 proves to be a viable approach, irrespective whether an IR-SV process is present or not. Consequently, by constructing the H2CV model, the corresponding H2CH model version (where IR-SV contributions are neglected), is automatically included as limiting case. Albeit small, there are systematic differences between H2CV and full HCV caplet impled volatilities recognizable. These

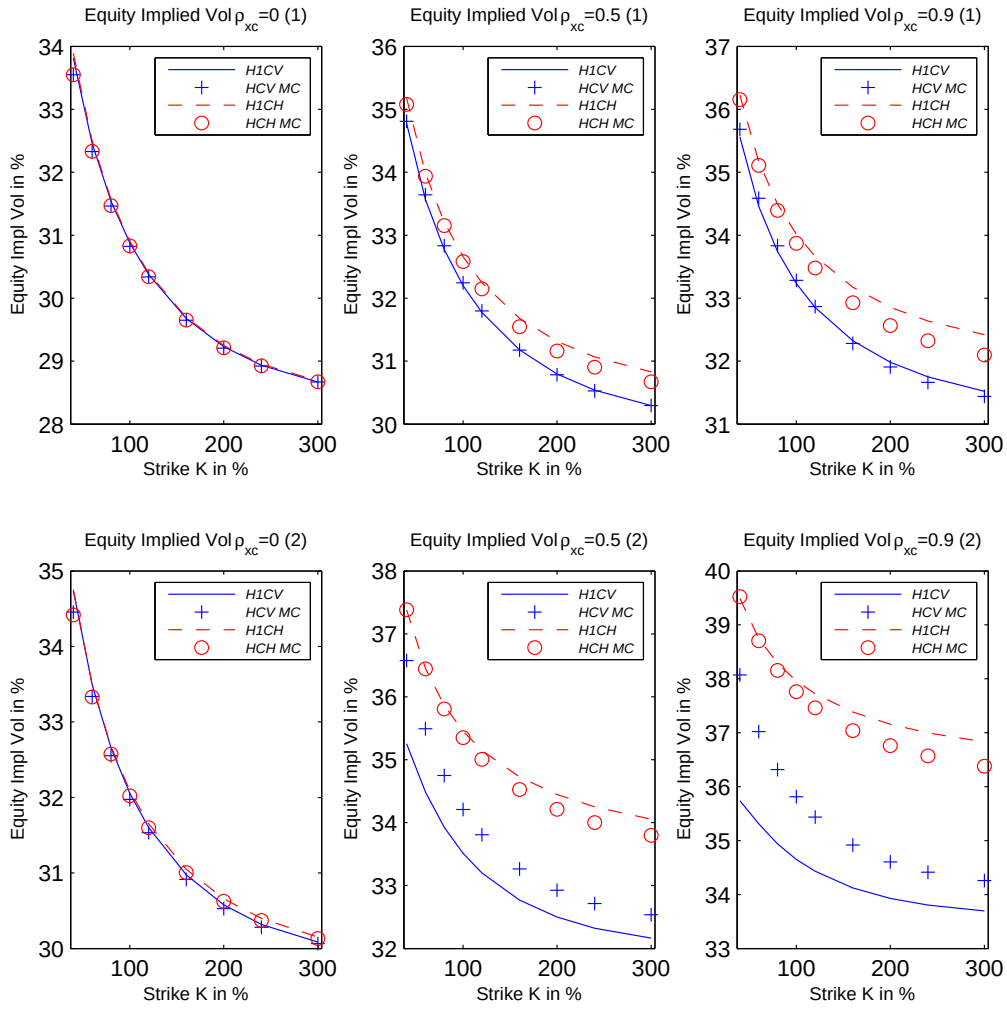

Figure 3.5: Implied volatilities corresponding to the option values shown in Fig. 3.4. Since implied volatilities are highly sensitive quality indicators, even slight deviations between affine approximation and original hybrid model become visible. Apparently the H1CV model introduced in the discussion at hand performs extremely well for the Set 1 over a wide range of EQ-IR correlations, albeit this scenario imposes already high IR-SV conditions in order to prove the validity of approximations. When pushing the limits even further in Set 2, fidelity of affine approximations tends to weaken, though deviations are comparable with the H1CH model without IR-SV characteristics and are still hardly recognizable in the corresponding EQ option prices.

deviations increase towards longer maturities T, at higher b_k values when DD effects are stressed, and in the presence of IR-SV processes, respectively. The reason for these empirical observations is motivated straightforwardly: By construction of the affine limit 2, the affine proxy $\alpha(t)$ in equation (3.72) is obtained with an approximative expected value of $x_{c,t}$ based on the presumption that η_0 is *frozen*; the expectation of $x_{c,t}$ is determined disregarding DDSV contributions 'a priori'. Consequently, deviations between H2CV and HCV models accumulate over maturity, and become more

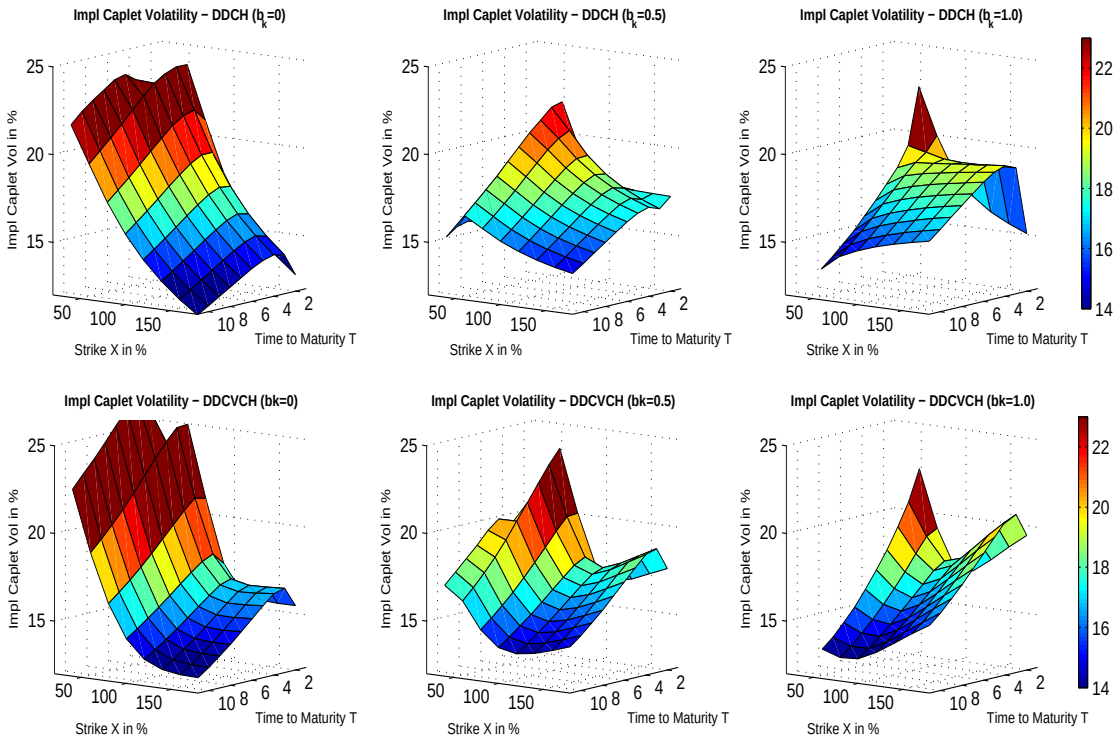

Figure 3.6: Implied caplet volatilities obtained for the DDSV Cheyette model (i.e. the IR component of the HCV model, abbreviated by DDCV CH). Different displaced-diffusion (DD) settings are selected by the choice of $b_k = \{0, 0.5, 1.0\}$, both without (plot series in upper half, abbreviated by DD CH) and with (lower half, abbreviated by DDCV CH) IR-SV contributions. The EQ option results shown in Figs. 3.4, 3.5 correspond to b_k=0, since the affine limit 1 precludes DD model features. Apparently DD contributions increase with growing b_k. When IR-SV is representable in the hybrid model (as is the case for the DDSV contributions in the CH model), the IR smile features appear superposed onto the DD base skew structure. Implied caplet volatilities are obtained for CH model parameters $f(0,t) = 0.05$, $\lambda = 0.1$, $s_k = 0.0125$ and SV parameters β=0.3, ϵ=1.2, respectively, by means of MC simulations conducted with 10^6 paths and 800 time steps/ΔT (and again $\Delta T = 1$). MC results obtained in $\mathbb{Q}^B$ and $\mathbb{Q}^T$ measures are equivalent within the typical error level of 0.1 bp.

pronounced in the presence of significant IR-SV contributions. The model bias introduced by the affine limit 2 approximations can be thought of as a systematic bias in the drift component of the $x_{c,t}$ propagation - consequently the systematic differences in caplet volatilities are independent of moneyness.

As DD effects are reproducable in the IR component, the H2CV model also succeeds in reproducing DDSV effects in the hybrid model in this case. Comparing EQ derivative prices evaluated by H2CV and full HCV models (lower level plot series in Fig. 3.8) proves that the H2CV model performs better than the H1CV model in reproducing call option prices. The H2CV model reproduces the characteristics of the HCV model particularly in the OTM regime, where hybrid model contributions are most important. The H2CV gives results close to the HCV model at the high EQ-IR correlations $\rho_{xc} = 0.9$ under discussion, where correlation effects are most critical and most important for hybrid

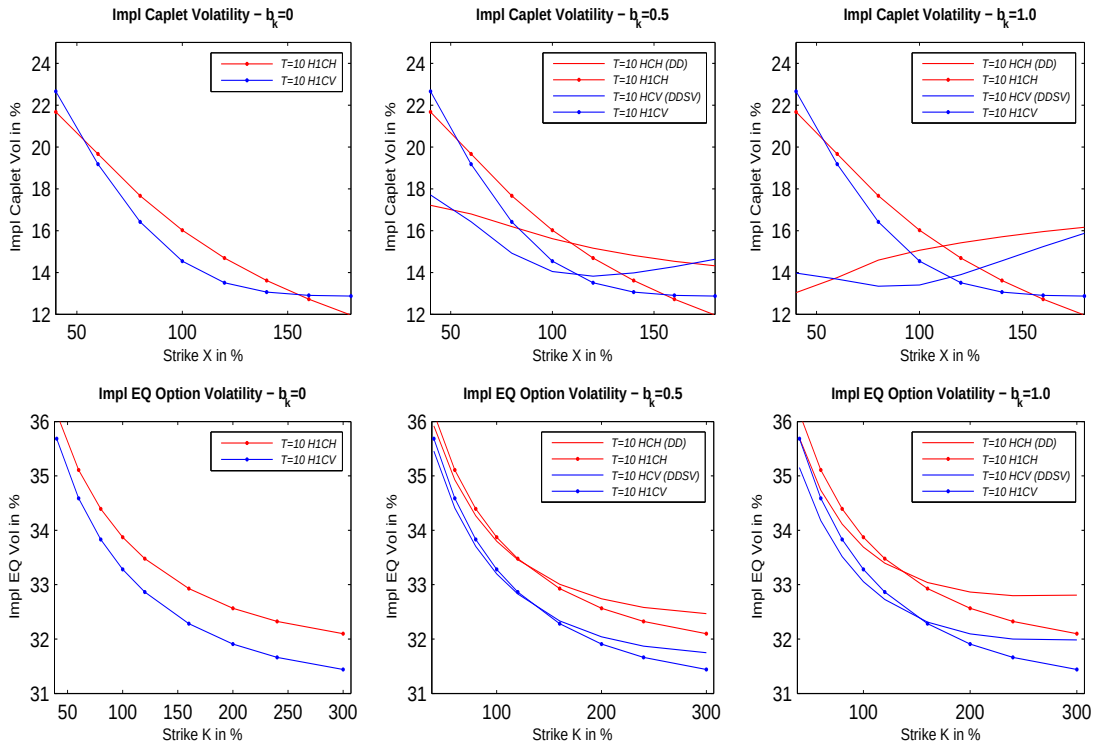

Figure 3.7: Implied caplet volatilities corresponding to the caplet values shown in Fig. 3.6 (plot series in the upper figure half), and the associated EQ option prices (lower half) where the very same IR component (serving as basis of caplet prices) is combined with the Heston process in EQ. All implied volatilities are shown for $T = 10$, the models without IR-SV process in red, and the models with IR-SV contributions in blue, respectively. Compared are the full models (lines with dots) and the corresponding affine approximations, employing the parameter Set 1 (as in Fig. 3.4), and focusing on the case ρ_{xc}=0.9 where hybrid model features are most prominent. Whereas for b_k=0 the affine approximations exhibit an excellent representation of the full model, the affine limit 1 shows difficulties to reproduce the base skew features introduced with increasing b_k parameter. The deviations to the full model are understandable as the short rates are *frozen* in the initial state as one of the presumptions of the affine limit 1.

product evaluations in our tests. In conclusion, the H2CV model is a very promising affine model approximation showing accurate model prices when reproducing DDSV hybrid model extensions.

Finally, it is important to note that the conclusions here are based on numerical experiments. Though we tested our model implementations over a range of parameters around the selected scenarios presented in this thesis, the validity of the models under discussion is possibly limited to certain parameter regimes. Understanding the model behaviour over the entire available parameter space would rely on a more rigorous error analysis to be conducted in future studies.

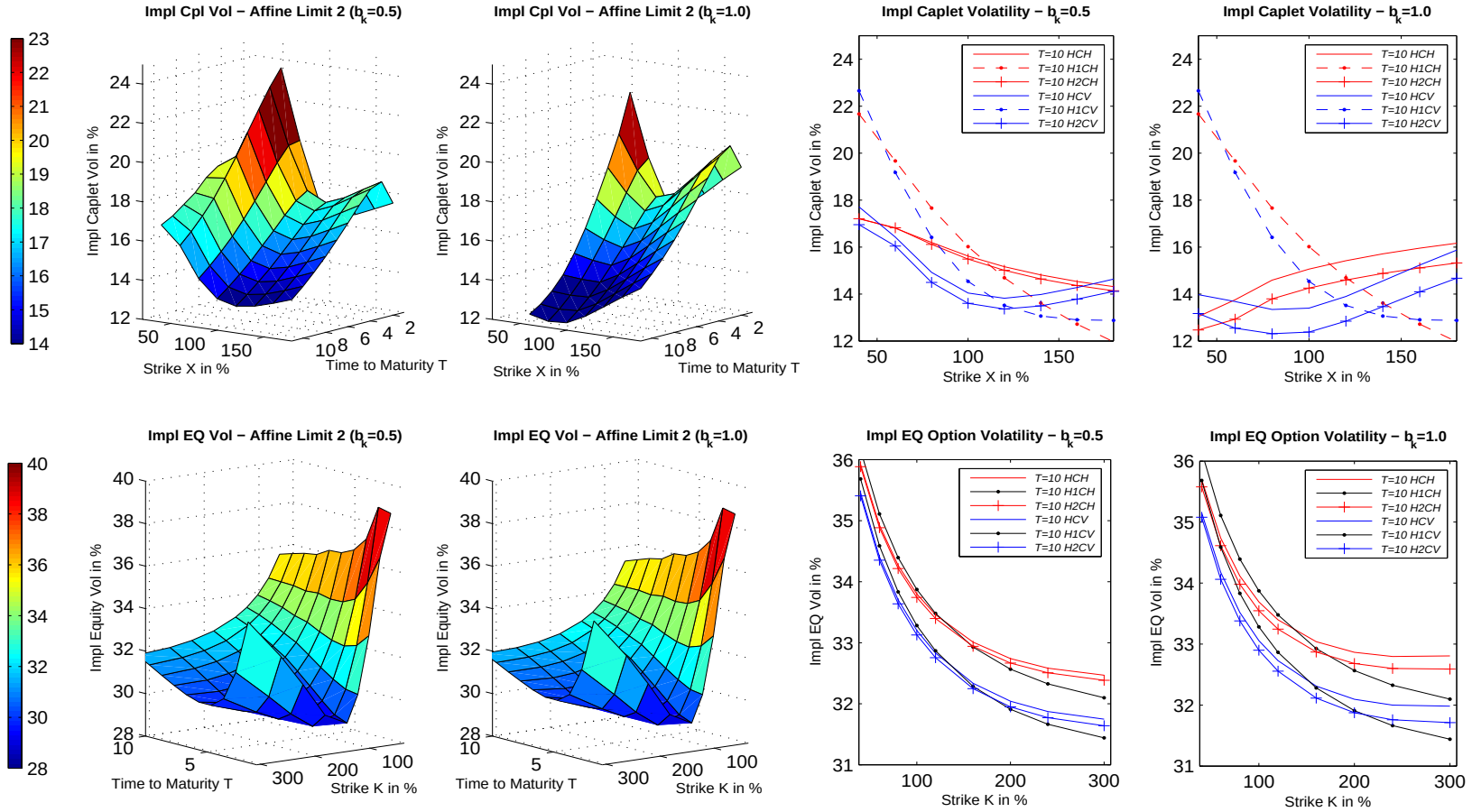

Figure 3.8: Left half: Implied caplet (top) and EQ option (bottom) volatility surfaces for scenarios with significant DD base skew features, which are reproducable within the affine model limit 2 (H2CV). Right half: Quantitative evidence of H2CV (Heston DDSV Cheyette model in affine limit 2) validity. The H2CV model reproduces DD base skew features very well up to b_k=0.5. IR-SV contributions are also incorporated (equivalent to the H1CV model). Deviations between H2CV and HCV models arise at higher base skews, though the crucial point to reproduce the log-normal IR characteristics is well incorporated as key feature of the affine limit 2. The affine models in limit 1 are shown to contrast the case where DD base skew features are completely neglected. Model parameters correspond to Set 1, inverse transform and MC evaluation details are identical to the specifications in the preceding figures.

Chapter 4

Model Validation

4.1 Calibration

In the preceding chapter hybrid models with varying degree of sophistication were introduced along with the corresponding approximations within the class of AJD processes. The potential of each hybrid model is defined by how well the model can reproduce realistic market features in certain numerical experiments. The quality of the corresponding affine model approximation is given by how well the original hybrid model features are retained. Each hybrid model under consideration has certain features and limitations which are summarized in the following list:

- Heston Hull-White (HHW) model features implied volatility smile and skew in the EQ component. Implied volatility features are limited to the inherent skew of Gaussian IR models. All these basic model characteristics are retained in the affine H1HW approximation.

- Heston Cheyette (HCH) model contains the HHW as limiting case when the Cheyette model is based on a single factor constant volatility specification. Then, also the corresponding affine model versions H1CH and H1HW are equivalent. The HCH model characteristics are determined by the choice of the volatility function of the IR component.

- Heston DDSV Cheyette (HCV) model reflects smile and skew features in EQ and IR components. Therewith, as argued in the preceding chapter, the HCV is capable to generate *hybrid smiles* based on *IR stochastic volatility*. IR smiles are reproducable by the affine H1CV version; IR smiles and skew as introduced by the DDSV extensions of the full-scale model are retained within the affine H2CV approximation. Though the HCV volatility spectrum is potentially narrowed in comparison to Heath-Jarrow-Morton based market models like the HLMM, the corresponding affine H1CV and H1LMM approximations are expected to have comparable information content in EQ and IR implied volatilities. From this point of view, the H2CV model is expected to perform superior to both the H1CV and the H1LMM model, respectively.

- Heston DDSV LMM (HLMM) model incorporates the implied volatility smile and skew in EQ and IR component. Like the HCV model the HLMM model is capable to reproduce *hybrid smiles*. High dimensionality and most of the HLMM complexity are abandoned by *freezing initial Libors* to derive the affine H1LMM model. As a consequence, H1LMM and H1CV models

are equivalent in system complexity. The intriguing differences are that the H1LMM model has a Libor based volatility specification and originates from a log-normal full-scale model, whereas the H1CV model is based on bond measure volatilities and a classical Gaussian short rate model.

The different hybrid models are compared in four hybrid scenarios defined by the implied volatility characteristics in equity and interest rates. Model calibration and validation proceeds along the following steps:

(i) Calibration of the IR component of the hybrid model to implied volatility surfaces defined in section 4.1.1. The decisive differences between the hybrid models under investigation arise from the inclusion of DDSV extensions in the IR component. Four different IR scenarios are devised to point out particular DDSV features.

(ii) With the correlation between EQ and IR model components fixed to $\rho_{xc} = \rho_{xr} = 0.5$, the hybrid model calibration set is completed with the EQ components in section 4.1.2. The EQ component corresponding to each of the four IR scenarios is calibrated to the same EQ call option volatility surface. Hence, in total four calibration sets result for each model representing four different hybrid model scenarios.

(iii) Pricing of the hybrid products introduced in section 4.2 with the calibrated full and affine models. Full and affine model characteristics and performance are validated in section 4.2 based on the pricing results.

4.1.1 Calibration of Hybrid Model Interest Rate Component

The four qualitatively different interest rate (IR) scenarios controlled by the DDSV extensions are shown in Fig. 4.1. The displaced-diffusion (DD) concept controls the base skew of the implied volatility surface. The choice $b_k = 0.5$ implies large base skew, and $b_k = 0.9$ corresponds to the 'quasi'-lognormal case with flat implied volatility. The parameters of the IR-SV process determine the IR smile characteristics. A steep IR smile is obtained for $\beta = 0.3$ and $\epsilon = 1.2$, and small smile effects result for $\beta = 1.0$ and $\epsilon = 0.1$. The four different DDSV parameter combinations are summarized in the following scenarios:

$$\begin{aligned}
&\text{Scenario 1}: \quad \text{DD}\, s_k^{LMM} = 0.25, \quad b_k = 0.5; \quad \text{IR}-\text{SV}\, \beta = 1.0, \quad \epsilon = 0.1; \\
&\text{Scenario 2}: \quad \text{DD}\, s_k^{LMM} = 0.25, \quad b_k = 0.9; \quad \text{IR}-\text{SV}\, \beta = 1.0, \quad \epsilon = 0.1; \\
&\text{Scenario 3}: \quad \text{DD}\, s_k^{LMM} = 0.25, \quad b_k = 0.5; \quad \text{IR}-\text{SV}\, \beta = 0.3, \quad \epsilon = 1.2; \\
&\text{Scenario 4}: \quad \text{DD}\, s_k^{LMM} = 0.25, \quad b_k = 0.9; \quad \text{IR}-\text{SV}\, \beta = 0.3, \quad \epsilon = 1.2.
\end{aligned} \tag{4.1}$$

$k = \{1, .., 10\}$ are the Libor rates relevant to the underlying DDSV LMM implementation - this is the IR component of the HLMM model discussed in section 3.3.2 above. The corresponding IR implied volatility surfaces shown in Fig. 4.1 are computed by the DDSV LMM model. The other parameters of the HLMM IR component are identical to the specification in the reference publication [4] (section 5.1 and Appendix E therein). Fig. 4.1 shows results for $T = 5$, albeit the complete caplet

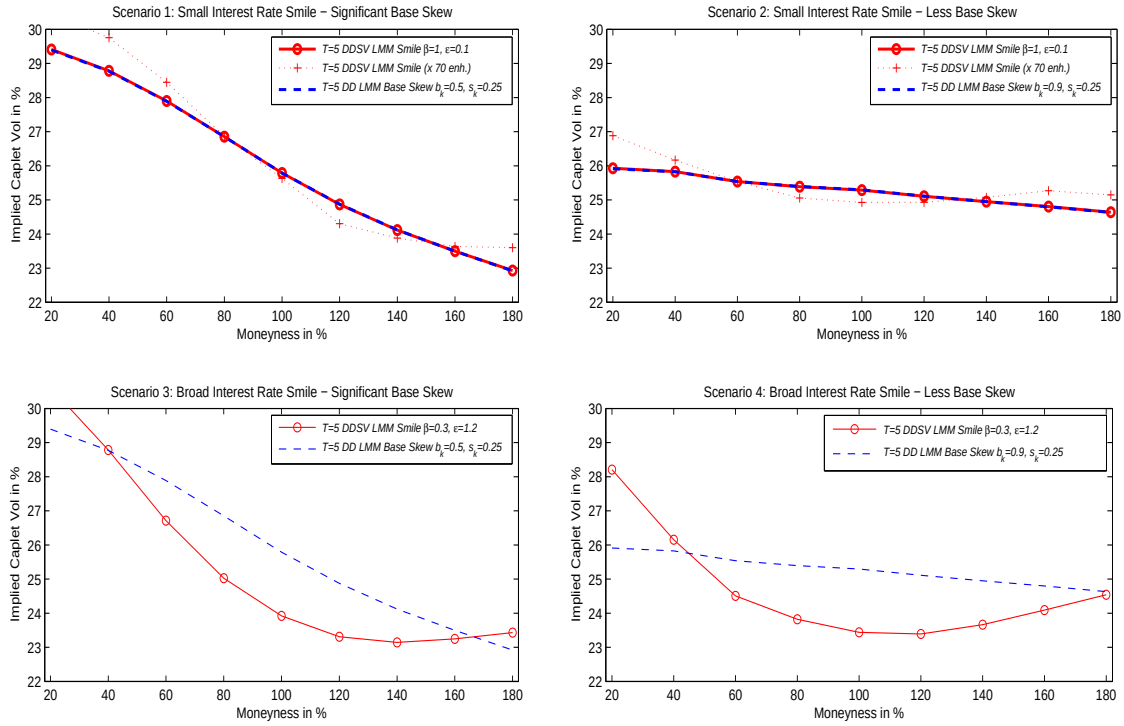

Figure 4.1: Caplet implied volatility smiles generated by the DDSV LMM - this is the IR component of the HLMM model which is the most sophisticated of the hybrid models under discussion. The interest rate (IR) caplets serve as calibration basis for the IR component of the other hybrid models in the subsequent comparison. Four scenarios are under discussion: Significant base skew (1, top left panel) and less base skew (2, top right) combined with hardly noticable IR smile. Steep IR smile is combined with large base skew (3, bottom left) and less skew (4, bottom right), respectively. Calibration data is obtained for $\mathcal{T} = \{T_k\} = \{T_1, T_2, T_3, T_4, T_5, T_6, T_7, T_8, T_9, T_{10}\}$, though solely the snapshot at T_5 is shown here for clarity.

implied volatility surface for the time set $\mathcal{T}$ and strike set $\mathcal{K} = \{20, 40, 60, 80, 100, 120, 140, 160, 180\}$ is computed and employed as calibration basis. Details of the calibration process are shown in Fig. E.4, where the parameters fixing the Cheyette volatility specification are determined to

$$\lambda = 0.0074 \qquad \text{and} \quad \eta = 0.0125 \equiv s_k^{CH} \quad \text{with} \quad k = 1.$$

With these calibration results - combined with the DDSV parameter sets corresponding to the four IR scenarios given in equation (4.1) above - all parameters of the IR components of all hybrid models under discussion are fully determined. The remaining task is to calibrate the Heston EQ model component in the subsequent section.

4.1.2 Calibration of Hybrid Model Equity Component

Calibration of the equity (EQ) component of all hybrid models is based on the equity call option data from the reference publication [4] (section 5.1 and Appendix E therein). The reference data

and the corresponding implied call option volatility surface was reproduced in section 3.3.2 above. In the respective sections the HLMM full model and H1LMM affine version were discussed, and the implementation of the HLMM via a MC scheme and the H1LMM employing the COS method were benchmarked with the data published in [4]. Benchmark results are shown in Fig. 3.2 for selected times of the set $\mathcal{T}$.

The EQ call option values of the complete benchmark set $\mathcal{T}$ serve as the basis of the calibration process for the EQ component. As all models share a standard Heston process as common element, the EQ calibration results apply to all hybrid models under discussion. The calibration is performed employing a Levenberg-Marquardt algorithm. The quality and effectiveness of the calibration procedure are demonstrated in Fig. E.5, where the calibration results are shown in the context of the reference data from [4].

With the EQ-IR correlation set to $\rho_{xr} = 0.5$ the Levenberg-Marquardt calibration of the EQ component yields the following Heston parameters:

$$\kappa = 0.446, \quad \bar{v} = 0.0628, \quad v_0 = 0.101, \quad \gamma = 0.462, \quad \rho_{xv} = -0.215.$$

Therewith the parameters of each individual hybrid model are determined for all four scenarios and the calibration process is concluded. The calibrated models are used for pricing hybrid derivative products in the subsequent section.

4.2 Model Performance Characteristics

Evaluation performance and pricing results are compared for the full-scale models and affine approximations under investigation. In the following two hybrid derivative products are introduced and priced on the basis of the previously obtained calibration sets:

- **Hybrid Derivative Product 1 (HD1)**: *Plain Diversification Hybrid*

  A diversification hybrid is a derivatives product combining several asset classes with diverse risk and rate of return profiles. When constructed appropriately, the hybrid is supposed to have a risk exposure less than that of any individual contributing asset, and a rate of return higher than the one of the least risky asset - by virtue of imperfect correlation between the assets as argued in [41].

  The most simple version of a *Plain Diversification Hybrid* is to combine a stock with value S_t at time t with a zero coupon bond $P(t, T_N)$ maturing at T_N. Within the hybrid the contribution of the stock is weighed by w_1, and of the bond by w_2, respectively. Positive weight corresponds to a long position, negative weight to a short position. The structure with the option expiry date $t = T_i$ would formally be priced under the risk-neutral measure according to the following equation:

  $$\Pi_{HD1}(t) \quad = \quad \mathbb{E}^{\mathbb{Q}}[\tfrac{1}{B_{T_i}}(w_1 F^{\mathbb{Q}}_{T_i} + w_2 P(T_i, T_N)^+ | \mathcal{F}_t], \tag{4.2}$$

  where $F^{\mathbb{Q}}_{T_i}$ is the T-forward stock price at time $t = T_i$. In this formulation the pricing equation $\Pi(t)$ is rather tedious to handle, as the conditional distribution of the money market account

$1/B_t$ (with $B_0 = 1$) and the derivative payoff $(...)^+$ is unknown. However, like in many pricing problems with hybrid derivatives, the pricing equation becomes accessible via transformation to the T_N-forward measure $\mathbb{Q}^{T_N}$. Applying the Radon-Nikodym derivative

$$\frac{\mathbb{Q}^{T_N}}{\mathbb{Q}}|_{\mathcal{F}_{T_i}} = \frac{B_0}{B_{T_i}} \frac{P(T_i, T_N)}{P(0, T_N)}, \tag{4.3}$$

the transformed pricing equation under $\mathbb{Q}^{T_N}$ changes to

$$\begin{aligned} \Pi_{HD1}(t) &= P(t,T_N)\mathbb{E}^{T_N}[\tfrac{1}{P(T_i,T_N)}(w_1 S_{T_i} + w_2 P(T_i,T_N))^+|\mathcal{F}_t] \\ &= P(t,T_N)\mathbb{E}^{T_N}[(w_1 F_{T_i}^{T_N} + w_2)^+|\mathcal{F}_t] \\ &= w_1 P(t,T_N)\mathbb{E}^{T_N}[(F_{T_i}^{T_N} + \tfrac{w_2}{w_1})^+|\mathcal{F}_t]. \end{aligned} \tag{4.4}$$

Apparently, the derivative price $\Pi_{HD1}(t)$ at time t is nothing more than a plain European call option with effective strike $K \equiv \frac{w_2}{w_1}$ at maturity T_N, multiplied by the weight factor w_1. The advantage of this hybrid product is that the corresponding pricing equation can be immediately evaluated via MC simulation as well as inverse transform methods.

- **Hybrid Derivative Product 2 (HD2)**: *Minimum of Several Assets Payoff*
  This is another diversification product and a variant of HD1. A straightforward realization is to combine a constant maturity swap (CMS) entered into at T_i and maturing at T_N with a simple stock S_t into a derivative contract with payoff structure

$$\Pi_{HD2}(t) = P(t,T_i)\mathbb{E}^{T_i}\left[\left(min\left(\frac{1 - P(T_i,T_N)}{\sum_{k=i+1}^{N} P(T_i,T_k)}, k \cdot \frac{S_{T_i}}{S_{T_N}}\right)\right)^+ |\mathcal{F}_t\right] \tag{4.5}$$

  as suggested in [4]. k controls the mixture between IR and EQ product contributions. Results of HD2 valuations were used to benchmark the HLMM MC implementation in section 3.3.2 above (and particularly Fig. E.6 therein).

Performance of Full and Affine Models in Pricing Hybrids

Evaluations of the HD1 product by the HCV model and the affine H1CV and H2CV approximations are shown in Fig. 4.2. HD1 prices are obtained for the four scenarios previously defined. In order to price the HD1 by the Carr-Madan FFT technique the pricing equation is reformulated:

$$\begin{aligned} \Pi_{HD1}(t) &= w_1 P(t,T_N)\mathbb{E}^{T_N}[(F_{T_i}^{T_N} + \tfrac{w_2}{w_1})^+|\mathcal{F}_t] \\ &= \mathbb{E}^{T_i}\left[w_1 P(t,T_N)\mathbb{E}^{T_N}[(F_{T_i}^{T_N} + \tfrac{w_2}{w_1})^+|\mathcal{F}_t]|\mathcal{F}_t\right] \\ &= w_1 P(t,T_i)\mathbb{E}^{T_i}\left[(F_{T_i}^{T_i} + \tfrac{w_2}{w_1}P(T_i,T_N))^+|\mathcal{F}_t\right] \\ &= w_1 P(t,T_i)\mathbb{E}^{T_i}\left[(\tfrac{S_t}{P(t,T_i)} + \tfrac{w_2}{w_1}\tfrac{P(t,T_N)}{P(t,T_i)})^+|\mathcal{F}_t\right] \end{aligned} \tag{4.6}$$

Both affine approximations of the HCV model show excellent results in reproducing HD1 prices in all four scenarios. The H2CV model is the better approximation to the full HCV model, essentially

because DD contributions are relevant in all four scenarios. Prices obtained with the H1CH model (where the IR-SV contributions in the scenarios are neglected) and the H1LMM model are given for comparison. In scenarios 1 and 2 IR-SV contributions are small. Consequently, the H1CV and H1CH model results are almost equivalent, and the differences to the HCV and H2CV models are due to DD effects. By comparison to the scenarios 3 and 4 we deduce that H1CV and H2CV models are more sensitive to IR-SV parameters than the H1LMM model. The HLMM and HCV models

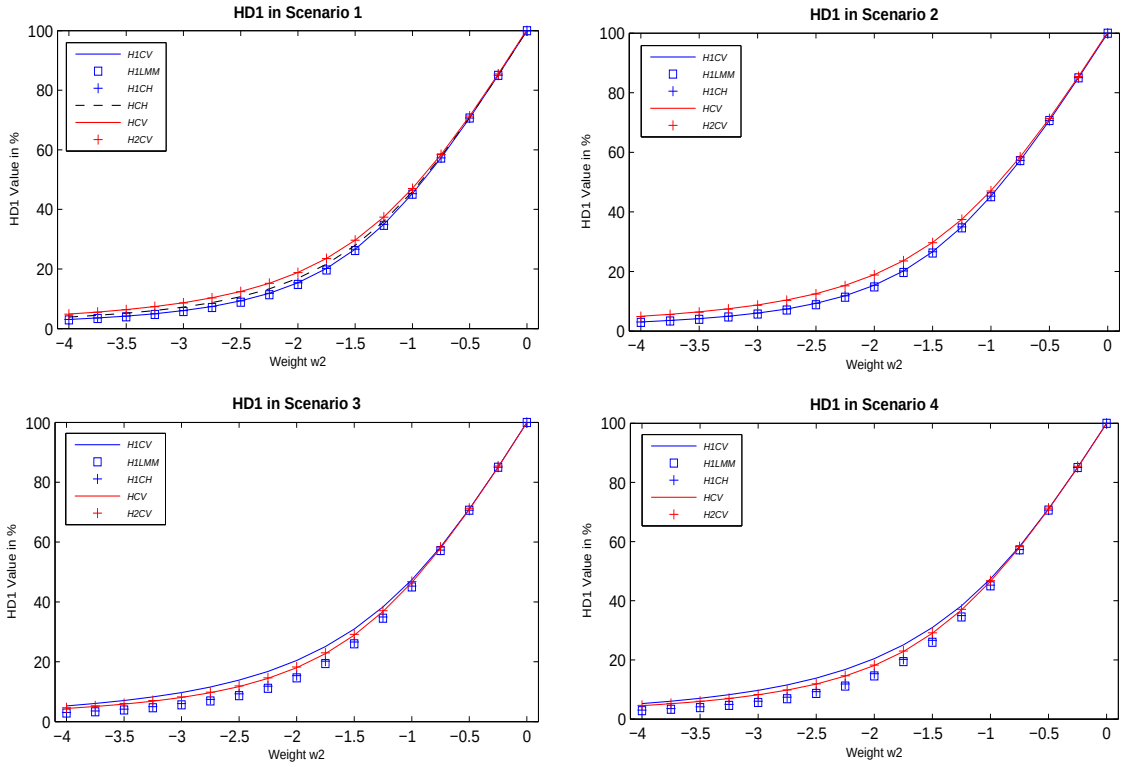

Figure 4.2: HD1 prices as function of relative bond asset weight w_2 for the hybrid models under discussion with the model calibration parameters shown in section 4.1.1, $S_0 = 1$, $P(0,T) = \exp[-0.05 \cdot T]$, $w_1 = 1$, option expiry at $T_i = 5$ and hybrid structure maturing at $T_N = 10$. Results of the full-scale models are obtained by Monte-Carlo simulations (MC errors are below the size of marker symbols). The affine model approximations are evaluated by the Carr-Madan FFT method (damping factor $\alpha = 0.75$). H1CV and H2CV models as affine approximations of the HCV model give excellent results in all four scenarios. The H2CV model performs slightly better than the H1CV approximation (this means the results are closer to the full HCV model), since all four scenarios have DD contributions.

both incorporate DDSV extensions, but are hybrid models with inherently different IR component approaches. Consequently pricing results differ in general between these models, as is shown by example of the HD2 in Fig. E.6. Here HD2 prices obtained for the affine H2CV approximations also give an accurate reproduction of the prices obtained with full model.

Chapter 5

Final Remarks

In the previous chapters we introduced the HCV hybrid model and the H1CV and H2CV models as the corresponding affine approximations. These models can represent *hybrid smiles* which in the present context are understood as implied volatility smiles in correlated EQ and IR hybrid components. By deriving the corresponding CHFs, the H1CV and H2CV models were made accessible to evaluation by inverse transforms. The HCV model was discussed in the context of the HHW and HLMM as alternative hybrid models. The corresponding affine H1HW and H1LMM approximations were derived in previous publications [1, 4]. The quality of the affine H1CV and H2CV model approximations was studied and compared to the characteristics of H1HW and H1LMM models.

The HCV model generates *hybrid smiles* by virtue of an IR-SV process. Originally descending from the short rate model ansatz, the displaced-diffusion (DD) extensions of the HCV model bridge towards log-normal model characteristics. The affine deterministic H1CV version gives an excellent representation of the Gaussian model characteristics of the HCV and hybrid smile features. The H2CV model is proposed as more sophisticated affine model where the DD model effects are retained. Hence, the H2CV model is an affine model incorporating hybrid smiles and DD contributions mixing classical short rate with the HJM relevant log-normal model characteristics.

The HCV model is inherently 5D irrespective whether $\mathbb{Q}^B$ or $\mathbb{Q}^T$ are the selected choice of measure. Due to the DDSV contributions the dimensional reduction applicable to simpler HHW/HCH hybrid models is rendered impossible. By suitable approximation assumptions - like *freezing* the initial interest rates within the volatility specification of the IR component - the EQ-IR hybrid models are reducable to 3D systems consisting of EQ, EQ-SV and IR-SV processes upon transformation to $\mathbb{Q}^T$. Such approximations are effective in the affine H1CV and H1LMM models.

Finally, a few words of caution about the limitations of the presented results. The statements about the quality of affine approximations, and the overall comparison of the characteristics of the various hybrid models, are based on numerical studies. Though we have tested a wide parameter set in addition to the selectively presented results in the figures, the statements are possibly limited to certain parameter regimes. Conducting a rigorous numerical error analysis would completely ensure the validity of affine model derivations. However, we leave this loose end as the connection to future studies.

Appendix A

Basic Characteristic Functions

A.1 Heston Process CHF in Gatheral's formulation

The Heston process incorporates stochastic volatility in equity prices by presuming CIR-type mean-reverting variance dynamics in the geometric Brownian motion of the underlying security S_t:

$$\begin{aligned} dx_t &= (r - \tfrac{v_t}{2})dt + \sqrt{v_t}dW_x(t), \\ dv_t &= \kappa(\bar{v} - v_t)dt + \gamma\sqrt{v_t}dW_v(t), \\ \text{with } dW_x dW_v &= \rho_{xv}dt, \text{ as correlated Brownian motions.} \end{aligned} \tag{A.1}$$

The following notations for the equity stochastic volatility (EQ-SV) process are used:

- Equity security price $x_t = x(t, W_x) = \log S_t$.
- Stochastic variance $v_t = v(t, W_v)$.
- Mean-reversion rate κ of stochastic variance towards the long-term mean-level $\bar{v}$ (as long as not indicated explicitly otherwise, $\bar{v} = v(0)$ is presumed throughout)
- Volatility γ of the variance process.
- Interest rate component $r_t = r(t)$, which in the Heston EQ-SV framework is deterministic and not a state variable (i.e. here within the stand-alone Heston model for simplicity presumed to be constant $\bar{r} = \int r_s ds$).

Apparently, the Heston EQ-SV process with state variable vector $\mathbf{X}_t = [x_t, v_t]^\dagger$ is within the class of affine jump-diffusion (AJD) processes (cf. section 2.1), since

$$\mu(\mathbf{X}_t) = \begin{pmatrix} 0 \\ \kappa\bar{v} \end{pmatrix} + \begin{pmatrix} 0 & -\frac{1}{2} \\ 0 & -\kappa \end{pmatrix} \begin{pmatrix} x_t \\ v_t \end{pmatrix}, \tag{A.2}$$

$$\Sigma_{\mathbf{X}} = \begin{pmatrix} v_t & \rho_{xv}\gamma v_t \\ \rho_{xv}\gamma v_t & \gamma^2 v_t \end{pmatrix} = \begin{pmatrix} 0 & 0 \\ 0 & 0 \end{pmatrix} + \begin{pmatrix} (0,1) & (0,\rho_{xv}\gamma) \\ (0,\rho_{xv}\gamma) & (0,\gamma^2) \end{pmatrix} \begin{pmatrix} x_t \\ v_t \end{pmatrix}, \tag{A.3}$$

$$r(\mathbf{X}_t) = r, \tag{A.4}$$

as interest rate component, respectively, assume affine characteristics.
Consequently, the Heston CHF is derived in the form

$$\hat{\Phi}_H(u, \mathbf{X}_t, t, T) = e^{A(u,\tau) + B(u,\tau)x_t + D(u,\tau)v_t}, \tag{A.5}$$

with the Fourier coefficients as solutions of the following ODEs and associated initial conditions:

$$\begin{aligned}
\frac{d}{d\tau}B(u,\tau) &= 0, && \text{(A.6)}\\
\frac{d}{d\tau}D(u,\tau) &= \tfrac{\gamma^2}{2}D(u,\tau)^2 + (\rho_{xv}\gamma B(u,\tau) - \kappa)D(u,\tau) + B(u,\tau)(B(u,\tau)-1)/2, && \text{(A.7)}\\
\frac{d}{d\tau}A(u,\tau) &= -r + D(u,\tau)\kappa\bar{v}, && \text{(A.8)}\\
\text{with} \quad B(u,0) &= iu,\ D(u,0) = 0,\ A(u,0) = 0. && \text{(A.9)}
\end{aligned}$$

With $B(u,\tau) = iu$, the Heston Riccati ODE simplifies

$$\begin{aligned}
\frac{d}{d\tau}D(u,\tau) &= \tfrac{\gamma^2}{2}D(u,\tau)^2 - \beta_0 D(u,\tau) + \alpha_0\\
&= \tfrac{\gamma^2}{2}(D(u,\tau) - \xi_0^+)(D(u,\tau) + \xi_0^-), && \text{(A.10)}
\end{aligned}$$

and, as a consequence thereof, an analytic solution is derivable in closed form via the method of separation of variables:

$$\begin{aligned}
-\int_{D(0)}^{D(\tau)} \frac{dD}{D-\xi_0^+} + \int_{D(0)}^{D(\tau)} \frac{dD}{D-\xi_0^-} &= -\int_0^\tau d\hat{\tau}\tfrac{\gamma^2}{2}\xi_0^+(1-g), && \text{(A.11)}\\
\ln\frac{(D-\xi_0^+)\xi_0^-}{(D-\xi_0^-)\xi_0^+} &= -\tau d.
\end{aligned}$$

Solving for $D(u,\tau)$ we obtain

$$\begin{aligned}
D(u,\tau) = D_0(u,\tau) \quad \text{with} \qquad & D_k(u,\tau) = \xi_k^- \frac{1-e^{-d_k\tau}}{1-g_k e^{-d_k\tau}}, && \text{(A.12)}\\
\text{where} \quad g_k = \xi_k^-/\xi_k^+ & \\
\text{and} \quad \xi_k^\pm &= \frac{\beta_k \pm (\beta_k^2 - 2\alpha_k\gamma^2)^{\frac{1}{2}}}{\gamma^2} = \frac{\beta_k \pm d_k}{\gamma^2},\\
\alpha_k &= iu(\tfrac{iu}{2} - \tfrac{1}{2} + k) = -\tfrac{u^2}{2} - \tfrac{iu}{2} + iuk\\
\beta_k &= \kappa - \rho_{xv}\gamma(k+iu) \qquad \forall \qquad k = \{0,1\}.
\end{aligned}$$

Then,

$$\begin{aligned}
A(u,\tau) &= -r\tau + \kappa\bar{v}\left(\xi_0^-\tau - \frac{2}{\gamma^2}\ln\left[\frac{1-g_0e^{-d_0\tau}}{1-g_0}\right]\right) && \text{(A.13)}\\
&= -r\tau + \kappa\bar{v}H_0(u,\tau), && \text{(A.14)}
\end{aligned}$$

is obtained by integration. It is important to denote the argument of the complex logarithm in Gatheral's reformulation [12] as shown above, which deviates from Heston's original derivation [8],

$$\tilde{H}_0(u,\tau) = \xi_0^+\tau - \frac{2}{\gamma^2}\ln\left[\frac{e^{d_0\tau}-g_0}{1-g_0}\right]. \qquad \text{(A.15)}$$

In Heston's original derivation the complex logarithm in $A(u,\tau)$ branches to another Riemann sheet when the contour path integration crosses the negative real axis of the complex plane. Gatheral's formulation ensures the evaluation of the real part of the logarithm argument remains positive in any event the imaginary part becomes zero (for the explicit proof cf. [27]), and hence, branching

never takes place.
Finally, the discounted Heston CHF reads

$$\hat{\phi}_{H,0}(u, \mathbf{X}_t, t, T) = e^{-r(T-t)+\kappa\bar{v}H_0(u,\tau)+iux_t+D_0(u,\tau)v_t} \tag{A.16}$$

In Heston's orginal publication [8] the value of a call option with strike K is given in the T-Forward measure $\mathbb{Q}^T \equiv \mathbb{T}$ and is constructed from the cumulative distribution functions represented as Fourier inversa in the following form:

$$C^{\mathbb{T}}(z_t, v_t, \tau) = F(\tau) f_{k=1}(z_t, v_t, \tau) - K f_{k=0}(z_t, v_t, \tau) \tag{A.17}$$

$$\text{with} \quad f_k(z_t, v_t, \tau) = \frac{1}{2} + \frac{1}{\pi} \int_0^\infty \mathcal{R}\left[\frac{e^{+r\tau}\hat{\phi}_{H,k}(u, \hat{\mathbf{X}}_t, t, T)}{iu}\right] \mathrm{d}u, \tag{A.18}$$

$$z_t = \ln F(t) = x_t + r\tau, \text{ and } \hat{\mathbf{X}}_t = [z_t, v_t]^\dagger, \tag{A.19}$$

where $F(t) = S(T) = \frac{S(t)}{P(t,T)}$ is the T-forward stock price at time $t = T - \tau$, and $P(t, T)$ is the zero bond value maturing at T, respectively.
By virtue of the fundamental (Lévy / Gil-Pelaez) Fourier inversion theorem the Cumulative Distribution Function (CDF)

$$CDF(x) = \mathbb{P}(X \leq x) = \tfrac{1}{2} - \tfrac{1}{\pi} \int_0^\infty \mathcal{R}\left[\frac{e^{-iux}\hat{\phi}_X(u)}{iu}\right] \mathrm{d}u \tag{A.20}$$

and its complement $\overline{CDF}(x) = \mathbb{P}(X > x) = 1 - CDF(x)$ are representable by the CHF of the underlying stochastic process.
By denoting that the change from $k = 1$ to $k = 0$ just corresponds to the simple substitution $u \to u - i$ (which represents just a simple shift in the complex plane)

$$\hat{\phi}_{H,k=0}(u - i, \hat{\mathbf{X}}_t, t, T) = \hat{\phi}_{H,k=1}(u, \hat{\mathbf{X}}_t, t, T), \tag{A.21}$$

the option pricing formula (here given in the spot measure $\mathbb{Q}$, for more details on the calculations cf. [34]) is reducable to the generic form

$$C(x_t, v_t, t, T) = S(t)\mathcal{D}_0(k) - Ke^{-r(T-t)}\mathcal{D}_1(k) \tag{A.22}$$

$$\text{with } \mathcal{D}_0(k) = \tfrac{1}{2} + \tfrac{1}{\pi} \int_0^\infty \mathcal{R}\left[\frac{e^{-iuk}\hat{\phi}_H(u - i)e^{-x_t - r(T-t)}}{iu}\right] \mathrm{d}u \tag{A.23}$$

$$\mathcal{D}_1(k) = \tfrac{1}{2} + \tfrac{1}{\pi} \int_0^\infty \mathcal{R}\left[\frac{e^{-iuk}\hat{\phi}_H(u)}{iu}\right] \mathrm{d}u \tag{A.24}$$

$$\text{and } k = \ln K \tag{A.25}$$

based solely on the Heston CHF

$$\hat{\phi}_H(u) = \hat{\phi}_H(u, \mathbf{X}_t, t, T) \equiv e^{-r(T-t)+\kappa\bar{v}H_0(u,T,t)+iux_t+D_0(u,T,t)v_t}. \tag{A.26}$$

A.2 CHF of the classical Hull-White process

A.2.1 Derivation without Hull-White decomposition

The Hull-White (HW) approach models stochastic interest rates by an Ornstein-Uhlenbeck-type process,

$$dr_t = \lambda(\theta(t) - r_t)dt + \eta dW_r(t) \tag{A.27}$$

- for the short rate $r_t = r(t, W_r(t))$ as the only state variable,
- with reversion rate λ towards the current HW mean reversion level $\theta(t)$; as shown below

$$\theta(t) \quad = \quad f(0,t) + \tfrac{1}{\lambda}\tfrac{\partial}{\partial t} f(0,t) + \tfrac{1}{2\lambda^2}(1 - e^{-2\lambda t}), \tag{A.28}$$

  resembles the connection to the initial yield curve by means of the instantaneous forward rate $f(0,t)$ of the initial term structure; constant mean reversion rate λ=const is presumed throughout the discussion to avoid unnecessary complexity in the model calibration,

- volatility η of the short rate (η is presumed constant for the moment.

Integrating $d(e^{\lambda t} r_t) = \lambda e^{\lambda t} r_t dt + e^{\lambda t}(\lambda(\theta(t) - r_t)dt + \eta dW_r(t)) = \lambda\theta(t)e^{\lambda t}dt + e^{\lambda t}\eta dW_r(t)$ with $t_0 = 0$ yields,

$$\begin{aligned} r_t &= r_0 e^{-\lambda t} + \lambda \int_0^t ds\, \theta(s) e^{-\lambda(t-s)} + \eta \int_0^t dW_r(s)\, e^{-\lambda(t-s)} \\ &= \psi(t) + \eta \int_0^t dW_r(s)\, e^{-\lambda(t-s)} = \psi(t) + \tilde{r}_t. \end{aligned} \tag{A.29}$$

Upon introduction of $\psi(t)$ we obtain the defining equation for $\theta(t)$ by

$$\begin{aligned} \tfrac{1}{\lambda}\tfrac{\partial}{\partial t}\psi(t) &= -r_0 e^{-\lambda t} - \lambda \int_0^t ds \theta(s) e^{-\lambda(t-s)} + \lambda\theta(t) = -\psi(t) + \theta(t), \\ \theta(t) &= \psi(t) + \tfrac{1}{\lambda}\tfrac{\partial}{\partial t}\psi(t). \end{aligned} \tag{A.30}$$

As shown in section A.2.3 $\psi(t)$ connects to the initial yield curve via

$$\psi(t) \quad = \quad f(0,t) + \tfrac{1}{\lambda}\tfrac{\eta^2}{2\lambda^2}(1 - e^{-\lambda t})^2 = f(0,t) + \tfrac{\eta^2}{2}\mu(0,t), \tag{A.31}$$

which is basically the initial instanteneous forward curve and an additional drift correction $\mu(0,t)$. The HW model is already in affine form, and hence, the CHF is composed of

$$\hat{\Phi}_{HW} \quad = \quad \mathbb{E}^{\mathbb{Q}}\left[e^{-\int_t^T r_s ds + i\mathbf{u}^\dagger \mathbf{X}_t} | \mathcal{F}_t\right] = e^{A_{HW}(u,\tau) + \tilde{C}(u,\tau) r_t} \tag{A.32}$$

$$\begin{aligned} \text{with} \quad \frac{d}{d\tau}\tilde{C}(u,\tau) &= -r_1 + (-\lambda)\tilde{C}(u,\tau) + 0 = -1 - \lambda\tilde{C}(u,\tau) \\ \frac{d}{d\tau}A(u,\tau) &= \lambda\theta(t)\tilde{C}(u,\tau) + 0 + \tfrac{1}{2}\tilde{C}(u,\tau)\eta^2\tilde{C}(u,\tau) \\ &= \lambda\theta(t)\tilde{C}(u,\tau) + \tfrac{\eta^2}{2}\tilde{C}^2(u,\tau) \\ \text{and} \quad \tilde{C}(u,0) &= iu,\ A_{HW}(u,0) = 0, \quad \text{for initial conditions.} \end{aligned}$$

$\tilde{C}(u,\tau)$ is a first order ODE solved by separation of variables, $A_{HW}(u,\tau)$ is straightforwardly integrated, and consequently

$$\begin{aligned}
\tilde{C}(u,\tau) &= -\tfrac{1}{\lambda}\left((1-iu\lambda)-e^{-\lambda\tau}\right) = -\tfrac{1}{\lambda}(1-e^{-\lambda\tau})+iue^{-\lambda\tau}, && \text{(A.33)}\\
A_{HW}(u,\tau) &= \tfrac{\eta^2}{2}\int_0^\tau d\tau\,\tilde{C}^2(u,\tau)+\lambda\int_0^\tau d\tau\,\theta(T-\tau)\tilde{C}(u,\tau)\\
&= \tfrac{\eta^2}{2}\tilde{I}_3(u,\tau)+\lambda\int_0^\tau d\tau\,\theta(t)\tilde{C}(u,\tau), && \text{(A.34)}\\
\text{since}\quad \tfrac{\eta^2}{2}\int_0^\tau d\tau\,\tilde{C}^2(u,\tau) &= \tfrac{\eta^2}{2}\tilde{I}_3(u,\tau)\\
&= \tfrac{\eta^2}{2\lambda^3}(\lambda\tau-2(1-e^{-\lambda\tau})+\tfrac{1}{2}(1-e^{-2\lambda\tau}))\\
&- iu\tfrac{\eta^2}{2\lambda^2}(1-e^{-\lambda\tau})^2-\tfrac{1}{2}u^2\tfrac{\eta^2}{2\lambda}(1-e^{-2\lambda\tau})^2. && \text{(A.35)}
\end{aligned}$$

In case of an initial yield curve specification in closed analytic form, $A_{HW}(u,\tau)$ is reducable to an explicit expression. For the calibration scenarios specified, the initial term structure is simply based on a constant initial instantaneous forward rate, $f(0,t)=f_0$,

$$f_0 = -\tfrac{\partial}{\partial T}\ln P(0,T), \quad P(0,T)=e^{-f_0T}. \tag{A.36}$$

and the quantities respectively are calculated as

$$\begin{aligned}
\psi(t) &= r_0e^{-\lambda t}+f_0(1-e^{-\lambda t})+\tfrac{\eta^2}{2\lambda^2}(1-e^{-\lambda t})^2, && \text{(A.37)}\\
\theta(t) &= f_0+\tfrac{\eta^2}{2\lambda^2}(1-e^{-2\lambda t}), && \text{(A.38)}\\
\lambda\int_0^\tau d\tau\,\theta(T-\tau)\tilde{C}(u,\tau) &= -(f_0+\tfrac{\eta^2}{2\lambda^2})\tau-\tfrac{\eta^2}{4\lambda^3}(e^{-2\lambda T}-e^{-2\lambda(T-\tau)})+\tfrac{1}{\lambda}(1+iu\lambda)\\
&\quad\left(f_0(1-e^{-\lambda\tau})+\tfrac{\eta^2}{2\lambda^2}(1-e^{-\lambda\tau})+\tfrac{\eta^2}{2\lambda^2}(e^{-2\lambda T}e^{-\lambda(2T-\tau)})\right) && \text{(A.39)}
\end{aligned}$$

adding up to the discounted HW CHF:

$$\begin{aligned}
A_{HW}(u,\tau) &= -f_0\tau+\tfrac{f_0}{\lambda}(1-e^{-\lambda\tau})+iuf_0(1-e^{-\lambda\tau})-\tfrac{1}{2}u^2\tfrac{\eta^2}{2\lambda}(1-e^{-2\lambda\tau}), && \text{(A.40)}\\
\hat{\Phi}_{HW}(u,r_t,T,t) &= e^{A_{HW}(u,\tau)+\tilde{C}(u,\tau)r_0}, && \text{(A.41)}
\end{aligned}$$

which, for the particular choice $r_0=f_0$, reduces to

$$\hat{\Phi}_{HW}(u,r_t,T,t) = e^{-r_0(T-t)+iur_0-\frac{1}{2}u^2\frac{\eta^2}{2\lambda^2}(1-e^{-2\lambda(T-t)})}. \tag{A.42}$$

Apparently, the initial term structure fixes only $\psi(t)$. HW reversion rate λ and volatility η are to be calibrated by means of liquid marked instruments, like IR caps and swaptions.

A.2.2 Connection to CHF employing Hull-White decomposition

The HW decomposition [30] is based on the separation of the mean reversion off-set $\tilde{r}_t = r_t-\psi(t)$, so that the short rate process is retained:

$$d\tilde{r}_t = -\lambda\tilde{r}_tdt+\eta dW_{\tilde{r}}(t). \tag{A.43}$$

The CHF is calculated as

$$\begin{aligned}
\hat{\Phi}_{HW-dc} &= \mathbb{E}^{\mathbb{Q}}\left[e^{-\int_t^T \tilde{r}(s)ds + i\mathbf{u}^\dagger \mathbf{X}_t}|\mathcal{F}_t\right] \\
&= e^{\tilde{A}(u,\tau)+\tilde{B}(u,\tau)\tilde{r}_t} = e^{\tilde{A}(u,\tau)+\tilde{B}(u,\tau)(r_t-\psi(t))}, \qquad \text{(A.44)} \\
\text{with} \quad \frac{d}{d\tau}\tilde{B}(u,\tau) &= -r_1 + -\lambda\tilde{B}(u,\tau) + 0 = -1 - \lambda\tilde{B}(u,\tau), \\
\frac{d}{d\tau}\tilde{A}(u,\tau) &= 0 + 0 + \tfrac{1}{2}\tilde{B}(u,\tau)\eta^2\tilde{B}(u,\tau) \\
&= \tfrac{\eta^2}{2}\tilde{B}^2(u,\tau), \qquad \text{(A.45)} \\
\text{and} \quad B(u,0) &= iu, \quad A(u,0) = 0 \quad \text{for initial conditions.}
\end{aligned}$$

The ODE solutions are known. Obviously, the solution $\tilde{B}(u,\tau) = B(u,\tau)$ is equivalent for both HW variants. The connection between the CHF of the decomposed and the standard HW model is established by

$$\begin{aligned}
\hat{\Phi}_{HW} = \mathbb{E}^{\mathbb{Q}}\left[e^{-\int_0^T ds\,(\psi(s)+\tilde{r}_s)+iu(\psi_T+\tilde{r}_T)}|\mathcal{F}_t\right] &= \mathbb{E}^{\mathbb{Q}}\left[e^{-\int_0^T ds\,\psi(s)+iu\psi_T}|\mathcal{F}_t\right]\cdot\hat{\Phi}_{HW-dc} \qquad \text{(A.46)} \\
-\int_0^\tau \psi(s)ds + iu\psi_T - B(u,\tau)\psi(t) &\equiv \lambda\int_0^\tau \theta(T-\tau)B(u,\tau)d\tau \\
\text{with} \quad -\int_t^T \psi(s)ds &= -\int_0^\tau \psi(t)d(T-t).
\end{aligned}$$

A.2.3 Zero coupon bond value derived from the HW CHF

Since the definition of the risk-neutral value at time t of the zero coupon bond maturing at T is

$$P(t,T) = \mathbb{E}^{\mathbb{Q}}\left[e^{-\int_t^T r_s ds}|\mathcal{F}_t\right], \qquad \text{(A.47)}$$

the zero bond value is obtained from the affine HW model CHF in the limit $u = 0$:

$$\begin{aligned}
\hat{\Phi}(0,\mathbf{X}_t,t,T) &= \mathbb{E}^{\mathbb{Q}}\left[e^{-\int_t^T r_s ds}\cdot 1|\mathcal{F}_t\right] = e^{A(0,\tau)+\mathbf{B}^\dagger(0,\tau)\mathbf{X}_t} \qquad \text{(A.48)} \\
\longrightarrow P(t,T) &= \hat{\Phi}_{HW}(0,r_t,t,T) = e^{A_{HW}(0,\tau)+\tilde{C}(0,\tau)r_t} \qquad \text{(A.49)} \\
&= e^{-\int_0^T \psi(s)ds+\tilde{A}(0,T)} \qquad \text{(A.50)}
\end{aligned}$$

The HW zero bond formula is frequently used, since there exists an analytic solution in closed form. The connection to the intial term structure is contained in the coefficent $A_{HW}(0,\tau) = A_{0,t,T,\theta(t)}$ via the mean-reversion level

$$\begin{aligned}
\theta(t) &= f^M(0,t) + \tfrac{1}{\lambda}\tfrac{\partial}{\partial T}f^M(0,t) + \tfrac{\eta^2}{2\lambda^2}(1-e^{-2\lambda t}) \qquad \text{(A.51)} \\
\text{with} \quad f^M(0,t) &= -\tfrac{\partial}{\partial T}\ln P^M(0,t).
\end{aligned}$$

The superscript 'M' points out that initial instantaneous forward rates and initial zero bond values are derived from market instruments. In order to emphasize the connection to the initial term

structure the HW zero bond formula is reformulated to

$$\begin{aligned}\hat{\Phi}(0,\mathbf{X}_t,t,T) &= \frac{P^M(0,T)}{P^M(0,t)}e^{B_c(t,T)f^M(0,t)-\frac{1}{2}B_c^2(t,T)\frac{\eta^2}{2\lambda}(1-e^{-2\lambda t})-B_c(t,T)r_t} \qquad (A.52)\\ &= \frac{P^M(0,T)}{P^M(0,t)}e^{B_c(t,T)f^M(0,t)-\frac{1}{2}B_c^2(t,T)y(t)-B_c(t,T)r_t},\\ \text{with}\quad B_c(t,T) &= -\tilde{C}(u,\tau)=\frac{1}{\lambda}(1-e^{-\lambda(T-t)}). \qquad (A.53)\end{aligned}$$

$y(t)$ is a quantity from the Cheyette model derived in the next section. It is used here to indicate the connection between the zero bond value derived in the HW model, and the corresponding zero bond expression obtained in the Cheyette model below. The definition $B_c(t,T)$ is introduced, since this relation is a structural element recurring in all IR and hybrid models under discussion.
When the simplifying assumptions on the initial yield curve structure ($f(0,t)=f_0$ and $f_0=r_0$) are in effect, the expression for the HW zero bond value reduces down to $P(0,T)=e^{-r_0T}$.

A.3 Cheyette model CHF

A.3.1 1D Markovian CHF derivation in the single factor volatility case

Presuming constant volatility η for the moment, the single factor Cheyette model remains affine and the CHF is obtained as

$$\begin{aligned}\hat{\Phi}_c(u,\mathbf{X}_t,t,T) &= \mathbb{E}^{\mathbb{Q}}\left[e^{-\int_t^T(f(0,t)+x_{c,t})\,ds+i\mathbf{u}^\dagger\mathbf{X}_t}|\mathcal{F}_t\right], = e^{A_c(u,\tau)+\tilde{C}(u,\tau)x_{c,t}+Y(u,\tau)y(t)},\\ \text{with spot rate}\quad r_t &= f(0,t)+x_{c,t}. \qquad (A.54)\end{aligned}$$

and instantaneous forward rate $f(t,T)$ in the limit $t\to 0$ and $T\to t$. Apparently, the Cheyette state variable $x_{c,t}$ establishes a link between the forward rates and the spot rates evolving in time. This is the decisive point, where the Cheyette model derives from the HJM framework and proceeds beyond basic short rate models.
Then, the affine model framework [21] assumes the representation

$$\begin{aligned}\mu(\mathbf{X}_t) &= \begin{pmatrix}\lambda f(0,t)+\frac{\partial}{\partial t}f(0,t)\\ \eta^2\end{pmatrix}+\begin{pmatrix}-\lambda & 1\\ 0 & -2\lambda\end{pmatrix}\begin{pmatrix}x_{c,t}\\ y(t)\end{pmatrix}, \qquad (A.55)\\ \Sigma_{\mathbf{X}} &= (c_0)_{ij}+(c_1)^\dagger_{ij,\mathbf{x}}\begin{pmatrix}x_{c,t}\\ y(t)\end{pmatrix}\\ &= \begin{pmatrix}\eta^2 & 0\\ 0 & 0\end{pmatrix}+((\mathbf{0},\mathbf{0}))_{ij,\mathbf{x}}\begin{pmatrix}x_{c,t}\\ y(t)\end{pmatrix},\\ \text{and}\quad r(\mathbf{X}_t) &= r_0+\mathbf{r_1}^\dagger\begin{pmatrix}x_{c,t}\\ y(t)\end{pmatrix}\\ &= f(0,t)+(1,0)\begin{pmatrix}x_{c,t}\\ y(t)\end{pmatrix},\end{aligned}$$

and consequently the Fourier coefficients result from the following defining ODEs and initial conditions:

$$\begin{aligned}
\frac{d}{d\tau}\tilde{C}(u,\tau) &= -1-\lambda\tilde{C}(u,\tau), && \text{(A.56)}\\
\frac{d}{d\tau}Y(u,\tau) &= -0+\tilde{C}(u,\tau)-2\lambda Y(u,\tau), && \text{(A.57)}\\
\frac{d}{d\tau}A_{CH}(u,\tau) &= -f(0,t)+\eta^2 Y(u,\tau)+\tfrac{1}{2}\eta^2\tilde{C}^2(u,\tau),\\
&= -f(0,t), && \text{(A.58)}\\
\text{and}\quad \tilde{C}(u,0) &= iu,\ Y(u,0)=0,\ A(u,0)=0 \quad \text{for initial conditions.}
\end{aligned}$$

The ODE solution for $\tilde{C}(u,\tau)$ is known from the HW model derivations above. Then, $Y(u,\tau)$ is solvable by standard first order ODE techniques and finally $A_{CH}(u,\tau)$ results from simple integration:

$$\begin{aligned}
\tilde{C}(u,\tau) &= \tfrac{1}{\lambda}\left((1+iu\lambda)e^{-\lambda\tau}-1\right) = -\tfrac{1}{\lambda}(1-e^{-\lambda\tau})+iue^{-\lambda\tau}, && \text{(A.59)}\\
Y(u,\tau) &= -\tfrac{1}{2\lambda^2}(1-2e^{-\lambda\tau}+e^{-2\lambda\tau}-2iu\lambda e^{-\lambda\tau}+2iu\lambda e^{-2\lambda\tau}),\\
A_{CH}(u,\tau) &= -\int_0^\tau f(0,t)d\tau+\eta^2\int_0^\tau Y(u,\tau)d\tau+\tfrac{\eta^2}{2}\int_0^\tau\tilde{C}^2(u,\tau)d\tau\\
&= -\int_0^\tau f(0,t)d\tau+\eta^2\tilde{I}_{CH,y}(u,\tau)+\tfrac{\eta^2}{2}\tilde{I}_3(u,\tau),\\
&\text{with}\\
\eta^2\tilde{I}_{CH,y}(u,\tau) &= \eta^2\int_0^\tau Y(u,\tau)d\tau\\
&= \tfrac{\eta^2}{2\lambda^3}[-\lambda\tau-2e^{-\lambda\tau}+\tfrac{1}{2}e^{-2\lambda\tau}+\tfrac{3}{2}]+iu\tfrac{\eta^2}{2\lambda^3}(1-e^{-\lambda\tau})^2,\\
\tfrac{\eta^2}{2}\int_0^\tau d\tau\,\tilde{C}^2(u,\tau) &= \tfrac{\eta^2}{2}\tilde{I}_3(u,\tau).
\end{aligned}$$

The integral $\tilde{I}_3(u,\tau)$ is obtained as part of the HW model derivations in the preceding section. For the particular case of constant volatility η the state variable $y(t)$ decouples from the Markovian process and the deterministic solution of the defining ODE is treatable in closed form by the method of variation of constants:

$$\begin{aligned}
y(t) &= \tfrac{\eta^2}{2\lambda}+(y_0-\tfrac{\eta^2}{2\lambda})e^{-2\lambda\tau} && \text{(A.60)}\\
\text{with}\quad y_0 &= y(0) \quad \text{as initial condition.}
\end{aligned}$$

Irrespective of the particular choice of y_0, apparently $y(t)$ tends towards the long-term mean $\frac{\eta^2}{2\lambda}$. With the coefficients given above, the discounted CHF of the 1D Markovian Cheyette system is given by

$$\begin{aligned}
\hat{\Phi}_{CH}(u,\mathbf{X}_t,T,t) &= e^{A_{CH}(u,\tau)+\tilde{C}(u,\tau)x_{c,t}+Y(u,\tau)y(t)},\\
&= e^{-\int_0^\tau f(0,t)d\tau+\tilde{C}(u,\tau)x_{c,t}+Y(u,\tau)y(t)}. && \text{(A.61)}
\end{aligned}$$

A.3.1.1 Connection to HW short rate model

Transition from the single volatility factor Cheyette to the HW model can be seen directly from the SDE system. Starting with the Cheyette model

$$\begin{aligned} dx_{c,t} &= (y_t - \lambda x_{c,t})dt + \eta_t dW_c(t), \\ y_t &= (\eta_t^2 - 2\lambda y_t)dt, \end{aligned} \tag{A.62}$$

for $\eta_t = \eta =$const the y_t decouples from the Markovian state variable $x_{c,t}$ and becomes deterministic. By the choices

$$\begin{aligned} dx_{c,t} &= dr_t - \tfrac{\partial}{\partial t} f(0,t), \\ y(t) &= \lambda\theta(t) - \lambda f(0,t) - \tfrac{\partial}{\partial T} f(0,t), \\ \text{so} \quad y(t) &= \tfrac{\eta^2}{2\lambda}(1 - e^{-2\lambda\tau}) \end{aligned} \tag{A.63}$$

the HW model is retained from $x_{c,t}$ dynamics:

$$\begin{aligned} dr_t - \tfrac{\partial}{\partial T} f(0,t) &= (\lambda\theta(t) - \lambda f(0,t) - \tfrac{\partial}{\partial T} f(0,t) - \lambda x_{c,t})dt + \eta dW_c(t), \\ dr_t &= \lambda[\theta(t) - (f(0,t) + x_{c,t})]dt + \eta dW_c(t), \\ \text{with} \quad r_t &= f(0,t) + x_{c,t}. \end{aligned}$$

An analogous argument is valid in Fourier space. Upon closer comparison of the Cheyette (CH) and HW CHFs, i.e.

$$\begin{aligned} \hat{\Phi}_{HW}(u, r_t, t, T) &= e^{A_{HW}(u,\tau) + \tilde{C}(u,\tau) r_t} \\ &= e^{\lambda \int_0^\tau \theta(t)\tilde{C}(u,\tau)d\tau + \frac{\eta^2}{2}\int_0^\tau \tilde{C}^2(u,\tau)d\tau + \tilde{C}(u,\tau) r_t} \\ &= e^{\lambda \int_0^\tau f(0,t)\tilde{C}(u,\tau)d\tau + \int_0^\tau \partial_T f(0,t)\tilde{C}(u,\tau)d\tau + \int_0^\tau y(0,t)\tilde{C}(u,\tau)d\tau} \\ &\cdot\ e^{\frac{\eta^2}{2}\int_0^\tau \tilde{C}^2(u,\tau)d\tau + \tilde{C}(u,\tau) r_t}; \end{aligned} \tag{A.64}$$

$$\hat{\Phi}_{CH}(u, x_{c,t}, y_t, t, T) = e^{A_{CH}(u,\tau) + \tilde{C}(u,\tau) x_{c,t} + Y(u,\tau) y(t)} \tag{A.65}$$

$$= e^{-\int_0^\tau f(0,t)d\tau + \eta^2 \tilde{I}_{CH,y}(u,\tau) + \frac{\eta^2}{2}\tilde{I}_3(u,\tau) + \tilde{C}(u,\tau)(x_{c,t} + f(0,t)) - \tilde{C}(0,t) f(0,t) + Y(u,\tau) y(t)},$$

the connection between individual Fourier constituent terms in the exponential becomes apparent by the reformulations

$$\text{HW}: \int_0^\tau \partial_T f(0,t)\tilde{C}(u,\tau)d\tau = -f(0,t)\tilde{C}(u,\tau) - \int_0^\tau f(0,\tau)d\tau - \lambda \in_0^\tau f(0,t)\tilde{C}(u,\tau)d\tau, \tag{A.66}$$

$$\begin{aligned} \text{CH}: \quad Y(u,\tau)y(t) &= \tfrac{\eta^2}{2\lambda^3}[-\tfrac{1}{2} + e^{-\lambda\tau} - \tfrac{1}{2}e^{-2\lambda\tau} + \tfrac{1}{2}e^{-2\lambda t} - e^{-2\lambda t}e^{-\lambda\tau} + \tfrac{1}{2}e^{-2\lambda t}e^{-2\lambda\tau}] \\ &+ iu\tfrac{\eta^2}{2\lambda}[(e^{-\lambda\tau} - e^{-2\lambda\tau})(1 - e^{-2\lambda t})]. \end{aligned} \tag{A.67}$$

Inserting the reformulations, most of the terms cancel out and the equivalence between HW and Cheyette terms reduces to the following identity:

$$\begin{aligned} \int_0^\tau \tilde{C}(u,\tau)y(t)d\tau &= \tfrac{\eta^2}{2\lambda^3}[-\lambda\tau + 1 - e^{-\lambda\tau} + \tfrac{1}{2}e^{-2\lambda t}(1 - e^{-\lambda\tau})^2] \\ &+ iu\tfrac{\eta^2}{2\lambda^2}[(1 - e^{-\lambda\tau})^2 + (1 - e^{-\lambda\tau})(1 - e^{-2\lambda t})e^{-\lambda\tau}] \\ &= \eta^2 \tilde{I}_{CH,y} + \tfrac{\eta^2}{2}\tilde{I}_3(u,\tau). \end{aligned} \tag{A.68}$$

Comparing coefficients has thus revealed the connection between HW and this most basic Cheyette model, as well as the relation to the initial yield curve:

$$\begin{aligned} \theta(t) &= f(0,t) + \tfrac{1}{\lambda}\tfrac{\partial}{\partial T} f(0,t) + \tfrac{\eta^2}{2\lambda^2}(1 - e^{-2\lambda t}) && \text{(A.69)} \\ &= f(0,t) + \tfrac{1}{\lambda}\tfrac{\partial}{\partial T} f(0,t) + \tfrac{1}{\lambda} y(t). && \text{(A.70)} \end{aligned}$$

For the particular specification of the initial term structure, $f(0,t) = f_0$ and $f_0 = r_0$, employed in the model calibration scenarios in the present context, the HW connection is established by the particular relation $\theta(t) = r_0 + \frac{1}{\lambda} y(t)$.

A.3.2 Zero coupon bond value in the Cheyette model

As elaborated in the context of the HW model above, the value of the zero coupon bond is obtained from the CHF corresponding to the respective model in the limit $u \to 0$:

$$\begin{aligned} P(t,T) &= \hat{\Phi}_{CH}(0, \mathbf{X}_t, t, T) = e^{A_{CH}(0,\tau) + C(0,\tau) x_{c,t} + Y(0,\tau) y(t)} \\ &= e^{-\int_0^\tau f(0,t)\, d\tau - \frac{1}{\lambda}(1 - e^{-\lambda\tau}) x_{c,t} - \frac{1}{2\lambda^2}(1 - e^{-\lambda\tau})^2 y(t)} \\ &= e^{-\int_t^T f(0,s)\, ds - B_c(t,T) x_{c,t} - \frac{1}{2} B_c^2(t,T) y(t)}, && \text{(A.71)} \end{aligned}$$

where $f(0,t)$ provides the connection to the market data via

$$\begin{aligned} P(t,T) &= \mathbb{E}^{\mathbb{Q}}\left[e^{-\int_0^T r_s\, ds} | \mathcal{F}_t \right] \\ &= e^{-\int_0^T f(t,s)\, ds} && \text{(A.72)} \\ \longrightarrow \frac{P^M(0,T)}{P^M(0,t)} &= e^{-\int_t^T f(0,s)\, ds}, && \text{(A.73)} \end{aligned}$$

and consequently, the Cheyette zero bond value is given by

$$P_{CH}(t,T,x_t,y_t) = \frac{P^M(0,T)}{P^M(0,t)} e^{-B_c(t,T) x_{c,t} - \frac{1}{2} B_c^2(t,T) y_t}. \qquad \text{(A.74)}$$

It is important to note that this zero bond value formulation is also valid in the context of model extensions towards stochastic volatility like in the Stochastic Volatility Cheyette model. Hence, the choice of y_t (instead of $y(t)$) in the final equation.
The reason is that the volatility contribution is completely absorbed in the state variable y_t, and is particularly noteworthy, because thereby the Cheyette model allows for stochastic volatility extension beyond the capability of the classical short rate models.
For the special case of the initial term structure, $f(0,t) = f_0$ and $f_0 = r_0$,

$$y_t = y(t) = \lambda r_0 + \tfrac{\eta^2}{2\lambda}(1 - e^{-2\lambda t}), \qquad \text{(A.75)}$$

is basically the variance of the HW process.

A.3.3 CHF of the DDSV Cheyette model

In the most general form the volatility specification in the Cheyette model is $\eta_t = \eta(x_{c,t}, y_t, z_t, t)$. A possible calibration approach is by means of the zero bond formula,

$$P_{DDSVCH}(t,T) \quad = \quad \frac{P^M(0,T)}{P^M(0,t)} e^{-B_c(t,T)x_{c,t} - \frac{1}{2}B_c^2(t,T)y_t}, \tag{A.76}$$

to be used in the analytic Black caplet formula. Critical point is the efficient numerical evaluation of the SDE for y_t.

Appendix B

Characteristic Functions of Full-Scale Hybrid Models in the Spot Measure

B.1 Single correlation Heston Hull-White (1F-HHW) model

B.1.1 Derivation of CHF 1F-HHW

Combining Heston EQ-SV and HW-IR process

$$\begin{aligned} dx_t &= (r_t - \tfrac{v}{2})dt + \sqrt{v_t}dW_x(t), \\ dv_t &= \kappa(\bar{v} - v_t)dt + \gamma\sqrt{v_t}dW_v(t), \\ dr_t &= \lambda(\theta - r_t)dt + \eta dW_r(t), \end{aligned} \tag{B.1}$$

with correlations $\rho_{xv}dt = dW_x dW_v$, $\rho_{rx}dt = dW_r dW_x$, $\rho_{rv}dt = dW_r dW_v$ the covariance matrix

$$\begin{aligned} \Sigma_{\mathbf{X}_t} &= \begin{pmatrix} v_t & \rho_{xv}\gamma v_t & \rho_{xr}\eta\sqrt{v_t} \\ \rho_{vx}\gamma v_t & \gamma^2 v_t & \rho_{vr}\gamma\eta\sqrt{v_t} \\ \rho_{rx}\eta\sqrt{v_t} & \rho_{rv}\gamma\eta\sqrt{v_t} & \eta^2 \end{pmatrix} = L_{\mathbf{X}_t} L_{\mathbf{X}_t}^{\dagger} \\ \text{with} \quad L_{\mathbf{X}_t} &= \begin{pmatrix} \sqrt{v_t} & 0 & 0 \\ \rho_{vx}\gamma\sqrt{v_t} & L_{xv}\gamma\sqrt{v_t} & 0 \\ \rho_{rx}\eta & L_{rv}\eta & L_{rx}\eta \end{pmatrix}, \\ \text{and} \quad & L_{xv} = \sqrt{1-\rho_{xv}^2},\ L_{rv} = (\rho_{rv} - \rho_{rx}\rho_{xv})/L_{xv},\ L_{rx} = \sqrt{1-\rho_{rx}^2 - L_{rv}^2}. \end{aligned} \tag{B.2}$$

contains non-linear terms $\Sigma_{1,3} = \Sigma_{3,1}$ and $\Sigma_{2,3} = \Sigma_{3,2}$ in the state variable $\sqrt{v_t}$. $L_{\mathbf{X}_t}$ is the Cholesky decomposition of the covariance matrix to express the HHW process in differential form by uncorrelated Brownian drivers,

$$\begin{pmatrix} dx_t \\ dv_t \\ dr_t \end{pmatrix} = \mu(\mathbf{X}_t)dt + L_{\mathbf{X}_t} \begin{pmatrix} d\tilde{W}_x(t) \\ d\tilde{W}_v(t) \\ d\tilde{W}_r(t) \end{pmatrix}. \tag{B.3}$$

This formulation is the basis of Monte-Carlo simulation schemes detailed in the description of computational evaluation methods.

By choosing EQ-IR correlation $\rho_{rx} = 0$ and SV-IR correlation $\rho_{rv} = 0$ the non-affine terms in the covariance matrix vanish. The remaining HHW model contains the Heston EQ-SV correlation ρ_{xv}

as correlation factor, and hence, the acronym 1F-HHW. An analytic solution for the CHF is then derivable in closed form by means of the commonly known techniques [21]. With the coefficients extracted from the affine model formulation

$$\begin{aligned}
\mu(\mathbf{X}_t) &= \begin{pmatrix} 0 \\ \kappa\bar{v} \\ \lambda\theta \end{pmatrix} + \begin{pmatrix} 0 & -\frac{1}{2} & 1 \\ 0 & -\kappa & 0 \\ 0 & 0 & -\lambda \end{pmatrix} \begin{pmatrix} x_t \\ v_t \\ r_t \end{pmatrix}, && \text{(B.4)} \\
\Sigma_{\mathbf{X}} &= (c_0)_{ij} + (c_1)^{\dagger}_{ij,\mathbf{x}} \begin{pmatrix} x_t \\ v_t \\ r_t \end{pmatrix} \\
&= \begin{pmatrix} 0 & 0 & 0 \\ 0 & 0 & 0 \\ 0 & 0 & \eta^2 \end{pmatrix} + \begin{pmatrix} (0,1,0) & (0,\rho_{xv}\gamma,0) & (0,0,0) \\ (0,\rho_{xv}\gamma,0) & (0,\gamma^2,0) & (0,0,0) \\ (0,0,0) & (0,0,0) & (0,0,0) \end{pmatrix} \begin{pmatrix} x_t \\ v_t \\ r_t \end{pmatrix}, && \text{(B.5)} \\
\text{and} \quad r(\mathbf{X}_t) &= r_0 + \mathbf{r_1}^{\dagger} \begin{pmatrix} x_t \\ v_t \\ r_t \end{pmatrix} && \text{(B.6)} \\
&= 0 + (0,0,1) \begin{pmatrix} x_t \\ v_t \\ r_t \end{pmatrix},
\end{aligned}$$

the defining ODEs for the Fourier coefficients $\mathbf{B}(\mathbf{u},\tau) = [B(u,\tau), D(u,\tau), C(u,\tau)]^{\dagger}$ and associated initial conditions are given by

$$\begin{aligned}
\frac{d}{d\tau}B(u,\tau) &= 0. && \text{(B.7)} \\
\frac{d}{d\tau}D(u,\tau) &= -0 + (-\tfrac{1}{2}, -\kappa, 0) \begin{pmatrix} B \\ D \\ C \end{pmatrix} + \tfrac{1}{2}(B,D,C) \begin{pmatrix} 1 & \rho_{xv}\gamma & 0 \\ \rho_{xv}\gamma & \gamma^2 & 0 \\ 0 & 0 & 0 \end{pmatrix} \begin{pmatrix} B \\ D \\ C \end{pmatrix} \\
&= -\tfrac{B}{2} - \kappa D + \tfrac{B^2}{2} + \rho_{xv}\gamma BD + \tfrac{\gamma^2}{2}D^2 \\
&= \tfrac{\gamma^2}{2}D^2 + (\rho_{xv}\gamma B - \kappa)D + \tfrac{B}{2}(B-1) \\
\frac{d}{d\tau}C(u,\tau) &= -1 + (1,0,-\lambda) \begin{pmatrix} B \\ D \\ C \end{pmatrix} = -1 + B - \lambda C, && \text{(B.8)} \\
\frac{d}{d\tau}A(u,\tau) &= \kappa\bar{v}D + \lambda\theta C + \tfrac{\eta^2}{2}C^2, && \text{(B.9)}
\end{aligned}$$

and initial conditions $B(u,0) = iu$, $D(u,0) = 0$, $C(u,0) = 0$, $A(u,0) = 0$.
Substituting the solution, $B(u,\tau) = iu$, the ODE for $D(u,\tau)$ becomes the Heston Riccati ODE with the solution already detailed in Appendix A.1. $C(u,\tau)$ is solved by standard techniques (only a slight variation from the Fourier coefficient B in the HW and Cheyette model context above). Finally $A(u,\tau)$ is obtained by straightforward integration, where the integral over $D(u,\tau)$ returns

the complex logarithm denoted in Gatheral's formulation (cf. to appendix A.1 for details):

$$
\begin{aligned}
B(u,\tau) &= iu, \qquad\qquad (B.10)\\
C(u,\tau) &= -\tfrac{1}{\lambda}(1-iu)(1-e^{-\lambda\tau}),\\
D(u,\tau) &= \xi^{-}\frac{1-e^{-d\tau}}{1-ge^{-d\tau}},\\
\text{where}\quad g &= \xi^{-}/\xi^{+},\\
\text{and}\quad \xi^{\pm} &= \frac{\beta \pm (\beta^2 - 2\alpha\gamma^2)^{\frac{1}{2}}}{\gamma^2} = \frac{\beta \pm d}{\gamma^2},\\
\alpha &= \tfrac{iu}{2}(iu-1) = -u^2/2 - iu/2 = \tfrac{B}{2}(B-1),\\
\beta &= \kappa - \rho_{xv}\gamma iu\\
A(u,\tau) &= \lambda\theta\int_0^\tau C(u,\tau)\,d\tau + \tfrac{\eta^2}{2}\int_0^\tau C^2(u,\tau)\,d\tau + \kappa\bar{v}\int_0^\tau D(u,\tau)\,d\tau\\
&= \lambda\theta I_1(u,\tau) + \tfrac{\eta^2}{2} I_3(u,\tau) + \kappa\bar{v} I_2(u,\tau), \qquad (B.11)
\end{aligned}
$$

with

$$
\begin{aligned}
\int_0^\tau C(u,\tau)\,d\tau &= \tfrac{1}{\lambda^2}(iu-1)\left(-\lambda\tau + (1-e^{-\lambda\tau})\right) \equiv I_1(u,\tau),\\
\int_0^\tau C^2(u,\tau)\,d\tau &= \tfrac{1}{\lambda^2}(-u^2-2iu+1)\int_0^\tau (1-2e^{-\lambda\tau}+e^{-2\lambda\tau})\,d\tau\\
&= \tfrac{1}{2\lambda^3}(i+u)^2(-2\lambda\tau - 4e^{-\lambda\tau} + 3 + e^{-2\lambda\tau}) \equiv I_3(u,\tau),\\
\int_0^\tau D(u,\tau)\,d\tau &= \xi^{-}\tau - \frac{2}{\gamma^2}\ln\left[\frac{1-ge^{-d\tau}}{1-g}\right] \equiv I_2(u,\tau).
\end{aligned}
$$

With the solution of the Fourier components completed, the CHF of the 1F-HHW model results

$$
\hat{\Phi}_{1F-HHW}(u,x_t,v_t,r_t,t,T) = e^{A_{1F}(u,\tau)+B(u,\tau)x_t+D(u,\tau)v_t+C(u,\tau)r_t}. \qquad (B.12)
$$

B.1.2 Analytic European call price in the 1F-HHW model

The result on the 1F-HHW CHF is consistent with the derivation of the valuation formula of a European call option in [29]. The derivation of the European call price within the 1F-HHW model is derived in [29] via solution of the Kolmogorov backward equation otained by the Feynman-Kac theorem. Heston already pointed out that the 1F-HHW is an affine model. Analoguos to the pure

Heston case the derivation is based on the formulation of the European call value.s

$$
\begin{aligned}
V_C(S,v,t,T,r0) &= S(t,T) f_{k=1}(X,v,t,T,r_0) - KP(t,T) f_{k=0}(S,v,t,T,r_0,u) \qquad \text{(B.13)}\\
\text{with} \quad f_k(S,v,t,T,r0) &= \frac{1}{2} + \frac{1}{\pi}\int_0^\infty \mathcal{R}\left[\frac{\exp(-iu\log K)\hat{\phi}_j(S,v,t,T,r_0}{iu}\right],\\
\hat{\phi}_k(S,v,t,T,r_0) &= \exp\left[F_k(t,T,u) + D_k(t,T,u)v + H_k(t,T,u)r_0\right]\cdot\\
&\qquad \exp\left[iu\log S + (k-1)b(t,T,r_0)\right] \qquad \text{(B.14)}\\
\text{with} \quad F_k(t,T,u) &= C_k(t,T,u)\bar{v} + (iu-(1-k))\left[\zeta_2(t,T) + (iu-(1-k))\zeta_3(t,T)\right]\\
\text{and} \quad H_k(t,T,u) &= \frac{iu-(1-k)}{\lambda}\left(1-\exp(-\lambda(T-t))\right)
\end{aligned}
$$

where $C_k(t,T,u)$ and $D_k(t,T,u)$ are defined in Appendix A.1; $\zeta_2(t,T)$ and $\zeta_3(t,T)$ are derived in conjunction with the zero bond value $P(t,T) = \exp(b_c(t,T,r_0))$ in the HW framework (cf. Appendix A.2.3), though in slightly alternative arrangement of constituent terms:

$$
\begin{aligned}
P(t,T) &= \exp[(b_c(r_0,t,T)], \qquad \text{(B.15)}\\
b_c(t,T,r_0) &= -\frac{r_0}{\lambda}\left(1-\exp(-\lambda(T-t))\right)\\
&\quad -\frac{1}{\lambda}\int_t^T \theta_{HW}(s)\left(1-\exp(-\lambda(T-s))\right)ds\\
&\quad +\frac{\eta^2}{2\lambda^2}\left(T-t+\tfrac{2}{\lambda}\exp(-\lambda(T-t)) - \tfrac{1}{2\lambda}\exp(-2\lambda(T-t)) - \tfrac{3}{2\lambda}\right)\\
&\equiv \zeta_1(t,T,r_0) + \zeta_2(t,T) + \zeta_3(t,T)\\
\text{with} \quad \theta_{HW}(t) &\rightarrow \theta_{HW} = \text{const} \quad \text{follows}\\
\zeta_2(t,T) &= \frac{\theta_{HW}}{\lambda^2}\left(1-\exp(-\lambda(T-t)) - \lambda(T-t)\right)
\end{aligned}
$$

In analogy to the pure Heston case, the 1F-HHW CHF results in the case $k = 0$.

B.1.3 Zero coupon bond price in the 1F-HHW model

In standard fashion the zero bond value is obtained from the CHF of The 1F-HHW in the limit $u \to 0$:

$$\hat{\Phi}_{1F-HHW} = e^{A(0,\tau)+B(0,\tau)x_t+D(0,\tau)v_t+C(0,\tau)r_t}. \qquad \text{(B.16)}$$

It is trivial to show $D(0,\tau) = 0$ and $B(0,\tau) = 0$ and the remaining terms coincide with terms of the zero bond value in the stand-alone HW model. Consequently the zero bond prices are equivalent in HW and 1F-HHW model environments, which is intuitively embraced by the consideration, that correlations between EQ and IR components are excluded 'a priori'.

B.1.4 Separability of interest rate process in 1F-HHW

A noteworthy feature is that the transformation of the 1F-HHW towards the T-forward measure corresponds to the simple displacement shift of the IR component of the CHF in the complex plane (quite analogously the Fourier coefficient corresponding to the IR component in the H1HW hybrid model changes to $C_B(u,\tau) \to C_T(u,\tau)$ upon transformation to $\mathbb{Q}^T$ as simple displacement in the complex plane). When only the EQ-SV correlation is non-vanishing $\rho_{xv} \neq 0$, the CHF separates into the interest rate $\hat{\phi}_{IR}$ and Heston process $\hat{\phi}_H$:

$$\hat{\phi}_{1F-HHW}(u,t,T) = \hat{\phi}_{IR}(u,t,T)\hat{\phi}_H(u,t,T). \tag{B.17}$$

Then, following [36], the CHF under the T-forward measure $\hat{\phi}_{IR}$ is derived straightforwardly, by splitting the underlying equity process $dS_t = rS_t dt + \sqrt{v}S_t dW_x$ into an interest rate drift and pure driftless Heston process:

$$\begin{aligned} d(\log S) &= (r - \tfrac{v}{2})dt + \sqrt{v}dW_x, \\ dX_t &= dX_{IR} + dX_H \end{aligned} \tag{B.18}$$

with $X_{IR}(t,T) = \int_t^T r(s)ds = D(t,T)$ the discount factor. Then, the CHF ensues to

$$\begin{aligned} \hat{\phi}^T_{HRHW}(t,T,u) &= \mathbb{E}^T[e^{iuX_T}|\mathcal{F}_t], \\ &= \mathbb{E}^{\mathbb{Q}}[e^{iuX_T}\frac{\mathbb{Q}^T}{\mathbb{Q}}|\mathcal{F}_t]/\mathbb{E}^{\mathbb{Q}}[\frac{\mathbb{Q}^T}{\mathbb{Q}}|\mathcal{F}_t], \\ \longrightarrow \hat{\phi}^T_{HRHW}(t,T,u) &= P^{-1}(t,T)\mathbb{E}[D(t,T)e^{iuX_T}] \qquad \text{(B.19)} \\ &= P^{-1}(t,T)\mathbb{E}[e^{-X_{IR}+iuX_T}] \\ &= P^{-1}(t,T)\mathbb{E}[e^{i^2X_{IR}+iu(X_{IR}+X_H)}] \qquad \text{(B.20)} \\ &= P^{-1}(t,T)\hat{\phi}_{IR}(u+i,t,T)\hat{\phi}_H(u,t,T) \end{aligned}$$

where $P(t,T)$ is the standard zero bond. Transformation of the CHF towards the T-forward measure is simply performed by substituting $u \to u+i$ in $\hat{\phi}_{IR}(u,t,T)$.

B.2 Heston Cheyette CHF in the Affine Deterministic Limit: H1CH Model

The Cheyette model in single-factor volatility formulation is comprised of the following set of SDEs:

$$\begin{aligned} dx_{s,t} &= (\pi_t - \tfrac{v_t}{2})dt + \sqrt{v_t}dW_x(t), \\ dv_t &= \kappa(\bar{v} - v_t)dt + \gamma\sqrt{v_t}dW_v(t), \\ dx_{c,t} &= (y_t - \lambda x_{c,t})dt + \eta_t dW_c(t), \\ dy_t &= (\eta_t^2 - 2\lambda y_t)dt, \\ \text{with} \quad \pi_t &= f(0,t) + x_{c,t}, \\ \eta_t &= \eta = \text{const.} \end{aligned} \tag{B.21}$$

For the IR component constant volatility η is considered for the moment, though this constraint is relaxed in the next section. Then, drift, volatility and IR specification assume the expressions:

$$\begin{aligned} \mu(\mathbf{X}_t) &= a_0 + a_1\mathbf{X}_t \\ &= \begin{pmatrix} 0 \\ \kappa\bar{v} \\ 0 \\ \eta^2 \end{pmatrix} + \begin{pmatrix} 0 & -\frac{1}{2} & 1 & 0 \\ 0 & -\kappa & 0 & 0 \\ 0 & 0 & -\lambda & 1 \\ 0 & 0 & 0 & -2\lambda \end{pmatrix} \begin{pmatrix} x_{s,t} \\ v_t \\ x_{c,t} \\ y_t \end{pmatrix}, \end{aligned} \tag{B.22}$$

$$\Sigma_{\mathbf{X}_t} = \begin{pmatrix} v_t & \rho_{xv}\gamma v_t & \rho_{xc}\eta\sqrt{v_t} & 0 \\ \rho_{vx}\gamma v_t & \gamma^2 v_t & \rho_{cv}\eta\gamma\sqrt{v_t} & 0 \\ \rho_{cx}\eta\sqrt{v_t} & \rho_{cv}\eta\gamma\sqrt{v_t} & \eta^2 & 0 \\ 0 & 0 & 0 & 0 \end{pmatrix}. \tag{B.23}$$

Deliberately setting $\rho_{cv} = 0$, and introducing the affine approximation

$$\mathbb{E}[\sqrt{v_t}] \simeq \delta_v(t) = a + be^{-ct} \tag{B.24}$$

the volatility can be written as

$$\begin{aligned} \hat{\Sigma}_{\mathbf{X}_t} &= (c_0)_{ij} + (c_1)_{ij,\mathbf{X}} \\ &= \begin{pmatrix} 0 & 0 & \rho_{xc}\eta\delta_v(t) & 0 \\ 0 & 0 & 0 & 0 \\ \rho_{cx}\eta\delta_v(t) & 0 & \eta^2 & 0 \\ 0 & 0 & 0 & 0 \end{pmatrix} + \\ &\quad \begin{pmatrix} (0,1,0,0) & (0,\rho_{xv}\gamma,0,0) & (0,0,0,0) & (0,0,0,0) \\ (0,\rho_{vx}\gamma,0,0) & (0,\gamma^2,0,0) & (0,0,0,0) & (0,0,0,0) \\ (0,0,0,0) & (0,0,0,0) & (0,0,0,0) & (0,0,0,0) \\ (0,0,0,0) & (0,0,0,0) & (0,0,0,0) & (0,0,0,0) \end{pmatrix} \begin{pmatrix} x_{s,t} \\ v_t \\ x_{c,t} \\ y_t \end{pmatrix}. \end{aligned} \tag{B.25}$$

Finally, the IR component is represented by

$$r(\mathbf{X}_t) = r_0 + r_1^\dagger \mathbf{X}_t = f(0,t) + (0,0,1,0) \begin{pmatrix} x_{s,t} \\ v_t \\ x_{c,t} \\ y_t \end{pmatrix}. \tag{B.26}$$

Then, the Fourier coefficients of the state variable vector $\mathbf{B}(u,\tau) = [B, D, C, Y]^\dagger$ are defined by the following set of ODEs

$$\begin{aligned}
\tfrac{d}{d\tau}B(u,\tau) &= 0, \qquad\qquad (B.27)\\
\tfrac{d}{d\tau}D(u,\tau) &= -0 + (-\frac{B}{2} - \kappa D) + \tfrac{1}{2}(B + \rho_{xv}\gamma D, B\rho_{xv}\gamma + \gamma^2 D, 0, 0)\begin{pmatrix} B \\ D \\ C \\ Y \end{pmatrix}\\
&= \tfrac{\gamma^2}{2}D^2(u,\tau) + (iu\rho_{xv}\gamma - \kappa)D(u,\tau) + \tfrac{B}{2}(B-1)\\
&= \tfrac{\gamma^2}{2}D^2(u,\tau) + (iu\rho_{xv}\gamma - \kappa)D(u,\tau) + \tfrac{iu}{2}(iu-1),\\
\tfrac{d}{d\tau}C(u,\tau) &= -1 + B - \lambda C = -(1-iu) - \lambda C(u,\tau),\\
\tfrac{d}{d\tau}Y(u,\tau) &= C(u,\tau) - 2\lambda Y(u,\tau),\\
\tfrac{d}{d\tau}A(u,\tau) &= -f(0,t) + \kappa\bar{v}D(u,\tau) + \eta^2 Y(u,\tau)\\
&+ \rho_{xc}\eta\delta_1(t)B(u,\tau)C(u,\tau) + \tfrac{\eta^2}{2}C^2(u,\tau),
\end{aligned}$$

and associated initial conditions $B(u,\tau) = iu$, $D(u,\tau) = 0$, $C(u,\tau) = 0$, $Y(u,\tau) = 0$. With the apparent solution, $B(u,\tau) = iu$, $D(u,\tau)$ is reduced to the well-known solution for the Heston-type Riccati equation, and the other Fourier coefficients are determined with standard techniques to solve first order ODEs:

$$\begin{aligned}
C(u,\tau) &= -\tfrac{1}{\lambda}(1-iu)(1-e^{-\lambda\tau}), \qquad (B.28)\\
Y(u,\tau) &= -\tfrac{1}{2\lambda^2}(1-iu)(1-e^{-\lambda\tau})^2 = -\tfrac{1}{2(1-iu)}C^2(u,\tau), \qquad (B.29)\\
A_{H1CH}(u,\tau) &= -\int_0^\tau f(0,t)\,d\tau + \kappa\bar{v}I_2(u,\tau) - \tfrac{\eta^2}{2(1-iu)}I_3(u,\tau)\\
&+ \rho_{xc}\eta I_4(u,\tau) + \tfrac{\eta^2}{2}I_3(u,\tau), \qquad (B.30)
\end{aligned}$$

with

$$\begin{aligned}
\int_0^\tau D(u,\tau)\,d\tau &= I_2(u,\tau),\\
\int_0^\tau Y(u,\tau)\,d\tau &= -\tfrac{1}{2(1-iu)}\int_0^\tau C^2(u,\tau)\,d\tau\\
&= -\tfrac{1}{2(1-iu)}I_3(u,\tau) = \int_0^\tau C(u,\tau)y(t)d\tau, \qquad (B.31)\\
\text{the last relation with } y(t) &= \tfrac{\eta^2}{2\lambda}(1-e^{-2\lambda\tau}) \text{ is the connection to the HW system,} \qquad (B.32)\\
\int_0^\tau \delta_v(T-\hat{\tau})C(u,\hat{\tau})d\hat{\tau} &= -\tfrac{1}{\lambda}iu(1-iu)\int_0^\tau (1-e^{-\lambda\hat{\tau}})(a_1 + b_1 e^{c_1(T-\hat{\tau})})\,d\hat{\tau}\\
&= I_4(u,\tau).
\end{aligned}$$

These Fourier coefficients define the CHF of the H1CH model:

$$\hat{\Phi}_{H1CH} = e^{A_{H1CH}(u,\tau) + iux_{s,t} + D(u,\tau)v_t + C(u,\tau)x_{c,t} + Y(u,\tau)y_t}. \qquad (B.33)$$

B.3 Heston DDSV Cheyette CHF in the Affine Limit 1: H1CV Model

The Heston DDSV Cheyette model combines the Heston process for EQ with a Cheyette framework for the interest rate (IR) component incorporating IR-SV by means of a displaced-diffusion (DD) stochastic volatility (SV) model, which captures IR skew and IR smile features. The model is defined by the following system of stochastic differential equations:

$$\begin{aligned} dx_{s,t} &= (\pi_t - \tfrac{v_t}{2})dt + \sqrt{v_t}dW_x(t), \\ dv_t &= \kappa(\bar{v} - v_t)dt + \gamma\sqrt{v_t}dW_v(t), \\ dx_{c,t} &= (y_t - \lambda x_{c,t})dt + \eta_t dW_c(t), \\ dz_t &= \beta(\bar{z} - z_t)dt + \epsilon\sqrt{z_t}dW_z(t), \\ dy_t &= (\eta_t^2 - 2\lambda y_t)dt, \\ &\text{with} \\ \pi_t &= f(0,t) + x_{c,t}, \\ \eta_t &= \sqrt{z_t}s_k(t)(b_k(t)\pi_t + (1 - b_k(t))\pi_0) \equiv \sqrt{z_t}s_k(t)\Phi_k(t) \end{aligned} \tag{B.34}$$

and correlations $\rho_{xv}dt = dW_x dW_v$, $\rho_{cx}dt = dW_c dW_x$, $\rho_{cz}dt = dW_c dW_z$, $\rho_{cv}dt = dW_c dW_v$, and $\rho_{vz}dt = dW_v dW_z$. The SV processes of the EQ and IR components are presumed to be uncorrelated ($\rho_{zv} = 0$). Substituting the limit 1 approximations (see section 3.6), the constituents of the affine model assume the following form:

$$\mu(\mathbf{X}_t) = \begin{pmatrix} 0 \\ \kappa\bar{v} \\ 0 \\ \beta\bar{z} \\ 0 \end{pmatrix} + \begin{pmatrix} 0 & -\frac{1}{2} & 1 & 0 & 0 \\ 0 & -\kappa & 0 & 0 & 0 \\ 0 & 0 & -\lambda & 0 & 1 \\ 0 & 0 & 0 & -\beta & 0 \\ 0 & 0 & 0 & s_k^2\Phi_k^2 & -2\lambda \end{pmatrix} \begin{pmatrix} x_{s,t} \\ v_t \\ x_{c,t} \\ z_t \\ y_t \end{pmatrix}, \tag{B.35}$$

$$
\begin{aligned}
\Sigma_{\mathbf{X}_t} &= \begin{pmatrix} 0 & 0 & \rho_{cx}s_k\Phi_k\delta_v(t)\delta_z(t) & 0 & 0 \\ 0 & 0 & 0 & 0 & 0 \\ \rho_{cx}s_k\Phi_k\delta_v(t)\delta_z(t) & 0 & 0 & 0 & 0 \\ 0 & 0 & 0 & 0 & 0 \\ 0 & 0 & 0 & 0 & 0 \end{pmatrix} \\
&+ \begin{pmatrix} (0,1,0,0,0) & (0,\rho_{xv}\gamma,0,0,0) & (0,0,0,0,0) & (0,0,0,0,0) & (0,0,0,0,0) \\ (0,\rho_{vx}\gamma,0,0,0) & (0,\gamma^2,0,0,0) & (0,0,0,0,0) & (0,0,0,0,0) & (0,0,0,0,0) \\ (0,0,0,0,0) & (0,0,0,0,0) & (0,0,0,s_k^2\Phi_k^2,0) & (0,0,0,\rho_{zc}s_k\Phi_k\epsilon,0) & (0,0,0,0,0) \\ (0,0,0,0,0) & (0,0,0,0,0) & (0,0,0,\rho_{zc}s_k\Phi_k\epsilon,0) & (0,0,0,\epsilon^2,0) & (0,0,0,0,0) \\ (0,0,0,0,0) & (0,0,0,0,0) & (0,0,0,0,0) & (0,0,0,0,0) & (0,0,0,0,0) \end{pmatrix} \\
&\begin{pmatrix} x_{s,t} \\ v_t \\ x_{c,t} \\ z_t \\ y_t \end{pmatrix}, \qquad \text{(B.36)}
\end{aligned}
$$

$$
r(\mathbf{X}_t) = f(0,t) + \begin{pmatrix} x_{s,t} & v_t & x_{c,t} & z_t & y_t \end{pmatrix} \begin{pmatrix} 0 \\ 0 \\ 1 \\ 0 \\ 0 \end{pmatrix}. \qquad \text{(B.37)}
$$

Then, with the vector of Fourier coefficients, $\mathbf{B} = [B, D, C, Z, Y]^\dagger$, the defining ODEs are

$$
\begin{aligned}
\tfrac{d}{d\tau}B(u,\tau) &= 0, \qquad \text{(B.38)} \\
\tfrac{d}{d\tau}D(u,\tau) &= -0 + (-\tfrac{1}{2}, \kappa, 0, 0, 0)\mathbf{B} \\
&\quad + \tfrac{1}{2}(B,D,C,Z,Y) \begin{pmatrix} 1 & \rho_{xv}\gamma & 0 & 0 & 0 \\ \rho_{xv}\gamma & \gamma^2 & 0 & 0 & 0 \\ 0 & 0 & 0 & 0 & 0 \\ 0 & 0 & 0 & 0 & 0 \\ 0 & 0 & 0 & 0 & 0 \end{pmatrix} \begin{pmatrix} B \\ D \\ C \\ Z \\ Y \end{pmatrix} \\
&= -\tfrac{1}{2}B - \kappa D + \tfrac{1}{2}(B^2 + 2\rho_{xv}\gamma BD + \gamma^2 D) \\
&= \tfrac{\gamma^2}{2}D^2(u,\tau) + (\rho_{xv}\gamma B(u,\tau) - \kappa)D(u,\tau) + \tfrac{B}{2}(B-1), \qquad \text{(B.39)} \\
\tfrac{d}{d\tau}C(u,\tau) &= -1 + (1,0,\lambda,0,0)\mathbf{B} + 0 = -1 + B(u,\tau) - \lambda C(u,\tau), \qquad \text{(B.40)} \\
\tfrac{d}{d\tau}Z(u,\tau) &= -0 + (0,0,0,-\beta, s_k^2\Phi_k^2)\mathbf{B} \\
&\quad + \tfrac{1}{2}(B,D,C,Z,Y) \begin{pmatrix} 0 & 0 & 0 & 0 & 0 \\ 0 & 0 & 0 & 0 & 0 \\ 0 & 0 & s_k^2\Phi_k^2 & \rho_{cz}s_k\Phi_k\epsilon & 0 \\ 0 & 0 & \rho_{cz}s_k\Phi_k\epsilon & \epsilon^2 & 0 \\ 0 & 0 & 0 & 0 & 0 \end{pmatrix} \begin{pmatrix} B \\ D \\ C \\ Z \\ Y \end{pmatrix} \\
&= \tfrac{\epsilon^2}{2}Z^2(u,\tau) + (\rho_{cz}s_k^2\Phi_k^2\epsilon C(u,\tau) - \beta)Z(u,\tau) \\
&\quad + s_k^2\Phi_k^2 Y(u,\tau) + \tfrac{1}{2}s_k^2\Phi_k^2 C^2(u,\tau), \qquad \text{(B.41)} \\
\tfrac{d}{d\tau}Y(u,\tau) &= -0 + (0,0,1,0,-2\lambda)\mathbf{B} + 0 = C(u,\tau) - 2\lambda Y(u,\tau), \qquad \text{(B.42)} \\
\tfrac{d}{d\tau}A(u,\tau) &= -f(0,t) + \kappa\bar{v}D(u,\tau) + \beta\bar{z}Z(u,\tau) + \tfrac{1}{2}\rho_{cx}s_k\Phi_k\delta_v(t)\delta_z(t)B(u,\tau)C(u,\tau), \qquad \text{(B.43)}
\end{aligned}
$$

with $t = T - \tau$ and initial conditions $B(u,0) = iu$, $D(u,0) = 0$, $C(u,0) = 0$, $Z(u,0) = 0$, $A(u,0) = 0$.

The underlying ODEs and corresponding solutions for $B(u,\tau)$, $C(u,\tau)$ and $D(u,\tau)$ are equivalent to the affine HHW models derived previously (cf. relevant appendices for the details).

$$\begin{aligned} B(u,\tau) &= iu, \\ C(u,\tau) &= -\tfrac{1}{\lambda}(1-iu)(1-e^{-\lambda\tau}), \\ D(u,\tau) &= \quad \text{Heston}-\text{type Riccati solution} \end{aligned}$$

$Y(u,\tau)$ is obtained by variation of constants:

$$Y(u,\tau) = -\tfrac{1}{2\lambda^2}(1-iu)(1-e^{-\lambda\tau})^2 = -\tfrac{1}{2(1-iu)}C^2(u,\tau). \tag{B.44}$$

$Z(u,\tau)$ is a Riccati-type differential equation for the SV of the IR component, though different to the Riccati equation obtained for the Heston EQ-SV component earlier, the coefficients are time-dependent. Employing the solutions for the other Fourier coefficients and presuming $\rho_{cz}=0$, the defining ODE is of the form

$$\begin{aligned} \tfrac{d}{d\tau}Z(u,\tau) &= \tfrac{\epsilon^2}{2}Z^2(u,\tau) - \beta Z(u,\tau) + q_1(u,\tau), \\ q_1(u,\tau) &= \tfrac{iu}{2-2iu}C^2(u,\tau) = \tfrac{iu(iu-1)}{2\lambda^2}s_k^2\Phi_k^2(1-e^{-\lambda\tau})^2. \end{aligned} \tag{B.45}$$

As a consequence, an elementary analytic solution is not available. One has to resort to standard numerical methods for ODE solution or to simplify towards $q_1(u,\tau)=q(u)$, time independent parameters where the solution is then a variation of the well-known Heston-type Riccati equation. Again, by straightforward integration $A(u,\tau)$ is given by

$$\begin{aligned} A(u,\tau) &= -\int_0^\tau f(0,t)\,d\tau + \kappa\bar{v}\int_0^\tau D(u,\tau)\,d\tau - \beta\bar{z}\int_0^\tau Z(u,\tau)\,d\tau \\ &+ \tfrac{1}{2}\rho_{cx}s_k\Phi_k\int_0^\tau \delta_v(t)\delta_z(t)B(u,\tau)C(u,\tau)\,d\tau \\ &= -\int_0^\tau f(0,t)\,d\tau + \kappa\bar{v}I_2(u,\tau) + \beta\bar{z}I_5(u,\tau) + \tfrac{1}{2}\rho_{cx}s_k\Phi_k I_7(u,\tau), \end{aligned} \tag{B.46}$$

where the integral $I_2(u,\tau)$ is found in the derivation of the H1HW model above, $I_5(u,\tau)$ references the integral resulting from the IR-SV process in the DDSV Cheyette model, and

$$\begin{aligned} I_7(u,\tau) &= -\tfrac{1}{\lambda}(1-iu)[a_1a_2(\tau+\tfrac{1}{\lambda}(e^{-\lambda\tau}-1)) + \tfrac{a_1b_2}{c_2}(e^{-c_2(T-\tau)}-e^{-c_2T}) + \tfrac{a_2b_1}{c_1}(e^{-c_1(T-\tau)-c_1T}) \\ &+ \tfrac{b_1b_2}{c_1+c_2}(e^{-(c_1+c_2)(T-\tau)}-e^{-(c_1+c_2)T}) \\ &- \tfrac{a_1b_2}{c_2-\lambda}e^{-c_2T}(e^{(c_2-\lambda)\tau}-1) - \tfrac{a_2b_1}{c_1-\lambda}e^{-c_1T}(e^{(c_1-\lambda)\tau}-1) \\ &- \tfrac{b_1b_2}{c_1+c_2-\lambda}e^{-(c_1+c_2)T}(e^{(c_1+c_2-\lambda)\tau}-1))]. \end{aligned} \tag{B.47}$$

With all Fourier coefficients well defined, the CHF of the Heston DDSV Cheyette model in the approximations of the affine limit 1 is determined:

$$\hat{\Phi}_{H1CV}(u,\mathbf{X}_t,t,T) = e^{A(u,\tau)+iux_{s,t}+D(u,\tau)v_t+C(u,\tau)x_{c,t}+Z(u,\tau)z_t+Y(u,\tau)y_t}. \tag{B.48}$$

B.4 Heston DDSV Cheyette CHF in the Affine Limit 2: H2CV Model

The approximations inherent to the H2CV model are introduced in section 3.6. The key idea is to use the volatility specification

$$\begin{aligned} \eta_t^A &\equiv \delta_z(t) s_k \Phi_k^A(t), \qquad \text{and} \quad (\eta_t^A)^2 \equiv z_t (s_k \Phi_k^A(t))^2, \\ \text{with} \quad s_k \Phi_k^A(t) &= s_k \left(b_k (f(0,t) + \alpha(t)) + (1-b_k)(f(0,0) + x_{c,0}) \right), \\ (s_k \Phi_k^A(t))^2 &= s_k^2 [b_k^2 \zeta^2(t) + 2 b_k (1-b_k) \pi_0 \zeta(t) + (1-b_k)^2 \pi_0^2], \\ \text{and} \quad \zeta(t) &= f(0,t) + \alpha(t), \\ \alpha(t) &\equiv \mathbb{E}[x_{c,t}] = \tfrac{\eta_0^2}{2\lambda^2}(1 - e^{-\lambda t})^2, \end{aligned} \tag{B.49}$$

in order to place the SDE system of the HCV model within the AJD process class. With this volatility specification the CHF derivation proceeds completely analogous to the preceding Appendix B.3, and the Fourier coefficients are obtained as the solution to the following first order ODEs:

$$\begin{aligned} \tfrac{d}{d\tau} B(u,\tau) &= 0, \\ \tfrac{d}{d\tau} D(u,\tau) &= \tfrac{\gamma^2}{2} D^2(u,\tau) + (\rho_{xv} \gamma B(u,\tau) - \kappa) D(u,\tau) + \tfrac{B}{2}(B-1), \\ \tfrac{d}{d\tau} C(u,\tau) &= -1 + B(u,\tau) - \lambda C(u,\tau), \\ \tfrac{d}{d\tau} Z(u,\tau) &= -\tfrac{\epsilon^2}{2} Z^2(u,\tau) + [\rho_{cz} (s_k \Phi_k^A(t))^2 \epsilon C(u,\tau) - \beta] Z(u,\tau) \\ &+ (s_k \Phi_k^A(t))^2 Y(u,\tau) + \tfrac{1}{2} (s_k \Phi_k^A)^2 C^2(u,\tau), \\ \tfrac{d}{d\tau} Y(u,\tau) &= C(u,\tau) - 2\lambda Y(u,\tau), \\ \tfrac{d}{d\tau} A(u,\tau) &= -f(0,t) + \kappa \bar{v} D(u,\tau) + \beta \bar{z} Z(u,\tau) + \tfrac{1}{2} \rho_{cx} s_k \Phi_k^A(t) \delta_v(t) \delta_z(t) B(u,\tau) C(u,\tau), \end{aligned} \tag{B.50}$$

with $t = T - \tau$ and initial conditions $B(u,0) = iu$, $D(u,0) = 0$, $C(u,0) = 0$, $Z(u,0) = 0$, $A(u,0) = 0$. The solutions of $B(u,\tau)$, $D(,u,\tau)$, $C(u,\tau)$, $Y(u,\tau)$ are equivalent to the preceding Appendix B.3. The coefficient $Z(u,\tau)$ is calculated as recursive as recursive solution to

$$\begin{aligned} \tfrac{d}{d\tau} Z(u,\tau) &= \tfrac{\epsilon^2}{2} Z^2(u,\tau) - \beta Z(u,\tau) + q_2(u,\tau), \\ q_2(u,\tau) &= \tfrac{iu}{2-2iu} C^2(u,\tau) = \tfrac{iu(iu-1)}{2\lambda^2} (s_k \Phi_k^A(T-\tau))^2 (1 - e^{-\lambda\tau})^2. \end{aligned} \tag{B.51}$$

We presume $q_2(u,\tau)$ to be piecewise constant in time $q_2(u,\tau) \simeq q_2(u,\tau_j)$ on intervals $\tau_j \in [T_j, T_{j+1}[$ for a particular choice of refinement $0 \le j \le j_{max}$. Then, the Cheyette SV process is recursively given by

$$Z_j(u,\tau_{j+1}) = Z(u,\tau_j) + \tfrac{\xi_{j+1}^-}{\epsilon^2} \frac{1 - e^{-d_{j+1}(\tau_{j+1} - \tau_j)}}{1 - \frac{\xi_{j+1}^-}{\xi_{j+1}^+} e^{-d_{j+1}(\tau_{j+1} - \tau_j)}}, \tag{B.52}$$

with coefficients

$$\begin{aligned} \hat{d}_{j+1} &= \sqrt{\beta^2 - 2\hat{\alpha}\epsilon^2}, \\ \hat{\xi}_j^{\pm} &= \beta \pm (d_{j+1} + d_j)/2 - \epsilon^2 Z_j, \\ \hat{\alpha} &= \tfrac{iu(iu-1)}{2\lambda^2} (s_k \Phi_k^A(T - \tau_j))^2 (1 - e^{-\lambda \tau_j})^2. \end{aligned}$$

The quality of the recursive approximation of $Z(u,\tau)$ with the term $q_2(u,\tau)$ is very close to the recursive solution of $Z(u,\tau)$ with $q_1(u,\tau)$ corrsponding to the H1CV model as shown in Fig. E.2. Finally, $A(u,\tau)$ is obtained by integration,

$$\begin{aligned} A(u,\tau) &= -\int_0^\tau f(0,t)\,d\tau + \kappa\bar{v}\int_0^\tau D(u,\tau)\,d\tau - \beta\bar{z}\int_0^\tau Z(u,\tau)\,d\tau \\ &+ \tfrac{1}{2}\rho_{cx}s_k\int_0^\tau \Phi_k^A(t)\delta_v(t)\delta_z(t)B(u,\tau)C(u,\tau)\,d\tau \\ &= -\int_0^\tau f(0,t)\,d\tau + \kappa\bar{v}I_2(u,\tau) + \beta\bar{z}I_8(u,\tau) + \tfrac{1}{2}\rho_{cx}s_k\Phi_k I_9(u,\tau). \end{aligned}$$

Though the integral $I_9(u,\tau)$ is straightforwardly derived in closed form, the numerical integration of $I_7(u,\tau)$ and $I_9(u,\tau)$ is a computationally practical approach.

Appendix C

Change of Measure

C.1 Derivation of H1HW CHF in the Forward Measure $\mathbb{Q}^T$

Forward Dynamics are obtained from the definition of the forward price $F_t = F(S_t, P_t) = S_t/P(t,T)$ by Ito's lemma:

$$\begin{aligned} dF_t &= \frac{\partial F}{\partial S} + \frac{\partial F}{\partial P} + \tfrac{1}{2}\frac{\partial^2 F}{\partial S^2} + \tfrac{1}{2}\frac{\partial^2 F}{\partial P^2} + \frac{\partial^2 F}{\partial P \partial S} \\ &= \frac{1}{P}dS - \frac{S}{P^2}dP + 0 + \tfrac{1}{2}\frac{2S}{P^3}(dP)^2 - \tfrac{1}{2}\frac{2}{P^2}dPdS \\ &= \frac{S_t}{P(t,T)}\frac{dS}{S} - \frac{S_t}{P(t,T)}\frac{dP}{P} + \text{drift terms} \\ &= F\left(\frac{dS}{S} - \frac{dP}{P}\right) + F\left[\left(\frac{dP}{P}\right)^2 - \frac{dS}{S}\frac{dP}{P}\right], \\ \frac{dF}{F} &= \frac{dS}{S} - \frac{dP}{P} + \left(\frac{dP}{P}\right)^2 - \frac{dS}{S}\frac{dP}{P}. \end{aligned} \tag{C.1}$$

The change of measure is to be applied to uncorrelated Brownian drivers. Therefore, the covariance matrix $\Sigma_{\mathbf{X}_t} = L_{\mathbf{X}_t} L^{\dagger}_{\mathbf{X}_t}$ is decomposed into Cholesky components:

$$\begin{aligned} \mathrm{d}\mathbf{X}_t &= \mu(\mathbf{X}_t)^0 dt + L_{\mathbf{X}_t}\mathrm{d}\tilde{\mathbf{W}}^{\mathbf{0}}, \\ \begin{pmatrix} dr_t \\ dv_t \\ \frac{dS_t}{S_t} \end{pmatrix} &= \begin{pmatrix} \lambda(\theta(t) - r_t) \\ \kappa(\bar{v} - v_t) \\ r_t \end{pmatrix} dt + \begin{pmatrix} \eta_t & 0 & 0 \\ \rho_{vr}\gamma\sqrt{v_t} & L_{vv}\gamma\sqrt{v_t} & 0 \\ \rho_{xr}\sqrt{v_t} & L_{xv}\sqrt{v_t} & L_{xx}\sqrt{v_t} \end{pmatrix} \begin{pmatrix} d\tilde{W}^0_r(t) \\ d\tilde{W}^0_v(t) \\ d\tilde{W}^0_x(t) \end{pmatrix}, \\ \text{with} \quad & L_{vv} = \sqrt{1-\rho^2_{rv}},\ L_{xv} = (\rho_{xv} - \rho_{xr}\rho_{rv})/L_{vv},\ L_{xx} = \sqrt{1-\rho^2_{xr} - L^2_{xv}}. \end{aligned} \tag{C.2}$$

The superscript $'0'$ indicates that at this point the drift and Brownian drivers are still considered in the spot measure $\mathbb{Q}^0$.

We have as **stock dynamics**

$$\frac{dS}{S} = r_t dt + \sqrt{v_t}dW^0_x = r_t dt + \rho_{xr}\sqrt{v_t}d\tilde{W}^0_r + L_{xv}\sqrt{v_t}d\tilde{W}^0_v + L_{xx}\sqrt{v_t}d\tilde{W}^0_x, \tag{C.3}$$

as **zero coupon bond dynamics**,

$$\frac{dP}{P} = r_t dt + \eta B_r dW^0_r = r_t dt + \eta B_r d\tilde{W}^0_r \quad \text{with} \quad B_r = -\tfrac{1}{\lambda}(1 - e^{-\lambda\tau}), \tag{C.4}$$

$$\left(\frac{dP}{P}\right)^2 = \eta^2 B^2_r dt \quad \text{and} \quad -\left(\frac{dP}{P}\right)\left(\frac{dS}{S}\right) = -\rho_{xr}\sqrt{v_t}\eta B_r dt. \tag{C.5}$$

Then, the forward dynamics read

$$\frac{dF_t}{F_t} = (\eta^2 B_r^2 - \rho_{xr}\eta B_r\sqrt{v_t})dt + (\rho_{xr}\sqrt{v_t} - \eta B_r)d\tilde{W}_r^0 + L_{xv}\sqrt{v_t}d\tilde{W}_v^0 + L_{xx}\sqrt{v_t}d\tilde{W}_x^0. \quad \text{(C.6)}$$

The **Girsanov kernel** obtained from the zero coupon bond dynamics to perform the transformation from the risk-neutral towards the T-forward measure, $\mathbb{Q}^0 \to \mathbb{Q}^T$ reads

$$\begin{pmatrix} d\tilde{W}_r^0 \\ d\tilde{W}_v^0 \\ d\tilde{W}_x^0 \end{pmatrix} = \begin{pmatrix} \eta B_r \\ 0 \\ 0 \end{pmatrix} dt + \begin{pmatrix} d\tilde{W}_r^T \\ d\tilde{W}_v^T \\ d\tilde{W}_x^T \end{pmatrix}. \quad \text{(C.7)}$$

Since the forward price is a martingale under the T-forward measure $F_t = \mathbb{E}^T[F_T|\mathcal{F}_t]$, the forward dynamics should be driftless:

$$\begin{aligned} \longrightarrow \frac{dF_t}{F_t} &= (\rho_{xr}\sqrt{v_t} - \eta B_r)d\tilde{W}_r^T + L_{xv}\sqrt{v_t}d\tilde{W}_v^T + L_{xx}\sqrt{v_t}d\tilde{W}_x^T \\ &= -\eta B_r dW_r^T + \sqrt{v_t}dW_v^T. \end{aligned} \quad \text{(C.8)}$$

However, drift components arise in the log-transform

$$\begin{aligned} d\hat{x}_t = d\log F &= -\tfrac{1}{2}[(\rho_{xr}^2 + L_{xv}^2 + L_{xx}^2)v_t - 2\rho_{xr}\eta B_r\sqrt{v_t} + \eta^2 B_r^2]dt + \\ &\quad (\rho_{xr}\sqrt{v_t} - \eta B_r)d\tilde{W}_r^T + L_{xv}\sqrt{v_t}d\tilde{W}_v^T + L_{xx}\sqrt{v_t}d\tilde{W}_x^T \\ &= -\tfrac{1}{2}(v_t - 2\rho_{xr}\eta B_r\sqrt{v_t} + \eta^2 B_r^2)dt + \\ &\quad (\rho_{xr}\sqrt{v_t} - \eta B_r)d\tilde{W}_r^T + L_{xv}\sqrt{v_t}d\tilde{W}_v^T + L_{xx}\sqrt{v_t}d\tilde{W}_x^T \\ &= -\tfrac{1}{2}(v_t - \xi(t))dt + \\ &\quad (\rho_{xr}\sqrt{v_t} - \eta B_r)d\tilde{W}_r^T + L_{xv}\sqrt{v_t}d\tilde{W}_v^T + L_{xx}\sqrt{v_t}d\tilde{W}_x^T. \end{aligned} \quad \text{(C.9)}$$

For the state vector $\mathbf{X}_t = [r_t, v_t, \hat{x}_t]^\dagger$ the affine decomposition of the SDE system in the T-Forward measure assumes the form:

$$\mu(\mathbf{X}_t) = a_0 + a_1\mathbf{X}_t \quad \text{(C.10)}$$

$$= \left(\begin{array}{c} \lambda(\theta(t) - r_t) - \eta^2 B_r \\ \hline \kappa(\bar{v} - v_t) \\ \rho_{xr}\eta B_r\delta_v - \frac{\eta^2}{2}B_r^2 - \frac{v_t}{2} \end{array}\right) = \left(\begin{array}{c} \lambda\theta(t) - \eta^2 B_r \\ \hline \kappa\bar{v} \\ \frac{1}{2}\xi(t) \end{array}\right) + \left(\begin{array}{c|cc} -\lambda & 0 & 0 \\ \hline 0 & -\kappa & 0 \\ 0 & -\frac{1}{2} & 0 \end{array}\right)\left(\begin{array}{c} r_t \\ \hline v_t \\ \hat{x}_t \end{array}\right),$$

$$\Sigma_{\mathbf{X}_t} = LL^\dagger = c_0 + c_1^\dagger\mathbf{X}_t \quad \text{(C.11)}$$

$$= \left(\begin{array}{c|cc} \eta^2 & \rho_{rv}\gamma\eta\delta_v & \rho_{rx}\eta\delta_v \\ \hline \rho_{rv}\gamma\eta\delta_v & 0 & 0 \\ \rho_{rx}\eta\delta_v & 0 & 0 \end{array}\right) + \left(\begin{array}{c|cc} (0,0,0) & (0,0,0) & (0,0,0) \\ \hline (0,0,0) & (0,\gamma^2,0) & (0,\rho_{xv}\gamma,0) \\ (0,0,0) & (0,\rho_{xv}\gamma,0) & (0,1,0) \end{array}\right)^\dagger \mathbf{X}_t,$$

$$r = r_0 + \mathbf{r_1}^\dagger\mathbf{X}_t = 0 + (1,0,0)^\dagger\mathbf{X}_t.$$

As indicated by the broken lines, in the T-forward measure the matrices separate into IR and EQ components without cross terms; in particular the coefficients on the EQ side are independent of r_t. Therefore, the Browian drivers $d\tilde{W}_r^T$ and $d\tilde{W}_x^T$ are combined without any loss of information

$$\begin{aligned} &\rho_{xr}\sqrt{v_t} - \eta B_r)d\tilde{W}_r^T + L_{xx}\sqrt{v_t}d\tilde{W}_x^T + L_{xv}d\tilde{W}_v^T, \\ &[(\rho_{xr}\sqrt{v_t} - \eta B_r)^2 - L_{xx}^2 v(t)]^{\frac{1}{2}}d\tilde{W}_F^T + \rho_{xv}d\tilde{W}_v^T \\ = &[\eta^2 B_r^2 - 2\rho_{xr}\eta B_r\delta_v(t) + v_t - \rho_{xv}^2 v_t]^{\frac{1}{2}}d\tilde{W}_F^T + \rho_{xv}\sqrt{v_t}d\tilde{W}_v^T \\ \equiv &[(v_t - \xi(t)) - \rho_{xv}^2 v_t]^{\frac{1}{2}}d\tilde{W}_F^T + \rho_{xv}\sqrt{v_t}d\tilde{W}_v^T = (v_t - \xi(t))^{\frac{1}{2}}d\tilde{W}_F^T, \end{aligned} \quad \text{(C.12)}$$

to form the Brownian drivers under the T-forward measure. This is in effect a dimensional reduction from $3D$ to $2D$. With the corresponding state vector $\hat{\mathbf{X}}_t = [v_t, \hat{x}_t]^\dagger$ the affine decompositon of the H1HW hybrid model gives rise to the following form under $\mathbb{Q}^T$:

$$\begin{aligned}
\mu^F(\mathbf{X}_t) &= a_0 + a_1\hat{\mathbf{X}}_t \qquad (C.13)\\
&= \begin{pmatrix} \kappa(\bar{v} - v_t) \\ \rho_{xr}\eta B_r\delta_v - \frac{\eta^2}{2}B_r^2 - \frac{v_t}{2} \end{pmatrix} = \begin{pmatrix} \kappa\bar{v} \\ \frac{1}{2}\xi(t) \end{pmatrix} + \begin{pmatrix} -\kappa & 0 \\ -\frac{1}{2} & 0 \end{pmatrix}\begin{pmatrix} v_t \\ \hat{x}_t \end{pmatrix},\\
\Sigma^F_{\mathbf{X}_t} &= \begin{pmatrix} \gamma^2 v_t & \rho_{xv}\gamma v_t \\ \rho_{xv}\gamma v_t & v_t - \xi(t) \end{pmatrix} = c_0 + c_1^\dagger\hat{\mathbf{X}}_t\\
&= \begin{pmatrix} 0 & 0 \\ 0 & -\xi(t) \end{pmatrix} + \begin{pmatrix} (\gamma^2, 0) & (\rho_{xv}\gamma, 0) \\ (\rho_{xv}\gamma, 0) & (1, 0) \end{pmatrix}^\dagger \hat{\mathbf{X}}_t,\\
r &= r_0 + \mathbf{r_1}^\dagger\hat{\mathbf{X}}_t = 0 + (1, 0, 0)^\dagger\hat{\mathbf{X}}_t.
\end{aligned}$$

For the corresponding Fourier state vector, $\mathbf{B} = [D, B]^\dagger$, the coefficients of the CHF are defined by ODEs

$$\begin{aligned}
\tfrac{d}{d\tau}\mathbf{B}(u,\tau) &= -\mathbf{r_1} + a_1^\dagger\mathbf{B} + \tfrac{1}{2}\mathbf{B}^\dagger(c_1)_{\hat{\mathbf{X}}_t}\mathbf{B}, \qquad (C.14)\\
\tfrac{d}{d\tau}D(u,\tau) &= \tfrac{\gamma^2}{2}D^2 + (\rho_{xv}\gamma B - \kappa)D + \tfrac{B}{2}(B-1),\\
\tfrac{d}{d\tau}B(u,\tau) &= 0,\\
\text{and}\quad \tfrac{d}{d\tau}A(u,\tau) &= -r_0 + \mathbf{B}^\dagger a_0 + \tfrac{1}{2}\mathbf{B}^\dagger c_0\mathbf{B},\\
\tfrac{d}{d\tau}A(u,\tau) &= \kappa\bar{v}D + \tfrac{\xi(t)}{2}B - \tfrac{\xi(t)}{2}B^2\\
&= \kappa\bar{v}D + (\rho_{xr}\eta B_r\delta_v - \tfrac{\eta^2}{2}B_r^2)\tfrac{B}{2}(1-B).
\end{aligned}$$

with initial conditions $B(u,0) = iu$, $D(u,0) = 0$, $A(u,0) = 0$ given by the choice $\mathbf{u}^\dagger = [0, 0, u]^\dagger$. The corresponding solutions are

$$\begin{aligned}
C_T(u,\tau) &= -\tfrac{1}{\lambda}(1 - e^{-\lambda\tau}) = B_r, \qquad (C.15)\\
D(u,\tau) &= (\text{Heston Riccati solution}),\\
B(u,\tau) &= iu,\\
A_{H1HW}(u,\tau) &= \int_0^\tau [\tfrac{d}{d\tau}A(u,\tau)]d\tau
\end{aligned}$$

Since the IR dynamics separate, the CHF of the H1HW model in the T-forward measure reduces to

$$\begin{aligned}
\hat{\Phi}^T(\mathbf{u}, \hat{\mathbf{X}}_t, T, t) &= \mathbb{E}^T\left[e^{i\mathbf{u}^\dagger\hat{\mathbf{X}}_t}|\mathcal{F}_t\right] = \mathbb{E}^T\left[e^{iu\hat{x}_t}|\mathcal{F}_t\right] = e^{A^T_{H1HW}(u,\tau) + B(u,\tau)\hat{x}_t + D(u,\tau)v_t}, \qquad (C.16)\\
&\quad \text{with initial condition} \quad \hat{\Phi}^T(u, \hat{\mathbf{X}}_t, T, T) = e^{i\mathbf{u}^\dagger\hat{\mathbf{X}}_T} = e^{iu\hat{x}_T},\\
\text{and}\quad \tfrac{d}{d\tau}A^T_{H1HW}(u,\tau) &= \kappa\bar{v}D + (u^2 + iu)(\rho_{xr}\eta B_r\delta_v - \tfrac{\eta^2}{2}B_r^2), \qquad (C.17)\\
A^T_{H1HW}(u,\tau) &= \kappa\bar{v}\int_0^\tau D(u,\tau)d\tau + (u^2+iu)\rho_{xr}\eta\int_0^\tau \delta_v C_T(u,\tau)d\tau - (u^2+iu)\tfrac{\eta^2}{2}\int_0^\tau C_T^2(u,\tau)d\tau\\
&= \kappa\bar{v}I_2(u,\tau) + \rho_{xr}\eta I_4^T(u,\tau) - \tfrac{\eta^2}{2}I_3^T(u,\tau), \qquad (C.18)
\end{aligned}$$

with integrals modified with respect to the spot measure results obtained earlier (cf. sections B.1 and 3.2.1):

$$\begin{aligned}
\rho_{rx}\eta I_4^T(u,\tau) &= \rho_{rx}\eta\int_0^T (u^2+iu)\delta_v(t)C(u,\tau)\,d\tau = (u^2+iu)\tfrac{\rho_{xr}\eta}{\lambda} \\
&\quad \left[-\tfrac{b}{c}e^{-cT}(1-e^{c\tau})+a\tau-\tfrac{a}{\lambda}(1-e^{-\lambda\tau})+\tfrac{b}{c-\lambda}(1-e^{-\tau(\lambda-c)})\right] \\
&= \tfrac{1}{iu-1}\rho_{xr}I_4, \\
\int_0^\tau C_T^2(u,\tau)\,d\tau &= \tfrac{u^2+iu}{\lambda^2}\int_0^\tau (1-2e^{-\lambda\tau}+e^{-2\lambda\tau})\,d\tau \\
&= \tfrac{u^2+iu}{2\lambda^3}(-2\lambda\tau-4e^{-\lambda\tau}+3+e^{-2\lambda\tau}) = I_3^T(u,\tau). \qquad \text{(C.19)}
\end{aligned}$$

C.2 Derivation of the H1CH CHF in the Forward Measure $\mathbb{Q}^T$

In order to derive the **forward dynamics**, we define the SDE system represented by the covariance matrix $\Sigma_{\mathbf{X}_t} = L_{\mathbf{X}_t}L_{\mathbf{X}_t}^\dagger$ in Cholesky components, i.e.

$$\begin{aligned}
\mathrm{d}\mathbf{X}_t &= \mu^0(\mathbf{X}_t)dt + L_{\mathbf{X}_t}\mathrm{d}\tilde{\mathbf{W}}^{\mathbf{0}}, \qquad \text{(C.20)} \\
\begin{pmatrix} dy_t \\ dx_{c,t} \\ \hdashline dv_t \\ \frac{dS_t}{S_t} \end{pmatrix} &= \left(\begin{array}{c} \eta^2-2\lambda y_t \\ y_t-\lambda x_{c,t} \\ \hdashline \kappa(\bar{v}-v_t) \\ r_t \end{array}\right)dt + \left(\begin{array}{cc:cc} 0 & 0 & 0 & 0 \\ 0 & \eta & 0 & 0 \\ \hdashline 0 & \rho_{vc}\gamma\sqrt{v_t} & L_{vv}\gamma\sqrt{v_t} & 0 \\ 0 & \rho_{xc}\sqrt{v_t} & L_{xv}\sqrt{v_t} & L_{xx}\sqrt{v_t} \end{array}\right)\begin{pmatrix} d\tilde{W}_y^0(t) \\ d\tilde{W}_c^0(t) \\ d\tilde{W}_v^0(t) \\ d\tilde{W}_x^0(t) \end{pmatrix}, \\
\text{with} \quad & L_{vv} = \sqrt{1-\rho_{vc}^2} \wedge L_{xv} = (\rho_{xv}-\rho_{xc}\rho_{vc})/L_{vv} \wedge L_{xx} = \sqrt{1-\rho_{xc}^2-L_{xv}^2}.
\end{aligned}$$

Superscript $'0'$ indicates that at this point the drift and Brownian drivers are in the spot measure $\mathbb{Q}^0$.

So, we find for the **stock dynamics**

$$\frac{dS}{S} = r_t dt + \sqrt{v_t}dW_x^0 = r_t + \rho_{xc}\sqrt{v_t}d\tilde{W}_c^0 + L_{xv}\sqrt{v_t}d\tilde{W}_v^0 + L_{xx}\sqrt{v_t}d\tilde{W}_x^0. \qquad \text{(C.21)}$$

For the **zero coupon bond dynamics** we have

$$\begin{aligned}
\frac{dP}{P} &= r_t dt + \eta B_c dW_x^0 = r_t dt + \eta B_c d\tilde{W}_c^0 \quad \text{with} \quad B_c = -\tfrac{1}{\lambda}(1-e^{-\lambda\tau}), \qquad \text{(C.22)} \\
\left(\frac{dP}{P}\right)^2 &= \eta^2 B_c^2 dt \quad \text{and} \quad -\left(\frac{dP}{P}\right)\left(\frac{dS}{S}\right) = -\rho_{xc}\sqrt{v_t}\eta B_c dt. \qquad \text{(C.23)}
\end{aligned}$$

Then, the forward dynamics are found as

$$\frac{dF}{F} = (\eta^2 B_c^2 - \rho_{xc}\eta B_c\sqrt{v_t})dt + (\rho_{xc}\sqrt{v_t}-\eta B_c)d\tilde{W}_c^0 + L_{xv}\sqrt{v_t}d\tilde{W}_v^0 + L_{xx}\sqrt{v_t}d\tilde{W}_x^0. \qquad \text{(C.24)}$$

The **Girsanov kernel** obtained from the zero coupon bond dynamics to perform the transformation from the risk-neutral towards the T-forward measure $\mathbb{Q}^0 \to \mathbb{Q}^T$ is given by

$$\begin{pmatrix} d\tilde{W}_c^0 \\ d\tilde{W}_v^0 \\ d\tilde{W}_x^0 \end{pmatrix} = \begin{pmatrix} \eta B_c \\ 0 \\ 0 \end{pmatrix}dt + \begin{pmatrix} d\tilde{W}_c^T \\ d\tilde{W}_v^T \\ d\tilde{W}_x^T \end{pmatrix}. \qquad \text{(C.25)}$$

Since the forward price is as a martingale under the T-forward measure, $F_t = \mathbb{E}^T[F_T|\mathcal{F}_t]$, the forward dynamics should be driftless:

$$\longrightarrow \frac{dF_t}{F_t} = (\rho_{xc}\sqrt{v_t} - \eta B_c)d\tilde{W}_c^T + L_{xv}\sqrt{v_t}d\tilde{W}_v^T + L_{xx}\sqrt{v_t}d\tilde{W}_x^T, \tag{C.26}$$

however, drift components arise in the log-transform

$$\begin{aligned} d\hat{x}_t = d\log F_t &= -\tfrac{1}{2}[(\rho_{xc}^2 + L_{xv}^2 + L_{xx}^2)v_t - 2\rho_{xc}\eta B_c\sqrt{v_t} + \eta^2 B_c^2]dt + \\ &\quad (\rho_{xc}\sqrt{v_t} - \eta B_c)d\tilde{W}_c^T + L_{xv}\sqrt{v_t}d\tilde{W}_v^T + L_{xx}\sqrt{v_t}d\tilde{W}_x^T \\ &= (-\tfrac{v_t}{2} + \rho_{xc}\eta B_c\sqrt{v_t} - \tfrac{\eta^2}{2}B_c^2)dt + \\ &\quad (\rho_{xc}\sqrt{v_t} - \eta B_c)d\tilde{W}_c^T + L_{xv}\sqrt{v_t}d\tilde{W}_v^T + L_{xx}\sqrt{v_t}d\tilde{W}_x^T. \end{aligned} \tag{C.27}$$

For the state vector, $\hat{\mathbf{X}}_t = [y_t, x_{c,t}, v_t, \hat{x}_t]^\dagger$, the affine decomposition of the SDE system in the T-forward measure is given by

$$\begin{aligned} \mu(\hat{\mathbf{X}}_t) &= a_0 + a_1\mathbf{X}_t = \begin{pmatrix} \eta^2 - 2\lambda y_t \\ y_t - \lambda x_{c,t} \\ \hline \kappa(\bar{v} - v_t) \\ \rho_{xc}\eta B_c\delta_v - \frac{\eta^2}{2}B_c^2 - \frac{v_t}{2} \end{pmatrix} \\ &= \begin{pmatrix} \eta^2 \\ f(0,t) \\ \hline \kappa\bar{v} \\ \frac{1}{2}\xi_c(t) \end{pmatrix} + \left(\begin{array}{cc:cc} -2\lambda & 0 & 0 & 0 \\ 1 & -\lambda & 0 & 0 \\ \hdashline 0 & 0 & -\kappa & 0 \\ 0 & 0 & -\frac{1}{2} & 0 \end{array}\right) \begin{pmatrix} y_t \\ x_{c,t} \\ \hline v_t \\ \hat{x}_t \end{pmatrix}, \\ \Sigma_{\hat{\mathbf{X}}_t} &= LL^\dagger = c_0 + c_1^\dagger\hat{\mathbf{X}}_t \qquad \text{(C.28)} \\ &= \left(\begin{array}{cc:cc} 0 & 0 & 0 & 0 \\ 0 & \eta^2 & \rho_{cv}\gamma\eta\delta_v & \rho_{cx}\eta\delta_v \\ \hdashline 0 & \rho_{vc}\gamma\eta\delta_v & 0 & 0 \\ 0 & \rho_{xc}\eta\delta_v & 0 & 0 \end{array}\right) + \left(\begin{array}{cc:cc} (0) & (0) & (0,0,0,0) & (0,0,0,0) \\ (0) & (0) & (0,0,0,0) & (0,0,0,0) \\ \hdashline (0) & (0) & (0,0,\gamma^2,0) & (0,0,\rho_{xv}\gamma,0) \\ (0) & (0) & (0,0,\rho_{xv}\gamma,0) & (0,0,1,0) \end{array}\right)^\dagger \hat{\mathbf{X}}_t, \\ r &= r_0 + \mathbf{r_1}^\dagger\hat{\mathbf{X}}_t = 0 + (0,1,0,0)^\dagger\hat{\mathbf{X}}_t. \qquad \text{(C.29)} \end{aligned}$$

As indicated by the broken lines, in the T-forward measure the matrices separate into IR and EQ components without cross terms; in particular the coefficients on the EQ side are independent of $x_{c,t}$ and y_t. Therefore

$$\begin{aligned} & \rho_{xc}\sqrt{v_t} - \eta B_c)d\tilde{W}_c^T + L_{xx}\sqrt{v_t}d\tilde{W}_x^T + L_{xv}d\tilde{W}_v^T \\ \longrightarrow\ & [(\rho_{xc}\sqrt{v_t} - \eta B_c)^2 - L_{xx}^2 v(t)]^{\frac{1}{2}}d\tilde{W}_F^T + \rho_{xv}d\tilde{W}_v^T \\ =\ & [\eta^2 B_c^2 - 2\rho_{xc}\eta B_c\delta_v(t) + v_t - \rho_{xv}^2 v_t]^{\frac{1}{2}}d\tilde{W}_F^T + \rho_{xv}\sqrt{v_t}d\tilde{W}_v^T \\ \equiv\ & [(v_t - \xi_c(t)) - \rho_{xv}^2 v_t]^{\frac{1}{2}}d\tilde{W}_F^T + \rho_{xv}\sqrt{v_t}d\tilde{W}_v^T = (v_t - \xi_c(t))^{\frac{1}{2}}d\tilde{W}_F^T, \end{aligned} \tag{C.30}$$

Again in analogy to the H1HW system discussed in the preceding section, this is in effect a dimension reduction from $3D$ to $2D$. With the corresponding state vector $\hat{\mathbf{X}}_t = [v_t, \hat{x}_t]^\dagger$ the affine decompositon

of the H1CH hybrid model assumes the following form under $\mathbb{Q}^T$:

$$\begin{aligned}
\mu^F(\mathbf{X}_t) &= a_0 + a_1\hat{\mathbf{X}}_t \qquad (C.31)\\
&= \begin{pmatrix} \kappa(\bar{v}-v_t) \\ \rho_{xc}\eta B_c\delta_v - \frac{\eta^2}{2}B_c^2 - \frac{v_t}{2} \end{pmatrix} = \begin{pmatrix} \kappa\bar{v} \\ \frac{1}{2}\xi_c(t) \end{pmatrix} + \begin{pmatrix} -\kappa & 0 \\ -\frac{1}{2} & 0 \end{pmatrix}\begin{pmatrix} v_t \\ \hat{x}_t \end{pmatrix},\\
\Sigma^F_{\mathbf{X}_t} &= \begin{pmatrix} \gamma^2 v_t & \rho_{xv}\gamma v_t \\ \rho_{xv}\gamma v_t & v_t - \xi_c(t) \end{pmatrix} = c_0 + c_1^\dagger\hat{\mathbf{X}}_t\\
&= \begin{pmatrix} 0 & 0 \\ 0 & -\xi_c(t) \end{pmatrix} + \begin{pmatrix} (\gamma^2,0) & (\rho_{xv}\gamma,0) \\ (\rho_{xv}\gamma,0) & (1,0) \end{pmatrix}^\dagger \hat{\mathbf{X}}_t. \qquad (C.32)\\
r &= r_0 + \mathbf{r_1}^\dagger\hat{\mathbf{X}}_t = 0 + (1,0,0)^\dagger\hat{\mathbf{X}}_t. \qquad (C.33)
\end{aligned}$$

For the corresponding Fourier state vector $\mathbf{B} = [D, B]^\dagger$ the coefficients of the CHF follow from the defining ODEs

$$\begin{aligned}
\tfrac{d}{d\tau}\mathbf{B}(u,\tau) &= -\mathbf{r_1} + a_1^\dagger\mathbf{B} + \tfrac{1}{2}\mathbf{B}^\dagger(c_1)_{\hat{\mathbf{X}}_t}\mathbf{B},\\
\tfrac{d}{d\tau}D(u,\tau) &= \tfrac{\gamma^2}{2}D^2 + (\rho_{xv}\gamma B - \kappa)D + \tfrac{B}{2}(B-1), \qquad (C.34)\\
\tfrac{d}{d\tau}B(u,\tau) &= 0,\\
\text{and}\quad \tfrac{d}{d\tau}A(u,\tau) &= -r_0 + \mathbf{B}^\dagger a_0 + \tfrac{1}{2}\mathbf{B}^\dagger c_0\mathbf{B},\\
\tfrac{d}{d\tau}A(u,\tau) &= \kappa\bar{v}D + \tfrac{\xi_c(t)}{2}B - \tfrac{\xi_c(t)}{2}B^2,\\
&= \kappa\bar{v}D + (\rho_{xc}\eta B_c\delta_v - \tfrac{\eta^2}{2}B_c^2)\tfrac{B}{2}(1-B),
\end{aligned}$$

with initial conditions $B(u,0) = iu$, $D(u,0) = 0$, $A(u,0) = 0$ given by the deliberate choice $\mathbf{u}^\dagger = [0,0,u]^\dagger$. The corresponding solutions are

$$\begin{aligned}
C_T(u,\tau) &= -\tfrac{1}{\lambda}(1-e^{-\lambda\tau}) = B_c, \qquad (C.35)\\
D(u,\tau) &= (\text{Heston Riccati solution}), \qquad (C.36)\\
B(u,\tau) &= iu, \qquad (C.37)\\
A_{H1CH}(u,\tau) &= \int_0^\tau [\tfrac{d}{d\tau}A(u,\tau)]d\tau
\end{aligned}$$

Since the IR dynamics separate, the CHF of the H1CH in the T-forward measure reduces to

$$\begin{aligned}
\hat{\Phi}^T(\mathbf{u},\hat{\mathbf{X}}_t,T,t) &= \mathbb{E}^T\left[e^{i\mathbf{u}^\dagger\hat{\mathbf{X}}_t}|\mathcal{F}_t\right] = \mathbb{E}^T\left[e^{iu\hat{x}_t}|\mathcal{F}_t\right] = e^{A^T_{H1CH}(u,\tau)+B(u,\tau)\hat{x}_t+D(u,\tau)v_t}, \qquad (C.38)\\
&\quad \text{with terminal condition}: \quad \hat{\Phi}^T(u,\hat{\mathbf{X}}_t,T,T) = e^{i\mathbf{u}^\dagger\hat{\mathbf{X}}_T} = e^{iu\hat{x}_T},\\
\text{and}\quad \tfrac{d}{d\tau}A^T_{H1CH}(u,\tau) &= \kappa\bar{v}D + (u^2+iu)(\rho_{xc}\eta B_c\delta_v - \tfrac{\eta^2}{2}B_c^2) \qquad (C.39)\\
\longrightarrow A^T_{H1CH}(u,\tau) &= \kappa\bar{v}\int_0^\tau D(u,\tau)d\tau + (u^2+iu)\rho_{xc}\eta\int_0^\tau \delta_v C_T(u,\tau)d\tau - (u^2+iu)\tfrac{\eta^2}{2}\int_0^\tau C_T^2(u,\tau)d\tau\\
&= \kappa\bar{v}I_2(u,\tau) + \rho_{xc}\eta I_4^T(u,\tau) - \tfrac{\eta^2}{2}I_3^T(u,\tau) \qquad (C.40)
\end{aligned}$$

with integrals modified with respect to the spot measure results obtained earlier (cf. appendix C.1). Evidently, the relation between H1HW and H1CH, which is somewhat more difficult to see in the spot measure and has to be made accessible via explicit reformulations under $\mathbb{Q}^B$, becomes perfectly obvious upon transformation to $\mathbb{Q}^T$.

Appendix D

Model Test Parameters

D.1 Heston Model Test Sets

The Heston model is the EQ component of all hybrid models under discussion in this thesis. Numerical evaluations of the Heston model need to be performed with care, in particular when the Feller condition is violated. In all hybrid model implementations the Heston model is retained in the limit of deterministic IRs. In order to ensure the quality of all numerical implementations, results for the Heston EQ component are calculated with test parameters. Test results are cross-checked with the corresponding published results, and compared between different implementation methods (Monte-Carlo, PDE, FFT and COS methods).

ID	T	S_0	v_0	κ	$\bar{v}$	γ	ρ_{xv}	r_0	Reference
H-1	10	100	0.05	0.3	0.05	0.6	-0.3	0.02	[1], Tbl. 4.1
H-2	0.5	1	0.0407	0.3	0.0823	0.5992	-0.5832	0.04	[1], Tbl. 6.1
H-3	10	1	0.0411	0.3	0.0828	0.6019	-0.4849	0.04	[1], Tbl. 6.1
H-4	0.5	1	0.0407	0.3	0.0822	0.5840	-0.6006	0.04	[1], Tbl. 6.2
H-5	10	1	0.0418	0.3	0.0826	0.4921	-0.6150	0.04	[1], Tbl. 6.2
H-6	1	100	0.04	1.5	0.04	0.3	-0.9	0.025	[39], Tbl. 1
H-7	1	100	0.12	3.0	0.12	0.04	0.6	0	[39], Tbl. 1
H-8	3	100	0.0707	0.6067	0.0707	0.2928	-0.7571	0	[39], Tbl. 1

Table D.1: Heston model test sets. Model parameters as introduced in Appendix A.1 above.

D.2 Hull-White Model Test Sets

Hull-White model test sets to ensure the quality of HW implementations by comparison with published results.

ID	λ	θ	η	ρ_{xr}	Reference
HW-1	0.01	0.02	0.01	$\{0.0, 0.2, 0.6\}$	[1], Tbl. 4.1
HW-2	0.501	0.04	0.005	$\{0.0, 0.2, 0.6\}$	[1], Ch.6

Table D.2: Hull-White Model test sets with HW parameters as introduced in Appendix A.2.1.

Appendix E

Additional Numerical Experiments

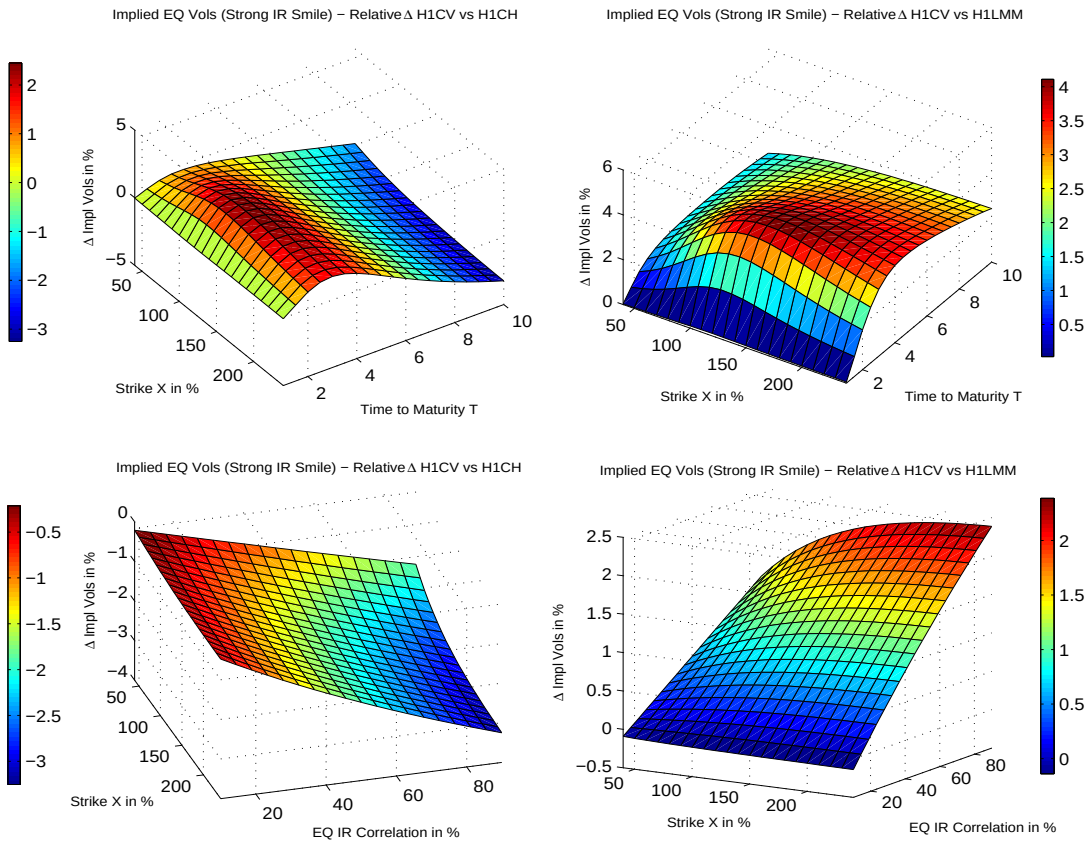

Figure E.1: Comparison of implied volatilities of affine hybrid model approximations in order to see DDSV effects. All results are obtained for equity call options in the *high IR smile* scenario (corresponding to $\beta = 0.2$, $\epsilon = 1.2$). Left: Difference in implied volatilities between H1CV (with DDSV) and H1CH (without DDSV) as function of maturity T (top) and of EQ-IR correlation (bottom), respectively. Apparently DDSV effects are relevant at all maturities $T > 0.5$, and become more pronounced with increasing EQ-IR correlation. Right: Differences between H1LMM (with DDSV, IR component LMM based) and H1CV (with DDSV, IR component Cheyette based). Differences are relevant at all maturities (top), increase with higher EQ-IR correlation and strikes X (bottom).

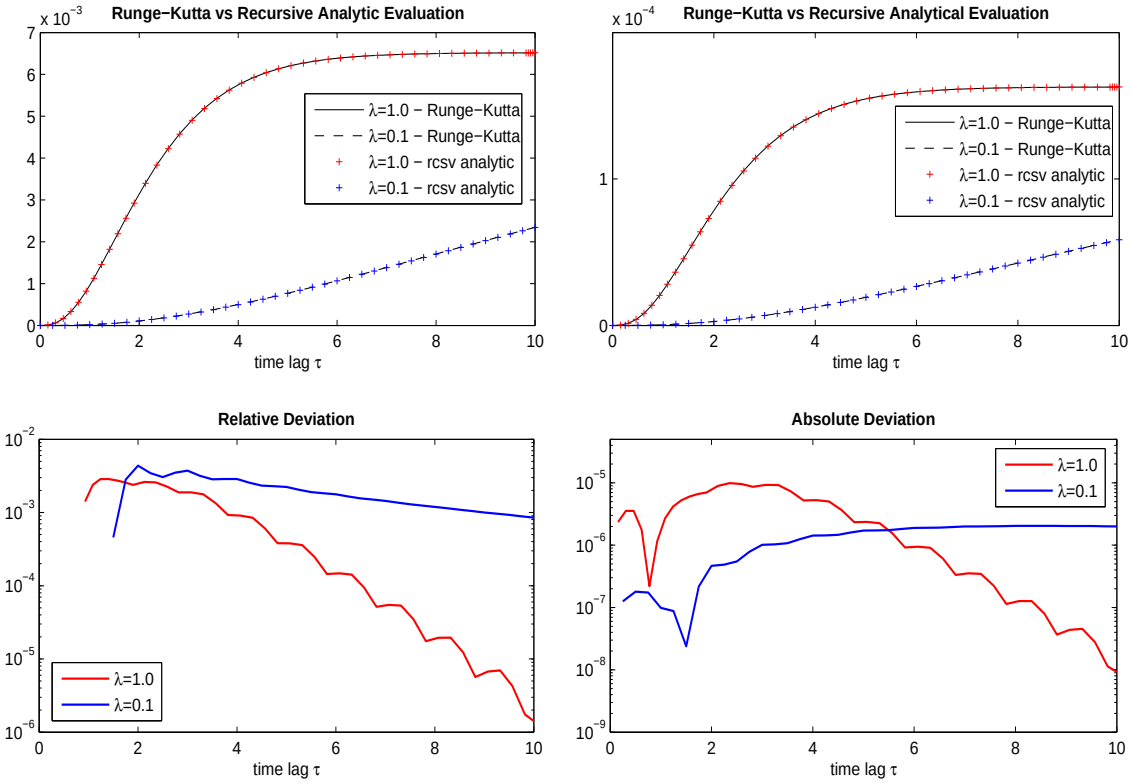

Figure E.2: $Z(u, \tau)$ computation by numerical evaluation of the ODE with the Runge-Kutta method in comparison to the recursive analytic approach. Evaluation of the recursive ansatz proves to be viable with respect to quality and superior in view of performance. The plotted time range is spaced into about 20 subintervals for the recursion.

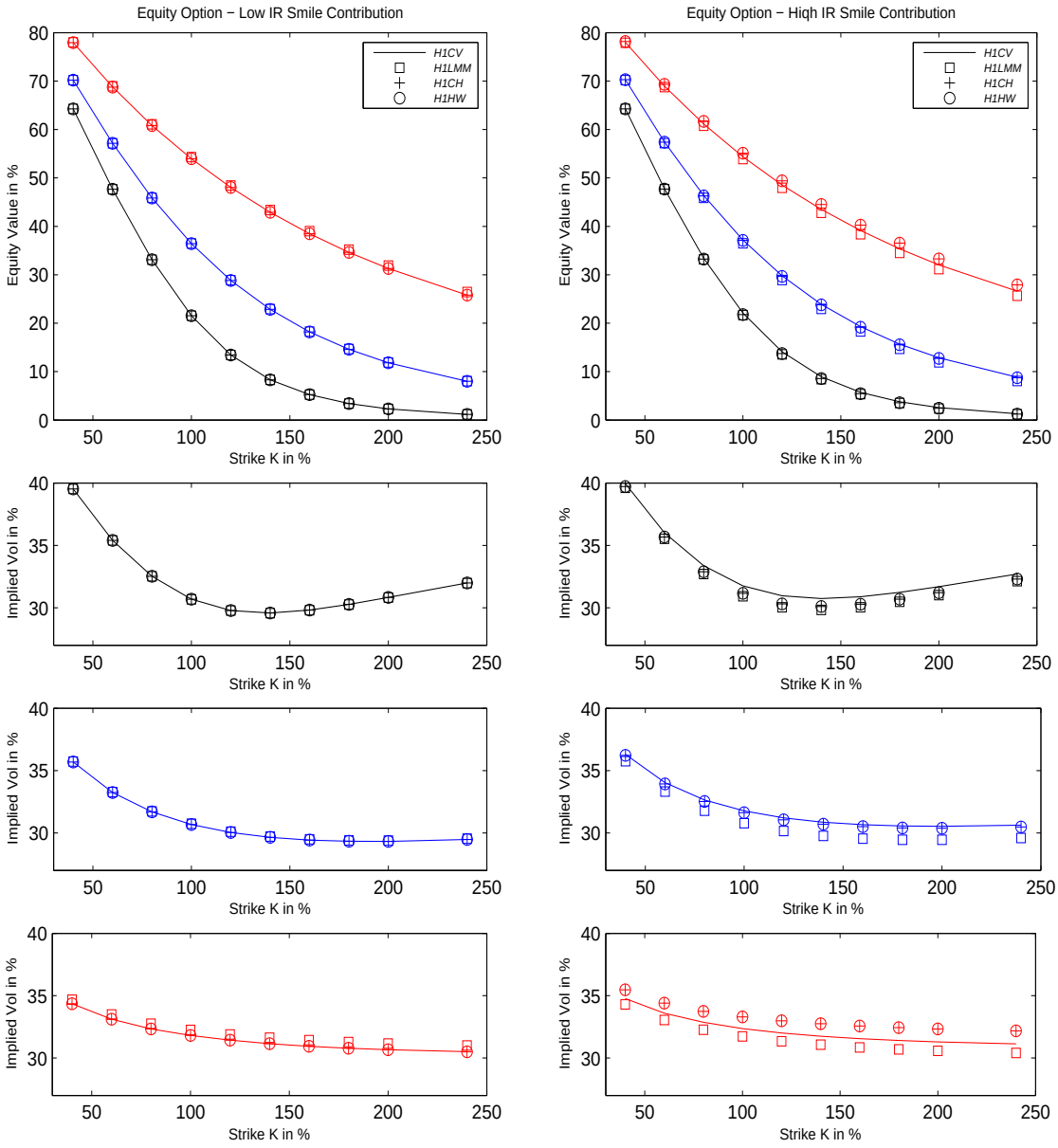

Figure E.3: Comparison of full-scale hybrid model affine approximations: The Heston EQ component is combined with a HW (H1HW), Cheyette (H1CH, H1CV) or LMM (H1LMM) IR component. EQ-IR correlation is set to $\rho_{xr} = 0.9$. Compared are European equity call options evaluated by Carr-Madan FFT (damping factor $\alpha = 0.75$) at maturities $T = 2$ (black), $T = 5$ (blue) and $T = 10$ (red), respectively. EQ option prices are shown in both top panels (model identification according to symbols in top level legend); corresponding implied volatilities are shown below, identified by the color code for maturities and symbol code for the models. Left half: Parameter limit where IR smile contributions are negligible ($\beta = 0$, $\epsilon = 0$). Right half: IR smile contributions are pushed to high limits ($\beta = 0.2$, $\epsilon = 1.2$). H1CV and H1LMM include DDSV extensions. Implied volatility results (particularly at long maturities) show that the H1CV *bridges* between classical hybrid short rate models and HJM based market models with DDSV extensions.

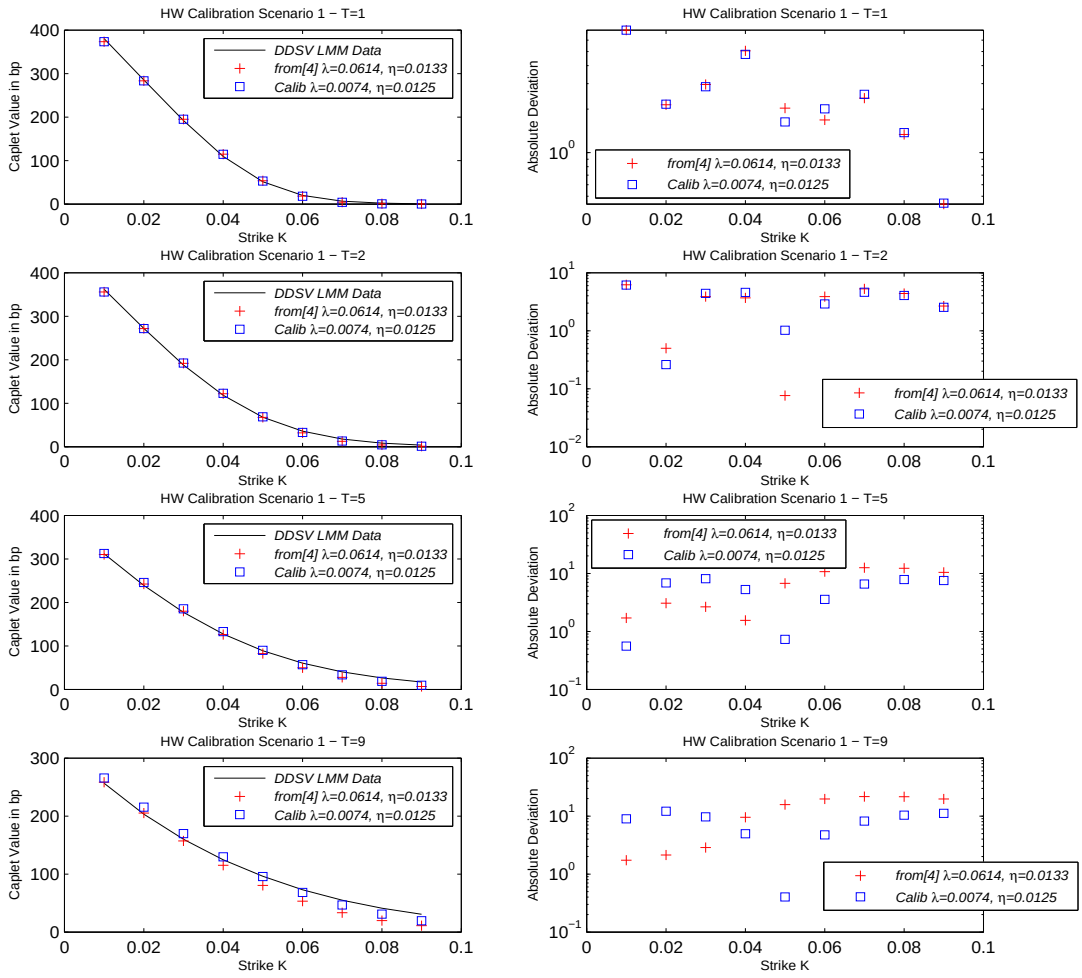

Figure E.4: Calibration results to fix the volatility specification of short rate based IR model components. Calibration proceeds on the basis of the caplet prices corresponding to the DD LMM implied volatility base skew surface in IR scenario 1. The results are compared with the reference data published in [4] (section 3 therein).

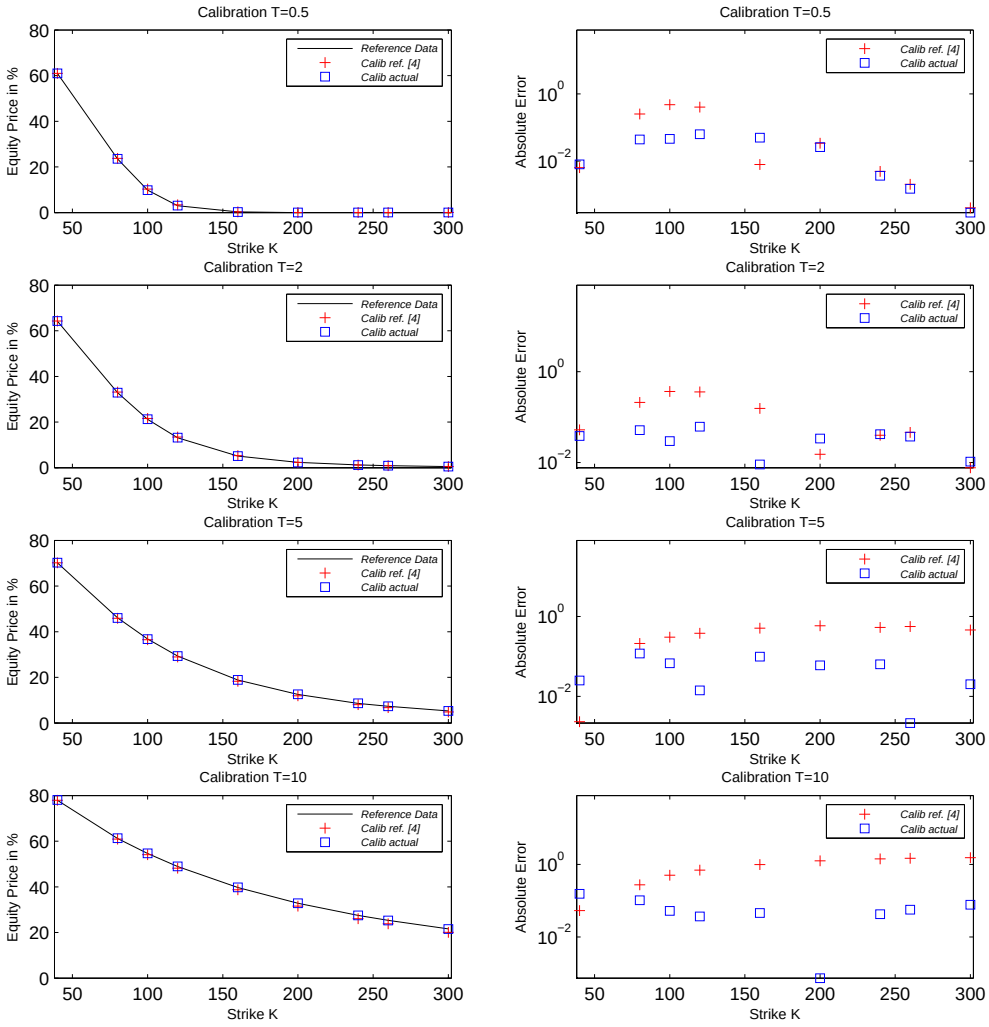

Figure E.5: Levenberg-Marquardt calibration of the Heston EQ component for selected snapshots of maturity. Calibration basis are the EQ call option quotes from [4] (section 5.1 and Appendix E therein). The calibration results are compared with the reference data and the corresponding calibration results of the reference publication [4] (section 5.3 therein).

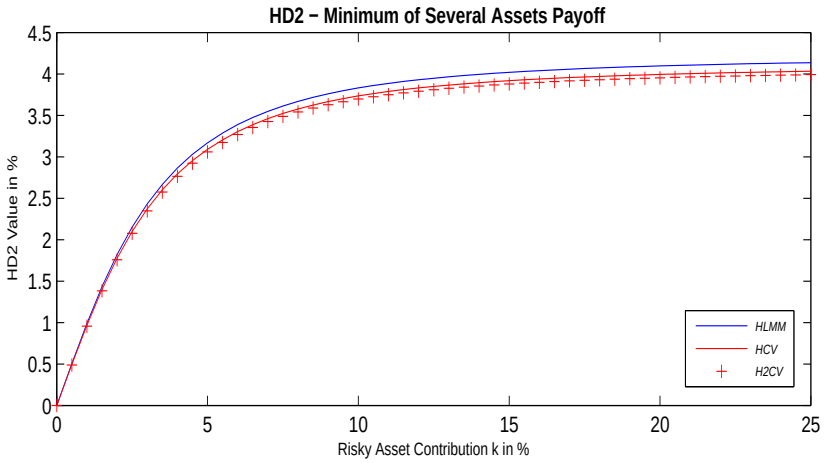

Figure E.6: HLMM Monte-Carlo results for the hybrid product HD2 - *Minimum Of Several Assets Payoff* for comparison with [4] (Fig 5.3, left panel therein). The hybrid product value (presuming $S_0 = 1, T_i = 5, T_N = 10$) as function of the relative equity contribution k is in very grood agreement with the reference results. Results for the same hybrid product and corresponding parameters are shown for the HCV and H2CV models for comparison.

Appendix F

Additional Derivations

HHW/HCH IR component: Analytic prices of contingent claims

In case of constant volatility an analytic valuation formula for contingent claims with European exercise features is constructable in the Cheyette framework in analogy to the Black pricing formula.In analogy to the HW model, the initial term structure fixes only the mean reversion level, and products of the IR market are employed to calibrate reversion rate λ and volatility η. For the simple 1D Markov Cheyette system (like in the HW model) analytic formulas exist to price IR caplets and swaptions. The calibration in the model validation context under consideration is performed using IR caplets. By definition,

$$V_{cpl}(t) = P(t,T_i)(T_{i+1}-T_i)\mathbb{E}^{T_i}\left[\frac{(L(T_i;T_i,T_{i+1})-K)^+}{1+(T_{i+1}-T_i)L(T_i;T_i,T_{i+1})}\right], \tag{F.1}$$

the caplet price V_{cpl} is the expected value of a call option on the forward Libor rate $L(T_i;T_i,T_{i+1})$ at $t=T_i$ with strike K and actual payoff at $t=T_{i+1}$ (so the payoff is discounted assuming simple compounding to $t=T_i$).

In order to use the analytic bond option valuation formula (obtained by Jamshidian's trick [30b]) the following reformulation is performed:

$$\begin{aligned} V_{cpl}(t) &= P(t,T_i)\mathbb{E}^{T_i}\left[\frac{1+(T_{i+1}-T_i)L(T_i;T_i,T_{i+1})-(1+(T_{i+1}-T_i)K)}{1+(T_{i+1}-T_i)L(T_i;T_i;T_{i+1})}\right]^+ \\ &= P(t,T_i)\mathbb{E}^{T_i}\left[1-\frac{1+\tau_i K}{1+\tau_i L(T_i;T_i;T_{i+1})}\right]^+ \\ &= P(t,T_i)\mathbb{E}^{T_i}\left[1-(1+\tau_i K)P(T_i;T_{i+1})\right]^+ \\ &= P(t,T_i)(1+\tau_i K)\mathbb{E}^{T_i}\left[K_p-F_p\right]^+. \end{aligned} \tag{F.2}$$

Hence, in short rate models caplets are understood as a portfolio of zero bond put options. The pricing is accomplished by an adoption of the Black formula for put options,

$$V_{cpl}(t) = P(t,T_i)(1+\tau_i K)\left(K_p N(-\bar{d}_2)-F_p N(\bar{d}_1)\right), \tag{F.3}$$

with generalized arguments for strike K_p, forward price F_p and bond volatility $\mathbb{V}_p$:

$$\begin{aligned} K_p &= \frac{1}{(1+\tau_i K)}, && \text{(F.4)} \\ F_p &= P(T_i, T_{i+1}), && \text{(F.5)} \\ \mathbb{V}_p &= \mathbb{V}[P(T_i, T_{i+1})] = b_c(T_i, T_{i+1})^2 \mathbb{V}[x_{c,t}] \\ &= \tfrac{1}{\lambda^2}(1 - e^{-\lambda(T_{i+1}-T_i)})^2 \tfrac{\eta^2}{2\lambda}(1 - e^{-2\lambda T_i}) && \text{(F.6)} \\ &\equiv \sigma_p^2, && \text{(F.7)} \\ \longrightarrow \bar{d}_1 &= \tfrac{1}{\sigma_p} \ln \tfrac{F_p}{K_p} + \tfrac{\sigma_p}{2} \quad \text{and} \quad \bar{d}_2 = \bar{d}_1 - \sigma_p. && \text{(F.8)} \end{aligned}$$

Here $\mathbb{V}[x]$ denotes the variance of the stochastic variable x. With the bond variance explicitly derivable, the Cheyette CHF based on the bond variance is known, i.e.

$$\hat{\Phi}_c^p = e^{iu(\ln F - \frac{1}{2}\mathbb{V}_p) - \frac{u^2}{2}\mathbb{V}_p}. \tag{F.9}$$

Therefore, it is in principle possible to calculate the caplet prices by Fourier valuation methods (cf. Appendix A.1) - as an alternative to the Black formula. It is important to note that the IR model calibration to caplets proceeds under the bond measure (with CH volatility η). Up to linear order the volatilities in the bond and T-forward measure η_f are related in the following fashion,

$$\eta \simeq f(0,t)\,\eta_f, \tag{F.10}$$

though the two caplet prices obtained in the respective measures are in principle not straightforwardly exchangeable.

Caplet prices to validate numerical implementations

Analytic caplet prices serve to validate numerical implementations of the HW and CH IR components of the hybrid models under discussion. The extension of the Cheyette (CH) IR component by a displaced-diffusion (DD) and stochastic volatility (SV) approach is an essential point of the present work, where the volatility specification assumes the form (for details and variable descriptions cf. section 3.4.2):

$$\begin{aligned} \eta_t(x_{c,t}, z_t) &= s_k(t)(b_k(t)\pi_t + (1 - b_k(t))\pi_0)\sqrt{z_t}, && \text{(F.11)} \\ \text{with} \quad \pi_t &= f(0,t) + x_{c,t} \\ dz_t &= \beta(\bar{z} - z_t)dt + \epsilon\sqrt{z_t}dW_z(t). \end{aligned}$$

Though caplet prices in DDSV model extensions have no analytic reference, the plain CH caplet price follows for limiting parameter sets. By *freezing* the initial short rates in the DD approach ($\beta_k \to 0$), and rendering the SV process quasi-deterministic by the choices $\beta \ll 1$ and $\epsilon \to 0$, analytical reference prices are applicable. In Fig. F.1 typical error levels for the caplet implied volatility surfaces are shown for Monte-Carlo (MC) implementations of the CH IR component in the spot measure $\mathbb{Q}^B$ and terminal measure $\mathbb{Q}^T$, respectively. In general, all numerical implementations presented are validated against limiting cases where analytical cross-checks are applicable.

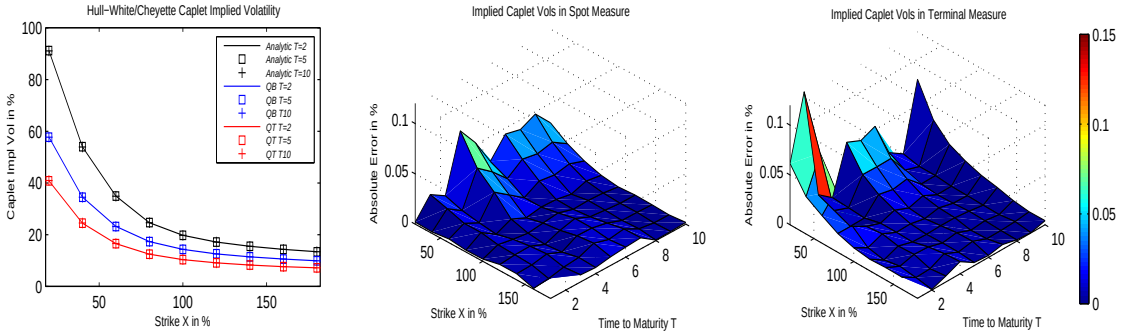

Figure F.1: HW/CH caplet prices obtained by Monte-Carlo (MC) simulation in the spot $\mathbb{Q}^B$ and $\mathbb{Q}^T$ measure are compared to the analytic reference value (with η=const) at times T=2, 5 and 10 (left subfigure). Simulations are performed with 10^6 MC paths and 800 timesteps per maturity tenor $\Delta T = T_{i+1} - T_i = 1$. The corresponding error levels measured as absolute difference to the analytical reference amount to much less than 0.5 % over most of the relevant caplet implied volatility surface in the spot measure $\mathbb{Q}^B$ (middle) as well as in the terminal measure $\mathbb{Q}^T$ (right), respectively. Cheyette parameters for this particular demonstration are $\lambda = 0.3$, $\eta = 0.125$; initial term structure is given by $P(0,T_i) = e^{-\int_0^{T_i} f(0,\tau)d\tau}$ with $f(0,t) = 0.05$. Number of paths and time discretization is typical for the model validation scenarios discussed below. Under these MC constraints, the error level is generally much below the symbol size of plot markers, and hence, the use of error bars is not applicable.

HHW/HCH hybrid models: Analytic prices of contingent claims

In the limit of vanishing EQ-IR correlations $\rho_{xr} = \rho_{xc} \to 0$ an analytic solution for European call options is derivable as detailed in Appendix B.1.2.

This limit corresponds to the uncorrelated hybrid 1F-HHW model introduced above and the analytical equity option prices serve as important consistency check to validate all numerical implementations of hybrid models.

References

[1] L.A. Grzelak and C.W. Oosterlee, On the Heston Model with Stochastic Interest Rates, SIAM Journal on Financial Mathematics, **2**, 255-286 (2011).

[2] L.A. Grzelak and C.W. Oosterlee, and S. van Weeren, The Affine Heston Model with Correlated Gaussian Interest Rated for Pricing Hybrid Derivatives, Quantitative Finance **11**, 1647-1663 (2011).

[3] L.A. Grzelak, C.W. Oosterlee, and S. v. Weeren, Extension of Stochastic Volatility Equity Models with Hull-White Interest Rate Process, Quantitative Finance, **12**(1), 89-105 (2012).

[4] L.A. Grzelak and C.W. Oosterlee, An Equity-Interest Rate Hybrid Model with Stochastic Volatility and the Interest Rate Smile, Delft Univ. of Technology Technical Report No. 10-01. Available at SSRN: http://ssrn.com/abstract=1543704 or http://dx.doi.org/10.2139/ssrn.1543704 (2010).

[5] F. Fang and C.W. Oosterlee, A novel pricing method for European options based on Fourier-cosine series expansions, SIAM Journal of Scientific Computation, **31**(2), 826-848 (2008).

[6] F. Fang and C.W. Oosterlee, Pricing early exercise and discrete barrier options using Fourier-Cosine expansions, Numerische Mathematik, **114**(1), 27-62 (2009).

[7] L.A. Anderson, Simple and Efficient Simulation of the Heston Stochastic Volatility Model, Journal of Computational Finance, **11**, 1-42 (2008).

[8] S.L. Heston, A closed-form solution for options with stochastic volatility with applications to bonds and currency options, The Review of Financial Studies, **6**(2), 327-343 (1993).

[9a] P.P. Carr and D.B. Madan, Option valuation using the fast Fourier transform, Journal of Computational Finance, **2**, 61-73 (1999).

[9b] A.L. Lewis, Option valuation under Stochastic Volatility, Finance Press, Chicago (2000).

[9c] R. Lee, Option Pricing by Transform Methods: Extensions, Unification, and Error Control, Journal of Computational Finance, **7**(3), 51-86 (2004).

[10] C. O'Sullivan and S. O'Sullivan, Pricing Options under Heston's Stochastic Volatiliy Model via Accelerated Explicit Finite Differencing Methods, UCD Geary Institute Discussion Paper Series, No. 201031 (2010).

[10a] A. van Haastrecht, R. Lord, A. Pelsser, and D. Schrager, Pricing Long-Maturity Equity and FX Derivatives with Stochastic Interest Rates and Stochastic Volatility, Ins.: Mathematics Econ., **45**(3), 436-448 (2009).

[11a] F. Ametrano and M. Joshi, Smooth Simultaneaous Calibration of the LMM to Caplets and Coterminal Swaptions, Quantitative Finance, **11**(4), 547-558 (2011).

[11b] M. Joshi, More Mathematical Finance: Chapter 17 and Chapter 18, Pilot Whale Press, Melbourne (2011).

[12] J. Gatheral, The volatility surface - A practitioner's guide, Wiley Finance, New York (2006).

[13] U. Cherubini et al., Fourier transform methods in finance, Wiley Finance, New York (2009).

[14] G. Hong, Forward Smile and Derivative Pricing, UBS presentation, Cambridge, (2004).

[15] H. Albrecher et al., The little Heston Trap, *Wilmott Magazine*, **January**, 83-92 (2006).

[16] C. Kahl and P. Jäckel, Not-so-complex logarithms in the Heston model, *Wilmott Magazine*, **March**, 94-103 (2005).

[17] C. Hunter, P. Jäckel and M. Joshi, Getting the Drift, *Risk*, **14**, 81-84 (2001).

[18] C. Hunter, P. Jäckel and M. Joshi, Drift Approximations in a Forward-Rate-Based LIBOR Market Model, working paper as basis of [17] (2001).

[17c] O. Cheyette, Markov Representation of the Heath-Jarrow-Morton Model, SSRN: http://ssrn.com/abstract=6073 (1996).

[17b] D. Heath, R. Jarrow and A. Morton, Bond Pricing and the Term Structure of Interest Rates: A new Methodology for Contingent Claim Valuation, *Econometrica*, **60**(1), 77-105 (1992).

[19] J. Hull and A. White, The Pricing of Options on Assets with Stochastic Volatilites, Journal of Finance **41**, 1011-1029 (1990).

[20] F. Black, The Pricing of Commodity Contracts, Journal of Financial Economics, **3**, 167-179 (1976).

[21] D. Duffie, J. Pan and K. Singleton, Transform analysis and asset pricing for affine jump-diffusions, *Econometrica*, **68**, 1343-1376 (2000).

[22] A. Lipton, The vol smile problem, *Risk*, **Febuary**, 61-65 (2002).

[23] M. Attari, Option Pricing using Fourier Transforms: A Numerically Effcient Simplification, Available at SSRN 520042 (2004).

[24] D.S. Bates, Maximum Likelihood Estimation of Latent Affine Processes, Review of Financial Studies, **19**, 909-965 (2006).

[25] U. Cherubini et al., Fourier transform methods in finance, Wiley Finance, New York (2009).

[26] G. Hong, Forward Smile and Derivative Pricing, UBS presentation, Cambridge (2004).

[27] H. Albrecher et al., The little Heston Trap, *Wilmott Magazine*, **January**, 73-82 (2007).

[28] C. Kahl and P. Jäckel, Not-so-complex logarithms in the Heston model, *Wilmott Magazine*, **March**, 94-103 (2005).

[29] K. in 't Hout et al., A semi-closed form analytic pricing formula for call options in hybrid Heston-Hull-White model, Proceedings of the 58th European Study Group Mathematics with Industry, eds. R.H. Bisseling et al., Utrecht (2007).

[30] B. Oksendal, Stochastic differential equations: An introduction with applications (3rd ed.), Springer, New York (1992).

[30a] D. Dufresne, The integrated square-root process, working paper, University of Montreal (2001).

[30b] F. Jamshidian, Bond and bond option evaluation in the Gaussian interest rate model, Research in Finance, **9**, 131-170 (1991).

[30] M. Joshi and A. Stacey, New and Robust Drift Approximations for the Libor Market Model, available at Mark Joshi's website (2005).

[31] L.B.G. Andersen and J. Andreasen, Volatility skews and extensions of the libor market model, Applied Mathematical Finance, **7**(1), 1-32 (2000).

[32] L.B.G. Andersen and J. Andreasen, Volatile volatilities, *Risk*, **15**(12), 163-168 (2002).

[33] L.B.G. Andersen and R. Brotherton-Ratcliffe, Extended libor market models with stochastic volatility, Journal of Computational Finance, **9**(1), 1-27 (2005).

[34] M. Schmelzle, Option Pricing Fomulae using Fourier Transform: Theory and Application, available under http://www.pathintegral.com (2010).

[35] B. Zhang and M. Giles, A Note on the implementation of the Libor Market model, Research Note, Oxford University (2009)

[36] J. Kienitz and M. Kammeyer, The Heston Hull-White Model Part I: Finance and Analytics, *Wilmott Magazine*, bf 57, 46-53 (2012).

[37] E.E. Kummer, Über die hypergeometrische Reihe $F(a;b;x)$, J. reine u. angew. Math., **15**, 39-83 (1936).

[38] J.P. Boyd, Chebyshev and Fourier spectral methods, Springer (Berlin) (1989).

[39] K.J. in 'T Hout and S. Foulon, ADI finite difference schemes for option pricing in the Heston model with correlation. Int. J. Numer. Anal. Mod., **7**, 303-320 (2010).

[40] T. Haentjens and K.J. in 't Hout, Journal of Computational Finance, **16**(1), 83-97 (2012).

[41] C. Hunter and G. Picot, Hybrid derivatives - financial engines of the future, The Euromoney-Derivatives and Riskmanagement Handbook, BNP Paribas (2006).